

# EXOPLANET EXPLORATION PROGRAM 2019 Technology Plan Appendix

Brendan Crill, Deputy Program Chief Technologist

Nick Siegler, Program Chief Technologist

## **Acknowledgments**

Important contributions and reviews were made by Peter Plavchan, Ben Mazin, Patrick Morrissey, Bala Balasubramanian, Eduardo Bendek, Laurent Puyeo, and Neil Zimmerman.

This document is cleared for public release (JPL CL #19-1070).

Cover Art Credit: NASA/JPL-Caltech/ R. Hurt (IPAC), [artist rendition of the TRAPPIST-1 system](#).

This research was carried out at the Jet Propulsion Laboratory, California Institute of Technology, under a contract with the National Aeronautics and Space Administration. Reference herein to any specific commercial product, process, or service by trade name, trademark, manufacturer, or otherwise, does not constitute or imply its endorsement by the United States Government, or the Jet Propulsion Laboratory, California Institute of Technology.

© 2019 California Institute of Technology. Government Sponsorship acknowledged.

**APPROVALS**

**Approved by:**

E-SIGNED by Gary Blackwood  
on 2019-03-13 23:30:37 GMT

---

Dr. Gary Blackwood  
Program Manager  
Exoplanet Exploration Program  
NASA / Jet Propulsion Laboratory  
California Institute of Technology

---

Date

E-SIGNED by Doug Hudgins  
on 2019-03-21 10:44:23 GMT

---

Dr. Douglas Hudgins  
Program Scientist for Programs  
Exoplanet Exploration Program  
Science Mission Directorate  
NASA Headquarters

---

Date

**Concurred by:**

E-SIGNED by Karl Stapelfeldt  
on 2019-03-13 23:39:53 GMT

---

Dr. Karl Stapelfeldt  
Program Chief Scientist  
Exoplanet Exploration Program  
NASA / Jet Propulsion Laboratory  
California Institute of Technology

---

Date

E-SIGNED by Keith Warfield  
on 2019-04-03 22:55:06 GMT

---

Keith Warfield  
Program Chief Engineer  
Exoplanet Exploration Program  
NASA / Jet Propulsion Laboratory  
California Institute of Technology

---

Date

**Prepared by:**

  
E-SIGNED by Brendan Crill  
on 2019-03-13 22:53:23 GMT

---

Dr. Brendan Crill  
Deputy Program Chief Technologist  
Exoplanet Exploration Program  
NASA / Jet Propulsion Laboratory  
California Institute of Technology

---

Date

  
E-SIGNED by Nicholas Siegler  
on 2019-03-13 23:00:13 GMT

---

Dr. Nicholas Siegler  
Program Chief Technologist  
Exoplanet Exploration Program  
NASA / Jet Propulsion Laboratory  
California Institute of Technology

---

Date

## Table of Contents

<b>A</b>	<b>Introduction</b>	<b>1</b>
A.1	Program Goals	1
A.2	Previously Funded Efforts	4
A.3	Technology Selection and Prioritization Criteria	7
<b>B</b>	<b>Visible/Near-Infrared Coronagraph/Telescope Technology Gaps</b>	<b>21</b>
B.1	Contrast	23
B.1.2	CG-2: Coronagraph Demonstrations and Modeling	27
B.1.3	CG-3: Deformable Mirrors	30
B.1.4	CG-4: Data post-processing Algorithms and Techniques	33
B.2	Contrast Stability	34
B.2.1	CG-5: Wavefront sensing and control	35
B.2.2	CG-6 Mirror Segment Phasing Sensing and Control	37
B.2.3	CG-7: Telescope Vibration Sensing and Control or Reduction	39
B.3	Angular Resolution	40
B.3.1	CG-1: Large Aperture Mirrors	41
B.3.2	Large Monolithic Mirrors	41
B.3.3	Large Segmented Mirrors	43
B.4	Detection Sensitivity	44
B.4.1	CG-8: Ultra-low Noise Visible Band Detectors	45
B.4.2	CG-9: Ultra-low Noise Near-Infrared Detectors	47
<b>C</b>	<b>Starshade Technology Gaps</b>	<b>50</b>
C.2	Starlight Suppression	54
C.2.1	S-1: Controlling Scattered Sunlight	55
C.2.2	S-2: Starlight Suppression and Model Validation	57
C.3	Formation Sensing and Control	59
C.3.1	S-3: Lateral Formation Sensing	59
C.4	Deployment Accuracy and Shape Stability	61
C.4.1	S-4: Petal Shape and Stability	62
C.4.2	S-5: Petal Positioning Accuracy and Opaque Structure	63
<b>D</b>	<b>Mid-IR Coronagraph/Telescope Technology Gaps</b>	<b>67</b>
D.1	Contrast	68
D.1.1	CG-15: Mid-infrared Coronagraph Optics and Architecture	69
D.1.2	CG-16: Cryogenic Deformable Mirror	70
D.2	Angular Resolution	71
D.2.1	CG-14: Mid-IR Large Aperture Telescopes	71
D.3	Detection Sensitivity	72
D.3.1	CG-13: Low-noise Mid-IR detectors	72
<b>E</b>	<b>Other Technology Gaps</b>	<b>73</b>
E.1	Contrast	73
E.1.1	CG-10: UV/V/NIR mirror coatings	73

<i>E.2</i>	<i>Detection Sensitivity</i>	75
E.2.1	CG-12: Ultra-low noise UV detectors	75
<i>E.3</i>	<i>Radial Stellar Motion Sensitivity (for planetary mass measurement)</i>	76
E.3.1	M-2: Laser Frequency Combs for Space-based EPRV	77
E.3.2	M-1: Extreme Precision Ground-based Radial Velocity	78
<i>E.4</i>	<i>Tangential Stellar Motion Sensitivity (for planetary mass measurement)</i>	79
E.4.1	M-3: Astrometry	79
<i>E.5</i>	<i>Mid-IR Transit and Secondary Eclipse Spectroscopy</i>	81
E.5.1	M-4: Ultra-Stable Mid-Infrared Detectors	82
<b>F</b>	<b>Technology Watch List</b>	<b>84</b>
F.1	<i>Advanced Cryocoolers</i>	84
F.2	<i>Sub-Kelvin Coolers</i>	84
<b>G</b>	<b>Prioritization</b>	<b>85</b>
<b>H</b>	<b>Conclusion</b>	<b>86</b>
<b>I</b>	<b>Document Change Log</b>	<b>87</b>
<b>J</b>	<b>Acronyms</b>	<b>88</b>
<b>K</b>	<b>References</b>	<b>90</b>

## A INTRODUCTION

The purpose of this Technology Plan Appendix is to guide near-term (1–5 year) technology development for future space observatories and ground-based support instruments related to NASA's Exoplanet Exploration Program (ExEP or Program). The ExEP responds to and supports the 2018 NASA Strategic Plan,<sup>1</sup> the 2014 NASA Science Plan,<sup>2</sup> and the 2014, 2016, and 2018 updates to the NASA Astrophysics Division Implementation Plan.<sup>3</sup>

This Appendix lists the enabling and enhancing technology needs of the ExEP that support the efforts of NASA's Astrophysics Division to respond to the 2010 Decadal Survey factoring in the Mid-Decadal (2016) recommendations.<sup>4</sup> This response is captured in the Astrophysics Division Implementation Plan (last updated in 2018).<sup>5</sup> The greatest emphasis is placed on technologies that enable the direct imaging and spectroscopic characterization of Earth-like planets in the habitable zone of Sun-like stars, though the program also tracks technologies that allow the study of broader classes of exoplanets and those that enable characterization such as mass. A possible path to developing the necessary technologies was presented in Crill and Siegler (2017).<sup>6</sup>

The Technology sections B, C, and D define the technology gaps and quantify, when possible, the difference between expected performance requirements and the current state-of-the-art. These sections also summarize recent key developments and communicate, when known, what is planned in the near future. Alternative technologies are also presented, as appropriate.

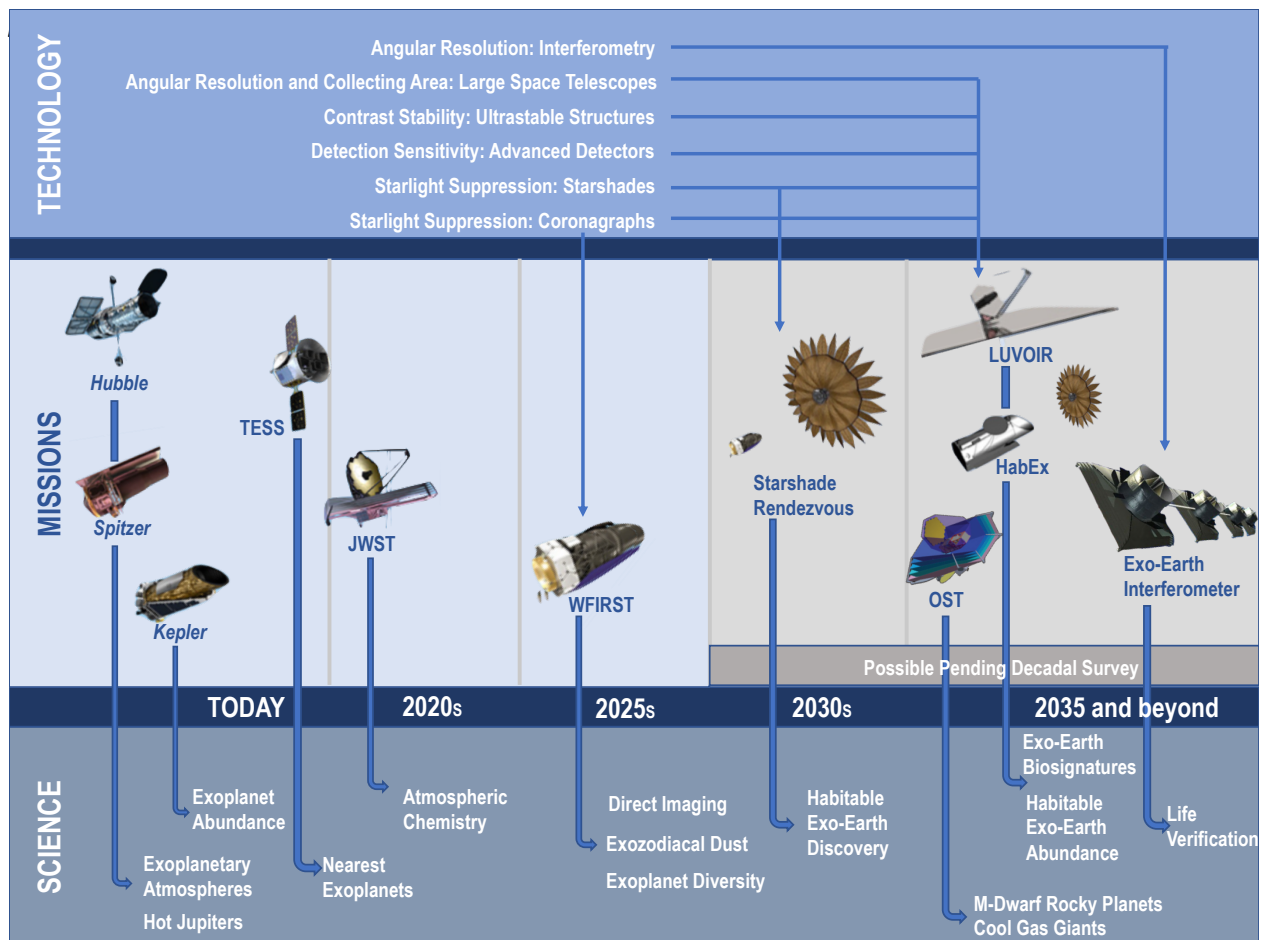
Note that, while the ExEP tracks all the listed technology gaps, a number of them are cross-cutting and important to all three Astrophysics Division science themes (Cosmic Origins, Physics of the Cosmos, and the ExEP). Several of the ExEP technology needs may be funded by the other Programs.

This Appendix communicates overall technology needs to aid scientists, engineers, and technology managers in academia, industry, research labs, and NASA centers in deciding which needed technology areas they are best suited to develop. However, not all the technologies to fly a New Worlds mission listed here are currently solicited under the Research Opportunities in Space and Earth Sciences (ROSES) Strategic Astrophysics Technology (SAT) Program (ROSES 2018, Appendix D.8). The specific technologies that are solicited under the SAT Program are described in the call for proposals. In general, an effort is made to identify and solicit proposals to mature the tallest technology tent poles within the limits of available funding, using the prioritization process described in this Appendix. Please note that in the case of a discrepancy between the ROSES language and this Appendix, the ROSES language has precedence.

### A.1 Program Goals

The 2010 Decadal Survey recommended the creation of a New Worlds Technology Development Program “to lay the technical and scientific foundation for a future mission to

Figure 1: NASA's timeline of past, current, planned, and possible Exoplanet missions.



study nearby Earth-like planets” (pp. 215–217). The Technology Development for Exoplanet Missions (TDEM) element of the SAT Program was established to support the maturation of key technologies that will enable NASA to achieve that goal. Previous work under the auspices of the SAT/TDEM Program, the results of the Exo-Coronagraph (Exo-C) and Exo-Starshade (Exo-S) probe studies,<sup>7</sup> which concluded in 2015, and the interim reports of the HabEx and LUVOIR large mission studies demonstrate that both coronagraphs and external occulters (starshades) are scientifically meritorious and their technology needs feasible for a future New Worlds mission.

The NASA Astrophysics Division response to the Decadal Survey’s recommendations (2018 Astrophysics Implementation Plan Update) describes a path for implementing the Wide-Field Infrared Survey Telescope (WFIRST),<sup>8</sup> the top large-scale mission recommendation and the next planned strategic mission after the James Webb Space Telescope (JWST). It also recommends concept development for future strategic missions for consideration by the 2020 Decadal Survey.

In 2018, NASA entered the preliminary design phase of the WFIRST mission, which makes use of a 2.4-m-diameter Astrophysics Focused Telescope Asset donated to NASA by another federal agency. A high-contrast coronagraph instrument with wavefront control has been baselined as a technology demonstration instrument within the planned WFIRST implementation. The WFIRST coronagraph will make important steps toward enabling starlight suppression necessary to directly image exo-Earths, but itself will not achieve the necessary contrast performance. Consequently, this Appendix describes the technologies devoted to instrument

performance on post-WFIRST missions capable of directly imaging and characterizing Earth-like planets.

Many of the exoplanet detection and characterization technology needs described here are intended to support the exoplanet science objectives of the two NASA Astrophysics Division 2020 Decadal Survey large mission concept studies—the Large Ultra-Violet Optical InfraRed (LUV OIR) Surveyor and the Habitable Exoplanet Imaging Observatory (HabEx; see Figure 2). Both telescope designs are driven by exo-Earth direct detection and characterization capabilities, and, unlike the case with WFIRST, the engineering requirements will drive the telescope requirements to meet the challenging contrast requirements when using a coronagraph. A third large mission concept, Origins, originally known as the Far-Infrared Surveyor and the Origins Space Telescope (OST), will include exoplanet transit spectroscopy as a central science theme, and is considering as an enhancement, a mid-infrared coronagraph capable of directly imaging Jupiter and Saturn analogs orbiting nearby stars.

The large mission concept studies commenced in 2016 for approximately three-year durations. The studies are led by Science and Technology Definition Teams (STDTs) and supported by NASA field centers for engineering and design work. Each mission concept STDT delivered Interim Reports

in 2018 which present a preliminary description of science goals, system architecture, and instrument suite.<sup>9</sup> In advance of the Interim Reports (and the Final Reports expected in 2019), the teams have also submitted, in the summers of 2016 and 2017, lists of technology gaps to the two NASA Program Offices<sup>10</sup> consisting of technology development needs for reaching the likely science objectives of each mission. Each of these STDT gap lists were reviewed as part of the annual ExEP technology selection and prioritization process, and the ExEP technology gap lists presented in this Appendix reflect our assessment of the STDTs's lists as of the end of 2017. As the work of the STDTs concludes, the technology needs may change in future editions of this Appendix.

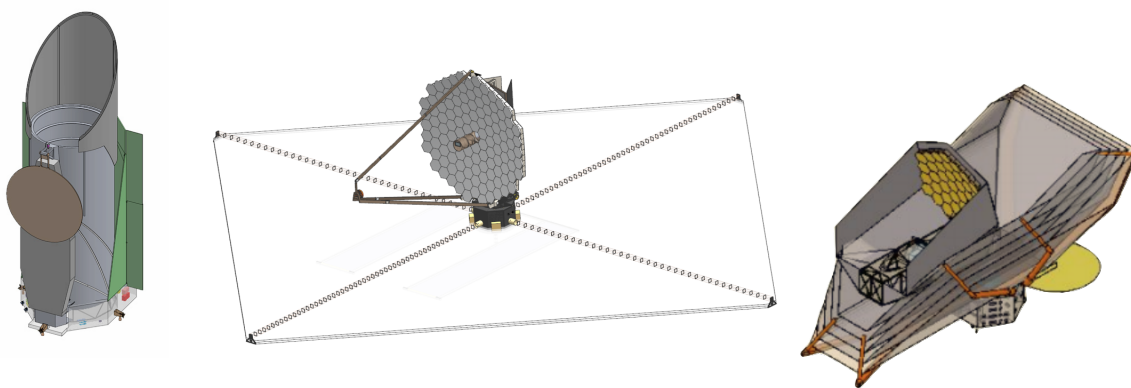


Figure 2: Renderings of the Decadal Survey large mission concepts HabEx (left), LUV OIR (center), and Origins (right). Each of these missions include exoplanet science as a driving science goal. HabEx and LUV OIR aim to directly image and characterize of rocky exoplanets orbiting nearby Sun-like stars in the visible and near-infrared bands. Origins aims to characterize the atmospheres of rocky exoplanets orbiting M dwarfs using transit spectroscopy and possibly to image directly cool gas giants in wide orbits. Primary telescope aperture diameter for the concepts rendered here are 4 m, 15m, and 9.1 m, respectively, for HabEx, LUV OIR, and Origins. Images courtesy of Keith Warfield, Matt Bolcar, and Origins team.

NASA's ExEP supports activities that contribute to the maturation of key technologies that will enable exoplanet missions. The Program funds and facilitates experiments and analyses selected by NASA HQ through yearly solicitations issued through the omnibus ROSES NASA Research Announcement (NRA). The Program also provides support in the form of infrastructure, modeling, expertise, and test facilities to selected Principal Investigators (PIs).

As a part of ROSES, NASA currently funds technology development through the Astrophysics Research and Analysis (APRA) solicitation and the SAT solicitations. APRA covers low Technology Readiness Level (TRL) technology research (TRL 1-2) while SAT covers maturation of mid-range TRL technologies (TRL 3-5). This two-stage approach is intended to support the advancement of technology envisaged by the 2010 Decadal Survey. All previous tasks funded under the 2009, 2010, 2012, 2013, 2014, 2015, 2016, and 2017 SAT solicitations are listed in **Table 1**; SAT whitepapers and abstracts can be found online.<sup>11</sup> Abstracts of funded APRA awards can also be found online.<sup>12</sup> In 2017, three SAT/TDEM awards, all related to advancing the state-of-art of coronagraphy, were funded. Note that for SAT 2018 and later, while the priority remains for NASA to mature key technologies for enabling exoplanet missions, the name TDEM is retired.

In 2018, at the direction of the U.S. Congress, the National Academies of Sciences, Engineering, and Medicine released an Exoplanet Science Strategy and an Astrobiology Science Strategy.<sup>13</sup> These documents represent important snapshot of the state of exoplanet science and technology and presents recommendations for the path forward. The Exoplanet Science Strategy included seven recommendations including “NASA should lead a large strategic direct imaging mission capable of measuring the reflected-light spectra of temperate terrestrial planets orbiting Sun-like stars.” The panel justified their recommendation with findings that “Recently acquired knowledge of the frequency of occurrence of small planets, and advances in the technologies needed to directly image them, have significantly reduced uncertainties associated with a large direct imaging mission.” And “A coronagraphic or starshade-based direct imaging mission is the only path currently identified to characterize Earth-size planets in the habitable zones of a large sample of nearby Sun-like stars in reflected light.”

The Astrobiology Science Strategy includes a recommendation “To advance the search for life in the universe, NASA should accelerate the development of life detection technologies... NASA should implement high-contrast starlight suppression technologies in near-term space- and ground-based direct imaging missions.”

These findings acknowledge the investments by NASA and others in advancing direct imaging technology. NASA may choose to respond to these recommendations or to wait for the full Astro2020 Decadal Survey which is now underway in 2019.

## **A.2 Previously Funded Efforts**

**Table 1** lists the previously funded TDEM awards, grouped by research area. Final Milestone Reports for completed TDEMs as well as Milestone Whitepaper Reports for those still in process

are posted on the ExEP Technology website<sup>14</sup> and in a common database with other NASA Astrophysics on the Astrophysics Strategic Technology Development database website.\*

**Table 1:** TDEM awards for calls for proposals beginning in 2009. Typically, technology work commences two years after the solicitation is released (column 1).

Year	PI	Institution	Proposal Title
<b>CORONAGRAPH STARLIGHT-SUPPRESSION DEMONSTRATIONS</b>			
2009	Mark Clampin	NASA Goddard Space Flight Center	Visible Nulling Coronagraph Technology Maturation: High Contrast Imaging and Characterization of Exoplanets
2009	Olivier Guyon	Univ. of Arizona	Phase-Induced Amplitude Apodization Coronagraphy Development and Laboratory Validation
2009	John Trauger	JPL	Advanced Hybrid Lyot Coronagraph Technology for Exoplanet Missions
2010	Olivier Guyon	Univ. of Arizona	Advances in Pupil Remapping (PIAA) Coronagraphy: improving Bandwidth, Throughput and Inner Working Angle
2010	Richard Lyon	NASA Goddard Space Flight Center	Compact Achromatic Visible Nulling Coronagraph Technology Maturation
2010	Jagmit Sandhu	JPL	Visible Nulling Coronagraph (VNC) Technology Demonstration Program
2010	Eugene Serabyn	JPL	Demonstrations of Deep Starlight Rejection with a Vortex Coronagraph
2013	Brian Hicks	NASA Goddard Space Flight Center	Segment Aperture Nulling Coronagraphy
2014	Eugene Serabyn	JPL	Broadband Light Rejection with the Optical Vortex Coronagraph
2016	John Trauger	JPL	Super Lyot ExoEarth Coronagraph
2016	Ruslan Belikov	NASA/Ames	Laboratory Demonstration of High Contrast Using PIAACMC on a Segmented Aperture
2016	Ruslan Belikov	NASA/Ames	Development of a Method for Exoplanet Imaging in Multi-Star Systems <sup>†</sup>
2017	Eugene Serabyn	JPL	Vortex Coronagraph High Contrast Demonstrations
2017	Rémi Soummer	Space Telescope Science Institute	First System-level Demonstration of High-Contrast for Future Segmented Space Telescopes

\* <http://www.astrostrategictech.us/>

<sup>†</sup> Funded by directed work package from NASA APD (not SAT)

Year	PI	Institution	Proposal Title
<b>STARSHADE STARLIGHT-SUPPRESSION DEMONSTRATIONS</b>			
2009	N. Jeremy Kasdin	Princeton Univ.	Starshades for Exoplanet Imaging and Characterization: Key Technology Development
2010	N. Jeremy Kasdin	Princeton Univ.	Verifying Deployment Tolerances of an External Occulter for Starlight Suppression
2012	Suzanne Casement	Northrop Grumman Aerospace Systems	Starshade Stray Light Mitigation through Edge Scatter Modeling and Sharp-Edge Materials Development
2012	Tiffany Glassman	Northrop Grumman Aerospace Systems	Demonstration of Starshade Starlight-Suppression Performance in the Field
2012	N. Jeremy Kasdin	Princeton Univ.	Optical and Mechanical Verification of an External Occulter for Straight Suppression ( <i>transferred to starshade technology activity</i> )
2013	Webster Cash	Univ. of Colorado	Development of Formation Flying Sensors
2013	N. Jeremy Kasdin	Princeton Univ.	Formation Flying for External Occulters ( <i>transferred to starshade technology activity</i> )
2014	Mark Thomson	JPL	Optical Shield for the Starshades Inner Disk Subsystem ( <i>transferred to starshade technology activity</i> )
<b>WAVEFRONT SENSING AND CONTROL OF SCATTERED STARLIGHT</b>			
2009	John Krist	JPL	Assessing the Performance Limits of Internal Coronagraphs Through End-to-End Modeling
2009	M. Charley Noecker	Ball Aerospace	Advanced Speckle Sensing for Internal Coronagraphs and Methods of Isolating Exoplanets from Speckles
2010	Paul Bierden	Boston Micromachines	MEMS Deformable Mirror Technology Development for Space-Based Exoplanet Detection
2010	Michael Helmbrecht	Iris AO	Environmental Testing of MEMS Deformable Mirrors for Exoplanet Detection
2010	N. Jeremy Kasdin	Princeton Univ.	Integrated Coronagraph Design and Wavefront Control using Two Deformable Mirrors
2017	Olivier Guyon	University of Arizona	Linear Wavefront Control for High Contrast Imaging
<b>OTHER TECHNOLOGIES</b>			
2009	Donald Figer	Rochester Inst. of Technology	A Photon-Counting Detector for Exoplanet Missions
2010	Stuart Shaklan	JPL	Coronagraph Starlight Suppression Model Validation: Coronagraph Milestone Report #3
2013	Eduardo Bendek	NASA Ames Research Center	Enhanced Direct Imaging Exoplanet Detection with Astrometric Mass Determination

Year	PI	Institution	Proposal Title
2015	Jim Breckinridge	University of Arizona	Threshold Raw Retrieved Contrast in Coronagraphs is Limited by Internal Polarization

### Flowdown from Capabilities to Gaps to Technologies

To show a coherent flowdown from the ExEP's most important science goals, we distinguish between capabilities, technology gaps, and technologies. *Capabilities* are broad desired technical abilities such as the capability to suppress starlight to sensitivities commensurate to rocky planets. Another is the capability to measure the mass of exoplanets.

Each desired capability has gaps between its desired state and the current state-of-the-art. We call these *technology gaps*. The technology gaps tracked by ExEP are listed in Table 3. Starlight suppression with coronagraphs and starshades, wavefront stability, and detection sensitivity are examples of technology gaps that remain in obtaining the capability to directly image exo-Earths.

ExEP tracks candidate *technologies* that may close the technology gaps. These are listed in Table 3. The technology list is updated each year as progress is made towards closing the technology gaps. The list is updated with new submissions from the community and is prioritized (see Section A.4).

### A.3 Technology Selection and Prioritization Process

The exoplanet science and technology community, including the large mission STDTs, submitted proposed technologies during an annual solicitation period during the summer of 2017. Along with the Technology List from the 2017 edition of the Technology Development Plan Appendix, these were first judged against a selection criterion to determine the relevance to ExEP:

***A technology considered for tracking by the ExEP enables or enhances the direct imaging or characterization of exoplanets.***

Technologies that address ExEP's technology gaps are the ones prioritized for development and considered for resource allocation. Some of these technologies may be funded outside of the ExEP. The remaining technologies considered to benefit exoplanet science (but not currently satisfying the selection criteria) are captured onto a Watch List.

The ExEP Technology List is listed in **Table 2**, in order of priority as described in the 2018 Technology Plan Appendix.

In order to better coordinate technology development across all of Astrophysics, the three NASA Astrophysics Division Program Offices ExEP, PCOS, and COR agreed to develop a new plan for a new, more unified, technology prioritization process. In addition, the technology gaps will be revised every two years. Hence there was no re-prioritization of the ExEP Technology Gap List in 2018, and the next selection and prioritization cycle will occur in calendar year 2019.

The PCOS/COR current approach to technology development can be found in Pham et al (2018)  
<sup>15</sup> The details of the new process are being defined in detail by technology teams from the three Program Offices.

**Table 2:** The 2018 ExEP Technology List. Technology ID's beginning with CG, S, and M refer to Coronagraph, Starshade and Miscellaneous technology, respectively. Changes with respect to the 2017 Technology List are indicated in blue font.

ID	Technology	Technology Gap	Technology Description	Current Performance	Needed Performance
CG-2	<b>Coronagraph Demo's and Modeling</b>	Coronagraph Contrast	Coronagraph optics and architecture that suppress diffracted starlight by a factor of $< 10^{-10}$ at visible and infrared wavelengths	<p><u>Lab:</u> <math>6 \times 10^{-10}</math> raw contrast at 10% bandwidth across angles of 3-15 <math>\lambda/D</math> demonstrated with a linear mask and an <u>unobscured</u> pupil in a static vacuum lab environment (Hybrid Lyot)</p> <p><math>&lt; 1.6 \times 10^{-9}</math> raw contrast at 10% bandwidth across angles of 3-9 <math>\lambda/D</math> demonstrated with a circularly-symmetric mask and <u>obscured</u> pupil in a static vacuum lab environment (WFIRST)</p> <p><u>Flight:</u> <math>10^{-4}</math> raw contrast 540 nm at 10 <math>\lambda/D</math> (HST)</p>	Coronagraph masks and optics capable of creating circularly symmetric dark regions in the focal plane enabling raw contrasts $\leq 10^{-10}$ , with minimal contribution from polarization aberration, IWA $< 3 \lambda/D$ for unobscured apertures, throughput $\geq 10\%$ , and bandwidth $\geq 10\%$ on obscured and segmented pupils in a simulated dynamic vacuum environment.
S-1	<b>Controlling Scattered Sunlight</b>	Starlight Suppression	Limit edge-scattered sunlight and diffracted starlight with optical petal edges that also handle stowed bending strain.	Edges manufactured with machining and electrical discharge machining do not meet scatter requirements; etched amorphous metal edges meet scatter specs integrated in-plane shape tolerance is to be demonstrated.	Integrated petal optical edges maintaining precision in-plane shape requirements after deployment trials and limit solar glint contributing $< 10^{-10}$ contrast at petal edges.
S-2	<b>Starlight Suppression and Model Validation</b>	Starlight Suppression	Experimentally validate at flight-like Fresnel numbers the equations that predict the contrasts achievable with a starshade.	Validated optical model with demonstrated $10^{-6}$ suppression at white light, 58 cm mask, and Fresnel number F (at the starshade tips) = 210; $6 \times 10^{-6}$ suppression demonstrated at F = 15; $4.6 \times 10^{-8}$ suppression demonstrated at F~27	Experimentally validated models with total starlight suppression $\leq 10^{-8}$ in scaled flight-like geometry, with F between 5 and 40 across a broadband optical bandpass. Validated models are traceable to $10^{-10}$ contrast system performance in space.

ID	Technology	Technology Gap	Technology Description	Current Performance	Needed Performance
S-3	<b>Lateral Formation Sensing</b>	Starshade Contrast Stability	Demonstrate lateral formation flying sensing accuracy consistent with keeping telescope in the starshade's dark shadow.	Sub-scale lab demonstration showing ability to center telescope within $\pm 1$ m of the center of the starshade shadow. <a href="#">The Starshade Contrast Stability Technology Gap is now closed.</a>	Demonstrate sensing lateral errors $\leq 0.24$ m $3\sigma$ accuracy at the flight signal-to-noise ratio at scaled flight separations. Demonstrate control algorithms with scaled lateral control error $\leq 1$ m radius.
S-5	<b>Petal Positioning Accuracy and Opaque Structure</b>	Deployment Accuracy and Shape Stability	Demonstrate that a starshade can be autonomously deployed to within its budgeted tolerances after exposure to relevant environments.	Petal deployment tolerance ( $\leq 1$ mm) verified with low fidelity 12 m prototype and no optical shield; no environmental testing (Exo-S design).	Deployment tolerances demonstrated to $\leq 1$ mm (in-plane envelope) with flight-like, minimum half-scale structure, with petal optical edge interfaces, that is optically opaque when deployed, and includes interfaces to launch restraint. Verify the structure will meet shape stability (petal edge position) after exposure to relevant environments <a href="#">throughout mission lifetime.</a>
S-4	<b>Petal Shape and Stability</b>	Deployment Accuracy and Shape Stability	Demonstrate a high-fidelity, flight-like starshade petal meets petal shape tolerances after exposure to relevant environments.	Manufacturing tolerance ( $\leq 100$ $\mu$ m) verified with low fidelity 6m prototype and no environmental tests. Petal deployment tests conducted but on prototype petals to demonstrate rib actuation; no shape measurements, no long-duration stowage tests.	Deployment tolerances demonstrated to $\leq 100$ $\mu$ m (in-plane tolerance profile for a 7 m petal on the 34m-diameter Exo-S design; tolerances scale roughly linearly with starshade diameter) with flight-like, minimum half-scale petal fabricated and maintains shape <a href="#">throughout mission lifetime</a> with exposure to relevant environments and is optically opaque.

ID	Technology	Technology Gap	Technology Description	Current Performance	Needed Performance
CG-3	<b>Deformable Mirrors</b>	Coronagraph Contrast	Flight-qualified large-format deformable mirrors and their electronics	<p><u>Lab</u>: Electrostrictive 64×64 actuator DMs have been demonstrated to meet <math>\leq 10^{-9}</math> contrasts and <math>&lt; 10^{-10}</math> stability in a vacuum environment and 10% bandwidth; 48×48 actuator DM passed random vibrate testing</p> <p><u>Flight</u>: No SOA</p>	<p>4 m primary mirror: <math>\geq 96 \times 96</math> actuators</p> <p>10 m primary mirror: <math>\geq 128 \times 128</math> actuators</p> <p>Enable raw contrasts of <math>\leq 10^{-9}</math> at <math>\sim 20\%</math> bandwidth and IWA <math>\leq 3 \lambda/D</math></p> <p>Flight-qualified device and drive electronics (radiation hardened, environmentally tested, life-cycled including connectors and cables)</p> <p>Mirror stability maintains <math>10^{-10}</math> contrast over observation time scales</p>
CG-1	<b>Large Aperture Primary Mirrors</b>	UVOIR Angular Resolution	Large monolith and multi-segmented mirrors that meet tight surface figure error, coating uniformity, and thermal control requirements at visible wavelengths	<p><u>Flight</u> Monolith:</p> <p>3.5-m sintered SiC with <math>&lt; 3 \mu\text{m}</math> SFE (Herschel)</p> <p>2.4 m ULE with <math>\sim 10</math> nm SFE (HST)</p> <p>Depth: Waterjet cutting is TRL 9 to 14", but TRL 3 to <math>&gt; 18"</math>. Fused core is TRL 3; slumped fused core is TRL 3 (AMTD).</p> <p>Segmented (no flight SOA): 6.5 m Be with 25 nm SFE (JWST)</p> <p>Non-NASA: 6 DOF, 1-m class SiC and ULE, <math>&lt; 20</math> nm SFE, and <math>&lt; 5</math> nm wavefront stability over 4 hr with thermal control</p>	<p>Aperture: 4–15 m; SFE <math>&lt; 10</math> nm rms (wavelength coverage 400–2500 nm)</p> <p>Wavefront stability better than 10 pm rms per wavefront control time step.</p> <p>Segmented apertures leverage 6 DOF or higher control authority meter-class segments for wavefront control.</p> <p>Environmentally tested</p>

ID	Technology	Technology Gap	Technology Description	Current Performance	Needed Performance
CG-6	<b>Mirror Segment Phasing Sensing &amp; Control</b>	Coronagraph Contrast Stability	Segmented or monolith large aperture mirrors require segment phasing and rigid-body sensing and control of the segments or the surface figure to achieve tight static and dynamic wavefront errors.	<p>6 nm rms rigid body positioning error and 49 nm rms stability (JWST error budget)</p> <p>SIM and non-NASA: nm accuracy and stability using laser metrology</p> <p>Capacitive gap sensors demonstrated at 10 pm.</p> <p>No flight SOA; ground-based (Keck) achieved 6 nm positioning error in operations</p>	Systems-level considerations to be evaluated but expect will require WFE stability less than 10 pm rms sensitivity and control over periods of tens of minutes
CG-7	<b>Telescope Vibration Sense/Control or Reduction</b>	Coronagraph Contrast Stability	Isolation, reduction, and/or damping of spacecraft and payload vibrational disturbances	<p>80 dB attenuation at frequencies &gt; 40 Hz (JWST passive isolation)</p> <p>Disturbance-Free Payload demonstrated at TRL 5 for JWST with 70 dB attenuation at "high frequencies" with 6-DOF low-order active pointing.</p> <p>GAIA cold gas microthrusters or LISA pathfinder colloidal microthrusters for fine pointing can reduce disturbance environment.</p>	Vibration isolation or reduction of vibration disturbance sources to a level that enables < 1 nm wavefront error stability.

ID	Technology	Technology Gap	Technology Description	Current Performance	Needed Performance
CG-9	<b>Ultra-Low Noise Near-Infrared Detectors</b>	NIR Detection Sensitivity	Near-infrared wavelength (900 nm to 2.5 $\mu\text{m}$ ), extremely low noise detectors for exo-Earth spectral characterization with Integral Field Spectrographs	<p><u>Lab:</u> HgCdTe photodiode arrays have read noise <math>\lesssim 2</math> e-rms with multiple nondestructive reads; 2k<math>\times</math>2k format; dark current &lt; 0.001 e-/s/pix; very radiation tolerant (JWST)</p> <p>HgCdTe APDs have dark current <math>\sim 10</math>–<math>20</math> e-/s/pix, RN <math>\ll 1</math> e- rms, and &lt; 1k<math>\times</math>1k format</p> <p>Sub-Kelvin photon-counting detectors (KID, TES): 0 read noise/dark current; radiation tolerance is unknown; &lt;1k<math>\times</math>1k format</p> <p><u>Flight:</u> HST WFC3/IR HgCdTe dark current 0.05 e-/px/s, 12 e- read noise, 1k<math>\times</math>1k format</p>	Read noise $\ll 1$ e- rms, dark current noise < 0.001 e-/pix/s, in a space radiation environment over mission lifetime $\geq 2\text{k}\times 2\text{k}$ format
CG-5	<b>Wavefront Sensing and Control</b>	Coronagraph Contrast Stability	Sensing and control of line-of-sight jitter and low-order wavefront drift	<p><u>Lab:</u> &lt; 0.5 mas rms per axis LOS residual error demonstrated in lab with a fast-steering mirror attenuating a 14 mas LOS jitter and reaction wheel inputs; <math>\sim 12</math> pm rms sensitivity of focus (WFIRST)</p> <p>Higher low-order modes sensed to 10–100 nm WFE rms on ground-based telescopes</p> <p><u>Flight:</u> No SOA</p>	Sufficient fast line-of-sight jitter (< 0.5 mas rms residual) and slow thermally-induced WFE sensing and control ( $\leq 10$ pm rms sensitivity) to maintain closed-loop < $10^{-10}$ raw contrast with an obscured/segmented pupil and simulated dynamic environment
CG-8	<b>Ultra-Low Noise Visible Detectors</b>	Vis Detection Sensitivity	Low-noise visible detectors for faint exoplanet characterization with an Integral Field Spectrograph	<p><u>Lab:</u> 1k<math>\times</math>1k silicon EMCCD detectors provide dark current of <math>7\times 10^{-4}</math> e-/px/sec; CIC of 0.01 e-/px/frame; zero effective read noise (in photon counting mode) after irradiation when cooled to 165.15K (WFIRST); 4k<math>\times</math>4k EMCCD fabricated but still under development</p> <p><u>Flight:</u> HST WFC3/UVIS CCD 3.1 e- read noise, dark current <math>2\times 10^{-3}</math>, format 2k<math>\times</math>2k</p>	Effective read noise < 0.1 e- rms; CIC < $3\times 10^{-3}$ e-/px/frame; dark current < $10^{-4}$ e-/px/sec tolerant to a space radiation environment over mission lifetime $\geq 2\text{k}\times 2\text{k}$ format

ID	Technology	Technology Gap	Technology Description	Current Performance	Needed Performance
M-4	<b>Ultra-Stable Mid-IR Detectors</b>	Transit Spectroscopy of Exo-Earths	Ultrastable detectors for the mid-infrared band (7 - 20 microns) enabling transit spectroscopy of rocky exoplanets in the Habitable Zone of M-dwarfs.	<u>Lab:</u> JWST/MIRI is expected to achieve 10-100 ppm transit stability  <u>Flight:</u> Spitzer IRAC Si:As detector data have demonstrated about 60 ppm precision in transit observations of several hours	< 5 ppm stability for 5 hours
M-3	<b>Astrometry</b>	Tangential Stellar Motion	Measure the mass and orbital parameters of Earth-like planets by performing astrometry of FGK stars to the sub-micro-arcsecond level.	<u>Flight:</u> GAIA typical uncertainty in astrometry for DR1 catalog is 300 microarcseconds; goal for V band magnitude 7-12 stars is 10 microarcseconds.	< 0.1 microarcsecond uncertainty enables survey of nearby FGK stars. Astrophysical limits (such as variable stellar surface structure) need to be well-understood. Telescope wavefront error stability and detector thermal and mechanical stability must enable sub-microarcsecond astrometry measurements.
CG-4	<b>Data Post-Processing Algorithms and Techniques</b>	Coronagraph Contrast	Data post-processing techniques to uncover faint exoplanet signals from residual speckle noise at the focal-plane detector	Few 100 × speckle suppression has been achieved by HST and by ground-based AO telescopes in the NIR and in contrast regimes of $10^{-4}$ to $10^{-5}$ , dominated by phase errors.	A 10-fold contrast improvement in the visible from $10^{-9}$ raw contrast where amplitude errors are expected to be important (or a demonstration of the fundamental limits of post-processing)
CG-10	<b>Mirror Coatings for UV/NIR/Vis</b>	Coronagraph Contrast	Mirror coatings that enable high reflectivity to wavelengths as short as 90 nm; <a href="#">coating uniformity enables <math>10^{-10}</math> coronagraph performance</a>	Al coating with combination of $MgF_2$ , LiF, and/or $AlF_3$ overcoat:  90-120 nm: < 50% reflectivity 120-300 nm: 85% reflectivity 300 nm-2 $\mu$ m: > 90% reflectivity  Polarization differences between orthogonal polarization states, uniformity, and durability of coatings on large optics is unknown.  <u>Flight:</u> HST uses $MgF_2$ ; 85% reflectivity $\lambda > 120$ nm; 20% reflectivity $\lambda < 120$ nm	A mirror coating that achieves:  90-120 nm: > 70% reflectivity 120-300 nm: > 90% reflectivity 300 nm-2 $\mu$ m: > 90% reflectivity  Polarization phase and amplitude difference < 1% between orthogonal polarization states.  <a href="#">Uniformity enables <math>10^{-10}</math> coronagraph contrast performance</a>

ID	Technology	Technology Gap	Technology Description	Current Performance	Needed Performance
M-2	<b>Laser Frequency Combs</b>	Radial Stellar Motion	Laser Frequency Combs (LFCs) are precise calibration sources for extreme-precision radial velocity measurement.	<p><u>Lab</u>: Electro-optic-modulation frequency combs demonstrated on ground-based observatories with needed mode spacing, need miniaturization and power reduction.</p> <p>Non-NASA work is advancing miniaturization.</p> <p><u>Flight</u>: Fiber laser-based optical frequency combs demonstrated on sounding rocket (TEXUS 51 4/15 and TEXUS 53 1/16) w/ ~ few hundred MHz mode spacing. System mass is &gt; 10 kg.</p>	<p>Space-based Laser Frequency Combs to calibrate high resolution, fiber-fed spectrographs for radial velocity precision better than 10 cm/s. Desired parameters are:</p> <ul style="list-style-type: none"> <li>• mode spacing of 5-10 GHz</li> <li>• bandwidth span 380 nm to 2400 nm</li> <li>• Allen deviation &lt; 10<sup>-10</sup></li> <li>• Low SWaP</li> </ul>
CG-13	<b>Ultra Low Noise Mid-IR detectors</b>	Mid-IR detection sensitivity	Low noise and detectors for the mid-infrared band (7 - 20 microns) enabling exoplanet direct imaging.	<u>Flight</u> : JWST/MIRI	< 5 ppm stability for 5 hr; noise requirements TBD, likely to be 10 x better than JWST/MIRI
M-1	<b>Extreme Precision Ground-based Radial Velocity</b>	Radial Stellar Motion	Ground-based radial velocity instrumentation capable of measuring the mass of candidate exo-Earths in the habitable zone and to maximize efficiency of space telescope surveys.	Stability of 28 cm/s over 7 hours (VLT/ESPRESSO).	Signal from exo-Earths is 10 cm/s; Need to reduce systematic errors to 1 cm/s on multi-year timescales; statistical uncertainties of 1 cm/s on monthly timescales for late F, G, and early K stars
CG-14	<b>Mid-IR Large Aperture Telescopes</b>	Mid-IR Angular Resolution	Cryogenic (4K), large-aperture (> 6m) telescopes to achieve high angular resolution needed to direct-image cool exoplanets in wide orbits (> 5 AU)	<p>JWST Be mirror segments may meet requirements now, so TRL 5 with an extremely expensive technology; TRL 3 exists for other materials like SiC.</p> <p>Cryogenic low-dissipation actuators exist at TRL 3-5.</p>	Develop a feasible and affordable approach to producing a 6-m-class telescope with sufficiently high specific stiffness, strength, and low areal density to be launched; while maintaining compatibility with cryogenic cooling and FIR surface quality/figure of ~1μm rms. Material property measurements at cryogenic temperatures for structures and optics such as damping, emissivity, thermal conductivity, etc.

ID	Technology	Technology Gap	Technology Description	Current Performance	Needed Performance
CG-15	<b>Mid-IR Coronagraph Optics and Architecture</b>	Mid-IR Coronagraph Contrast	Coronagraph optics and architecture that suppress diffracted starlight by a factor of $< 10^{-6}$ over a broad mid-IR band (7-30 microns)	The current state of the art for mid-infrared coronagraphs are the three four-quadrant phase masks of JWST-MIRI. These provide narrow-band imaging with contrasts up to $10^{-4}$ in three narrow bands from 10.65-15.5 micron with inner working angles of 0.33-0.49". The MIRI coronagraphs do not offer spectral dispersion.	Contrast should be $10^{-6}$ at IWA $3 \lambda/D$ at 10 $\mu\text{m}$ .
CG-16	<b>Cryogenic Deformable Mirrors</b>	Mid-IR Coronagraph Contrast	Flight-qualified deformable mirrors operable at cryogenic temperatures, and their drive electronics.	<u>Lab:</u> MEMS DM with 32x32 actuator count operated at 5k demonstrating 2.6 nm rms repeatability	Requirements on actuator stroke, stroke resolution, heat dissipation, and actuator count are TBD but must be operable at cryogenic temperatures.
CG-12	<b>Ultra-Low Noise UV Detectors</b>	UV Detection Sensitivity	Low-noise ultraviolet (200-400 nm) detectors to characterize exoplanets.	<u>Lab:</u> Micro-channel Plates (MCP): 0 read noise, $\lambda \sim 90 - 300$ nm, spurious count rate 0.05 - 0.5 counts/cm <sup>2</sup> /s; QE 20-45%; resolution element size 20 mm. EMCCD: 0 read noise, dark current $> 0.005$ e-/res/hr; QE 30-50%; resol. el. size 20 $\mu\text{m}$  <u>Flight:</u> HST HRC: In relevant UV band (250 nm): QE 33%, read noise 4.7 e-, dark current $5.8 \times 10^{-3}$ , 1024x1024	Read Noise: 0 e- Dark Current: 0 e-/resolution/s Spurious Count Rate: $< 0.05$ counts/cm <sup>2</sup> /s QE: 75% Resolution size $\leq 10 \mu\text{m}$ Tolerant to space radiation environment over mission lifetime.

<b>Technology Gap</b>	<b>Need</b>	<b>State-of-the-Art</b>	<b>Current Efforts</b>
<b>Coronagraph Contrast</b>	Maximized science yield for a direct imaging telescope/mission. $\leq 10^{-10}$ raw contrast, >10% system throughput, IWA $\leq 3 \lambda/D$ for unobscured pupil, obscured/segmented pupil	unobscured pupil: $6 \times 10^{-10}$ raw contrast at 10% bandwidth, angles of 3-15 $\lambda/D$ (HLC demo in HCIT); obscured pupil: $1.6 \times 10^{-9}$ raw contrast at 10% bandwidth across angles of 3-9 $\lambda/D$ (WFIRST)	SCDA in CY 2019 will answer the questions: 1. can a coronagraph provide high science yield on a segmented telescope, while maintaining robustness to wavefront error instabilities, levying unrealistic requirements on a space telescope. 2. can the necessary grayscale apodizer mask be built.  Decadal Survey Testbed (DST) in CY 2019, aims to demonstrate $10^{-10}$ on a clear aperture, enable future static (CY19) and dynamic (CY20) demos for segmented/obscured apertures  TDEM funded contrast demos in HCIT: Super Lyot (Trauger), PIAACMC (Belikov) aiming for $\sim 10^{-10}$ contrast demos in HCIT in CY19 and 20, Vortex (Serabyn) aiming for $10^{-9}$ in CY19
<b>Coronagraph Contrast Stability</b>	Contrast stability on time scales needed for spectral measurements (possibly as long as days). Achieving this stability requires an integrated approach to the coronagraph and telescope, possibly including wavefront sense/control, metrology and correction of mirror segment phasing, vibration isolation/reduction  This stability is likely to require wavefront error stability at the level of 10-100 pm per control step (of order 10 minutes).	WFIRST CGI demonstrated $\sim 10^{-8}$ contrast in a simulated dynamic environment using LOWFS (which obtained 12 pm focus sensitivity)  SIM and non-NASA work has demonstrated nm accuracy and stability with laser metrology  Capacitive gap sensors demonstrated at 10 pm  80 dB vibration isolation demonstrated  Gaia cold gas microthrusters and LISA pathfinder colloidal microthrusters can reduce vibrations	LUVOIR and HabEx concept studies are developing reference telescope and coronagraph architectures that includes the need for contrast stability as a driving requirement.  NASA APD Systems-level Segmented Telescope industry studies will generate system-level error budgets for a coronagraph/ telescope/ spacecraft systems and identify key trades.
<b>Angular Resolution (UV/Vis/NIR)</b>	Large (4–15 m) monolith and multi-segmented mirrors for space that meet SFE < 10 nm rms (wavelength coverage 400–2500 nm); Wavefront stability better than 10 pm rms per wavefront control time step; Segmented apertures leverage 6 DOF	<u>Monolith</u> : 3.5-m sintered SiC with < 3 $\mu\text{m}$ SFE (Herschel); 2.4-m ULE with $\sim 10$ nm SFE (HST); Depth: Waterjet cutting is TRL 9 to 14", but TRL 3 to >18". Fused core is TRL 3; slumped fused core is TRL 3 (AMTD).	HabEx and LUVOIR studies investigating monolith and segmented architectures, including materials (Si carbide, glass) manufacturing, coating, mounting, thermal control, vibration isolation.

	or higher control authority meter-class segments for wavefront control.	<u>Segmented</u> : (no flight SOA): 6.5 m Be with 25 nm SFE (JWST); Non-NASA: 6 DOF, 1-m class SiC and ULE, < 20 nm SFE, and < 5 nm wavefront stability over 4 hr with thermal control	SLSTC industry study is investigating manufacturability of large segmented mirrors  In-space assembly of future large telescopes (>20m) under study
<b>Vis/NIR Detection Sensitivity</b>	Near IR (900 nm to 2.5 μm) and visible-band (400-900nm) extremely low noise detectors for exo-Earth spectral characterization with Integral Field Spectrographs. NIR Read noise << 1 e <sup>-</sup> rms, dark current noise < 0.001 e <sup>-</sup> /pix/s, Vis band read noise < 0.1 e <sup>-</sup> rms; CIC < 3×10 <sup>-3</sup> e <sup>-</sup> /px/frame; dark current < 10 <sup>-4</sup> e <sup>-</sup> /px/sec, detection quantum efficiency (including all radiation effects) enables detection and characterization in a space radiation environment over mission lifetime; ≥ 2k×2k format	Vis: 1k×1k silicon EMCCD detectors provide dark current of 7×10 <sup>-4</sup> e <sup>-</sup> /px/sec; CIC of 0.01 e <sup>-</sup> /px/frame; zero effective read noise (in photon counting mode) after irradiation when cooled to 165.15 K (WFIRST); 4k×4k EMCCD fabricated but still under development  NIR: HgCdTe photodiode arrays have read noise ≤ 2 e <sup>-</sup> rms with multiple nondestructive reads; 2k×2k format; dark current < 0.001 e <sup>-</sup> /s/pix; very radiation tolerant (JWST); HgCdTe APDs have dark current ~10–20 e <sup>-</sup> /s/pix, RN << 1 e <sup>-</sup> rms, and < 1k×1k format  Cryogenic superconducting photon-counting detectors (MKID, TES): 0 read noise/dark current; radiation tolerance is unknown; <1k×1k format	HabEx and LUVOIR have baselined existing EMCCD (Vis) and HgCdTe (NIR) detectors while keeping an eye on potential improvements in other areas, particularly in read noise, dark current and radiation hardness  WFIRST CGI is advancing the EMCCD technology for the Vis band, in particular aiming to improve radiation hardness  Superconducting detectors (MKID, TES, etc.) developing under APRA for sub-orbital and ground-based efforts
<b>Starshade Starlight Suppression and Model Validation</b>	Experimentally validate at flight-like Fresnel numbers (F) the equations that predict starshade starlight suppression: total starlight suppression ≤ 10 <sup>-8</sup> in scaled flight-like geometry, F between 5 and 40 across a broadband optical bandpass. Contrast model accuracy validated to better than 25%.  Limit edge-scattered sunlight and diffracted starlight with optical petal edges that also handle any stowed bending strain. Limit solar scatter lobe brightness to better than visual magnitude (V) 25	Validated optical model with demonstrated 10 <sup>-6</sup> suppression at white light, 58 cm mask, and F (at the starshade tips) = 210; 6×10 <sup>-6</sup> suppression demonstrated at F =15; 4.6×10 <sup>-8</sup> suppression demonstrated at F ~ 27  Etched amorphous metal edges meet scatter specs integrated in-plane shape tolerance is to be demonstrated.	S5 is continuing sub-scale tests at Princeton that should achieve flight suppression. Currently limited by manufacture of the subscale starshade.  S5 developing amorphous metal edges that demonstrate shape specs.  The edge scatter technology scheduled to be at TRL 5 by the S5 project in 1-2 years  Suppression demos are high priority for S5  Because of reliance on models, once flight-like suppression is demonstrated, should also validate equations in a slightly wider range of parameters (wavelengths, subscale starshade size, etc.)

<b>Starshade Formation Sensing</b>	Demonstrate sensing lateral errors $\leq 0.24 \text{ m } 3\sigma$ accuracy at the flight signal-to-noise ratio at scaled flight separations. Demonstrate control algorithms with scaled lateral control error $\leq 1 \text{ m}$ radius.	Sub-scale lab demonstration showing ability to center telescope within $\pm 1 \text{ m}$ of starshade shadow. <u>This gap is now closed in early 2019 for a potential WFIRST rendezvous mission.</u>	WFIRST starshade accommodation and S5 created a scaled benchtop demonstration of using an out-of-band pupil-plane camera (For WFIRST, the LOWFS camera will suffice) to provide misalignment sensing  Control algorithms based on the sensor are also demonstrated at subscale.  The pupil-plane camera approach will be roughly independent of starshade and telescope diameter
<b>Starshade Deployment and Shape Stability</b>	A system that will deploy the petals from a launch-stowed configuration to the needed shape (to better than $\leq 1 \text{ mm}$ (in-plane envelope) and maintain petal edges to $\leq 100 \mu\text{m}$ (in-plane tolerance profile for a 7 m petal on the 34 m-diameter Exo-S design; tolerances scale roughly linearly with starshade diameter), and be optically opaque.	Manufacturing tolerance ( $\leq 100 \mu\text{m}$ ) verified with low fidelity 6 m prototype and no environmental tests. Petal deployment tests conducted but on prototype petals to demonstrate rib actuation; no shape measurements, no long-duration stowage tests.  Petal deployment tolerance ( $\leq 1 \text{ mm}$ ) verified with low fidelity 12 m prototype and no optical shield; no environmental testing (Exo-S design).	S5 is wrapping up a trade study that will select a deployment architecture to use as a baseline towards reaching TRL 5 by the early 2020s.  Work on this mechanical deployment will accelerate when the trade study is complete.  This technology gap is scheduled to be closed by early 2020s for a WFIRST rendezvous design (30m-diameter class starshade). A larger starshade may require a different autonomous deployment architecture or in-space assembly.
<b>Mid-IR Coronagraph Contrast</b>	Coronagraphy in the mid-IR to detect $\sim 100\text{-}300\text{K}$ planets in emission and perform spectroscopy between $10\text{-}30 \mu\text{m}$ .	The current state of the art for mid-infrared coronagraphs are the three four-quadrant phase masks of JWST-MIRI. These provide narrow-band imaging with contrasts up to $10^{-4}$ in three narrow bands from $10.65\text{-}15.5 \mu\text{m}$ with inner working angles of $0.33\text{-}0.49''$ . The MIRI coronagraphs do not offer spectral dispersion.	Origins is currently studying the science case for mid-infrared coronagraphy and technology development needed to achieve the science goals.  JAXA is studying the mid-IR instrument (MISC) in Origins.  If Origins uses a segmented telescope, this technology benefits from lessons learned in the Vis/NIR SCDA study.  The relatively modest contrast may not require small deformable mirrors such as those needed for speckle nulling in the visible band. If this is the case, this

			coronagraph could be ready on the time scale of a Vis/NIR coronagraph.
<b>Mid-IR Detection Stability</b>	Ultrastable detectors (< 10 ppm over 5 hours) for the mid-infrared band (7 - 20 microns) enabling transit spectroscopy of rocky exoplanets in the Habitable Zone of M-dwarfs.	JWST/MIRI is expected to achieve 10-100 ppm transit stability.  Spitzer IRAC Si:As detector data have demonstrated about 60 ppm precision in transit observations of several hours	Origins is currently studying the science case for transit spectroscopy and technology development needed to achieve the science goals.  Origins STDT is developing a detector technology roadmap, including mid-IR detectors with these stability requirements.  Analysis of MIRI transit spectroscopy data when JWST on-orbit performance will provide additional lessons
<b>Mid-IR Angular Resolution</b>	Cryogenic (4K), large-aperture (> 9m) telescopes to achieve high angular resolution needed to direct-image cool exoplanets in wide orbits (> 5 AU).	JWST Be mirror segments may meet requirements now, but other materials like SiC or simply aluminum may. Cryogenic low-dissipation actuators may play a role if active surface figuring is deemed necessary	Origins studying telescope technologies.  SLSTC industry study is investigating manufacturability of large cryogenic segmented mirrors
<b>Mid-IR Detection Sensitivity</b>	Low noise and detectors for the mid-infrared band (7 - 20 microns) enabling exoplanet direct imaging. noise requirements TBD, likely to be 10 x better than JWST/MIRI	JWST/MIRI's band-impurity detectors is the state of the art in this wavelength band.	OST's MISC instrument includes a coronagraph and will study sensitivity needs  JWST's performance on orbit will set the state of the art in this band.  NeoCAM is developing H2RGs with sensitivity at wavelengths as long as 12 microns.  The needs specified in OST's final report will determine the current level readiness. If improvement is needed in band-impurity-type detectors, building up an industrial base may be needed.
<b>UV Coronagraph Contrast</b>	Mirror coatings that enable high reflectivity to wavelengths as short as 90 nm while maintaining good performance in Vis/NIR band.  Coating uniformity must be good enough that polarization phase and amplitude difference < 1% between orthogonal polarization states across the whole wavelength band.	Al coating with combination of MgF <sub>2</sub> , LiF, and/or AlF <sub>3</sub> overcoat: 90-120 nm: < 50% reflectivity 120-300 nm: 85% reflectivity 300 nm-2 μm: > 90% reflectivity Polarization differences between orthogonal polarization states, uniformity, and durability of coatings on large optics is unknown. Flight: HST uses MgF <sub>2</sub> ;	HabEx and LUVOIR studies are both looking into trading ability to do coronagraphy across a wide band while maintaining UV sensitivity.  TDEM-funded study (PI Breckinridge) looking into sensitivity of polarization aberrations and possibly will set requirements from a

		85% reflectivity $\lambda > 120$ nm; 20% reflectivity $\lambda < 120$ nm	coronagraph on coating uniformity.
<b>UV Detection Sensitivity</b>	<p>Low-noise ultraviolet (200-400 nm) detectors to characterize exoplanets with an integral field spectrograph.</p> <p>Read Noise: 0 e<sup>-</sup>/resolution/s; Dark Current: 0 e<sup>-</sup>/resolution/s; Spurious Count Rate: &lt; 0.05 counts/cm<sup>2</sup>/s; QE: 75% ; Resolution size <math>\leq 10</math> nm; Tolerant to space radiation environment over mission lifetime.</p>	<p>Lab: Micro-channel Plates (MCP): 0 read noise, 90 – 300 nm, spurious count rate 0.05 - 0.5 counts/cm<sup>2</sup>/s; QE 20-45%; resolution element size 20 <math>\mu</math>m. EMCCD: 0 read noise, dark current &gt; 0.005 e<sup>-</sup>/res/hr; QE 30-50%; resol. el. size 20 <math>\mu</math>m</p> <p>Flight: HST HRC: In relevant UV band (250 nm): QE 33%, read noise 4.7 e<sup>-</sup>, dark current 5.8<math>\times 10^{-3}</math>, 1024<math>\times 1024</math> format</p>	<p>LUVOIR and HabEx studies determining whether these detectors are already good enough for their needs.</p> <p>APRA and SAT awards are advancing these detectors.</p> <p>These detectors are likely to be ready within a few years</p>
<b>Stellar Reflex Motion Sensitivity</b>	<p>Capability to measure exoplanet masses down to Earth-mass. The radial velocity semi-amplitude of a Solar-mass star due to an orbiting Earth-mass planet at 1 AU is 9 cm/s.</p> <p>Technology to make radial velocity mass measurements may include using a space-based instrument to avoid atmospheric telluric lines and simultaneous measurements of stellar lines across a broad band (both Vis and NIR).</p> <p>Theoretical understanding of astrophysical noise sources (stellar jitter) and how to mitigate them</p>	<p>Ground-based RV: state-of-the-art demonstrated stability is currently 28 cm/s over 7 hours (VLT/ESPRESSO).</p> <p>Laser frequency combs demonstrated on ground-based observatories with correct mode spacing, non-NASA work is advancing miniaturization. Fiber laser-based optical frequency combs demonstrated on sounding rocket though with closer line spacing than useful for RV.</p>	<p>NASA-chartered probe study (EarthFinder) investigating benefits of RV instrument on a space telescope.</p> <p>Ground-based RV instruments expected to achieve 20-30 cm/s single measurement precision by NN-EXPLORE's NEID instrument (WIYN telescope) and the iLocator instrument (LBT) both planned for 2019</p>
	<p>Capability to measure exoplanet masses down to Earth-mass. Astrometric detection of an exo-Earth at 10pc requires 0.1 microarcsecond uncertainty.</p> <p>Technology with the stability needed to make astrometric measurements to this level, possibly requiring detector metrology and/or diffractive pupils</p> <p>Theoretical understanding of astrophysical noise sources (star spots) and how to mitigate them.</p>	<p>GAIA preliminarily achieved 34 micro arcsecond error but ultimately could achieve 10 microarcseconds on bright targets after all systematics are calibrated</p> <p>TDEM-funded demonstration (Bendek) of diffractive pupil showed 5.75<math>\times 10^{-5}</math> <math>\lambda/D</math> or 1.4 microarcsecond on a 4m telescope (limited by detector calibration)</p> <p>Preliminary study of 1-m space telescope and instrument with in-situ detector calibration can achieve 0.8 micro arcsecond in 1 hr</p>	none

Table 3: ExEP Technology Gap List

## B VISIBLE/NEAR-INFRARED CORONAGRAPH/TELESCOPE TECHNOLOGY GAPS

Exo-Earth direct imaging and spectral characterization will require starlight suppression that exceeds the current best ground-based performances by several orders of magnitude. Coronagraphs come in numerous architectures, each with its own strengths and weaknesses with respect to telescope aperture (monolithic, segmented), pupil obscuration (unobscured, obscured by secondary mirror and its support struts), and wavefront error sensitivity (e.g. line-of-sight jitter, telescope vibration, polarization).

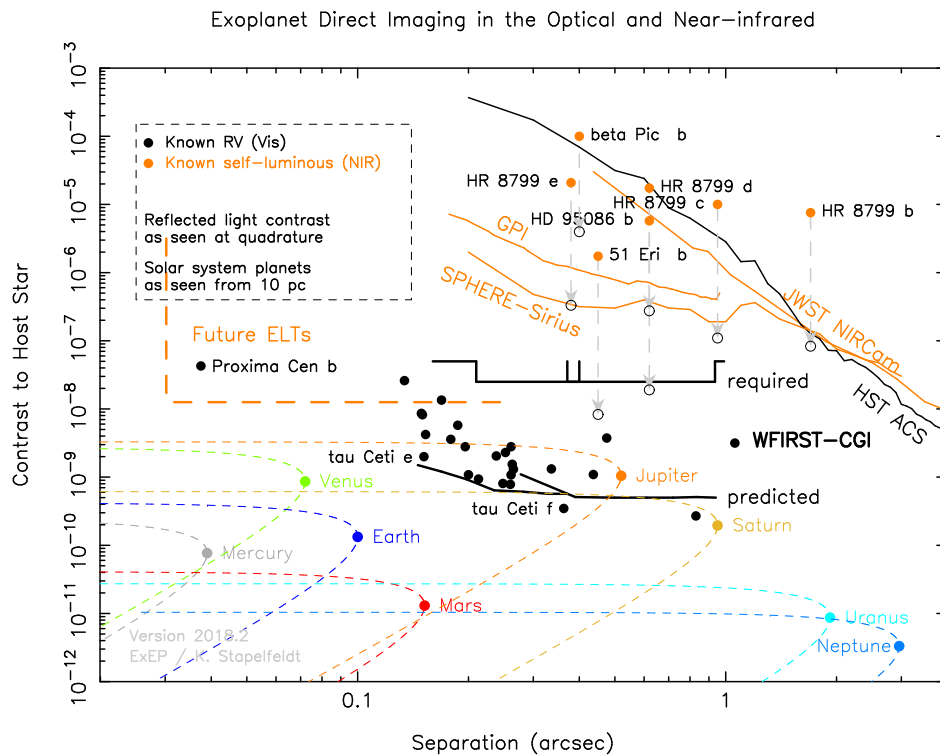


**Figure 3:** Contrast (ratio of planet brightness to host star brightness) versus apparent angular separation. The filled orange circles indicate the direct imaging of young, self-luminous planets imaged in the near-infrared by ground-based telescopes. Contrasts for the planets of the Solar System are for analogous planets placed 10 pc away. The solid black dots are contrast estimates of measured radial velocity planets, including Proxima Cen b. The orange curves show measured performance of ground-based coronagraphs. The GPI curve shows typical performance, while the SPHERE curve shows the best achieved performance to-date on Sirius. Achieved performance with HST/ACS coronagraphic masks, and the predicted performance of JWST/NIRCam masks are also shown. The predicted and required performance at 565 nm for the WFIRST coronagraph instrument (CGI) is shown as solid black curves. The “predicted” curves extending from 0.13” to 0.4” is based on performance achieved in a testbed. From 0.4” to 1”, performance is based on a coronagraph mask designed to maximize outer working angle. For consistency, the planets discovered in the near-infrared are shown with vertical arrows pointing to the predicted contrast ratios at visible wavelengths (WFIRST-CGI is expected to conduct science between 442 and 980 nm).

Residual wavefront errors that result in additional quasi-static noise on the detector (known as speckles) can be corrected with the use of an adaptive optics system: this is done through wavefront sensing and the use of deformable mirrors (Section B.1.3). As a final step, post-processing of the data images (Section B.1.4) can further improve the effective contrast.

The most important ongoing development in coronagraph technology is the baselining of a coronagraph instrument on the WFIRST space mission, as it will be the first coronagraph with wavefront control to fly in space, advancing both space and ground state-of-the-art starlight suppression. While both the Hubble Space Telescope (HST) and the JWST have onboard coronagraphs, neither have an adaptive optics system with corresponding wavefront sensing and control required to achieve better than  $10^{-8}$  contrast sensitivity and narrow inner working angles (IWA) ( $< 3 \lambda/D$ ). WFIRST will also have the first ultra-low noise visible detector and deformable mirrors to reach low-Earth orbit or beyond. **Figure 3** shows the predicted performance of WFIRST-CGI in contrast vs. angular separation.

The obscured pupil of the WFIRST telescope (due to its on-axis secondary mirror and support struts) introduces complex diffraction features that are absent in designs with unobscured pupils. Consequently, the WFIRST coronagraph architectures and optics have started the era of high-contrast/obscured pupil coronagraph design and demonstration that will serve on-axis and segmented telescope aperture designs of the future. The importance of investment by WFIRST in advancing technologies, performing systems engineering, and eventually in on-orbit demonstration is reflected in one of the seven recommendations of the National Academies' Exoplanet Science Strategy that "NASA should launch WFIRST to conduct its microlensing survey of distant planets and to demonstrate the technique of coronagraphic spectroscopy on exoplanet targets."

The ExEP Technology List (**Table 2**) targets the next-generation coronagraphs beyond WFIRST that will be capable of directly imaging exo-Earths around Sun-like stars in the solar neighborhood. As mentioned earlier, the list of coronagraph technologies have been broadened to include more of the telescope system since all contributing noise sources must be accounted for if contrasts of  $10^{-10}$  are to be reached at  $10^{-11}$  stability levels. The coronagraph can no longer be considered just a payload instrument designed in isolation of the observatory.

The coronagraph technologies listed in **Table 2** address four technology gaps shown in Figure 4 and listed in Table 3:

1. **Contrast (Section B.1)** – the ability to block the on-axis light from a target star creating a dark region in the science focal plane where the faint off-axis reflected light of a planet could be detected. Technologies listed by ExEP to close this gap are Coronagraph Demonstrations and Modeling (CG-2; Section B.1.2), Deformable Mirrors (CG-3; Section B.1.3), and Data Post-processing Algorithms and Techniques (CG-4; Section B.1.4).
2. **Contrast Stability (Section B.2)** – the ability to sense and control the incoming starlight maintaining the desired contrast long enough for full science integration. The technologies listed by ExEP that address this gap are Mirror Segment Phasing Sensing and Control (CG-6; Section B.2.2), Telescope Vibration Sense/Control or Reduction (CG-7; Section B.2.3), and Wavefront Sense/Control (CG-5; Section B.2.1).
3. **Detection Sensitivity (Section B.4)** – the ability to detect extraordinarily few photons dispersed across many pixels of a spectrograph and not be limited by the detector's efficiency or intrinsic noise properties. The technologies on ExEP's list that address this missing capability are Ultra Low-Noise Visible-band Detectors (CG-9; Section B.4.1) and Ultra Low-Noise Near-Infrared Detectors (CG-8; Section B.4.2).

4. **Angular Resolution (Section B.3)** – the ability to probe terrestrial regions around stars (e.g., the habitable zone) requires a minimum aperture size. The more distant the star, the larger the telescope aperture needed to probe these regions. Large apertures provide not just improved angular resolution but also improved sensitivity to faint objects (sharper point spread functions), higher throughput, lower integration times, better isolation of an exoplanet from diffuse exozodi background, and the capability to probe habitable zones of stars further away. The technology listed by ExEP to close this gap is Large Aperture Primary Mirrors (CG-1; Section B.3.1).

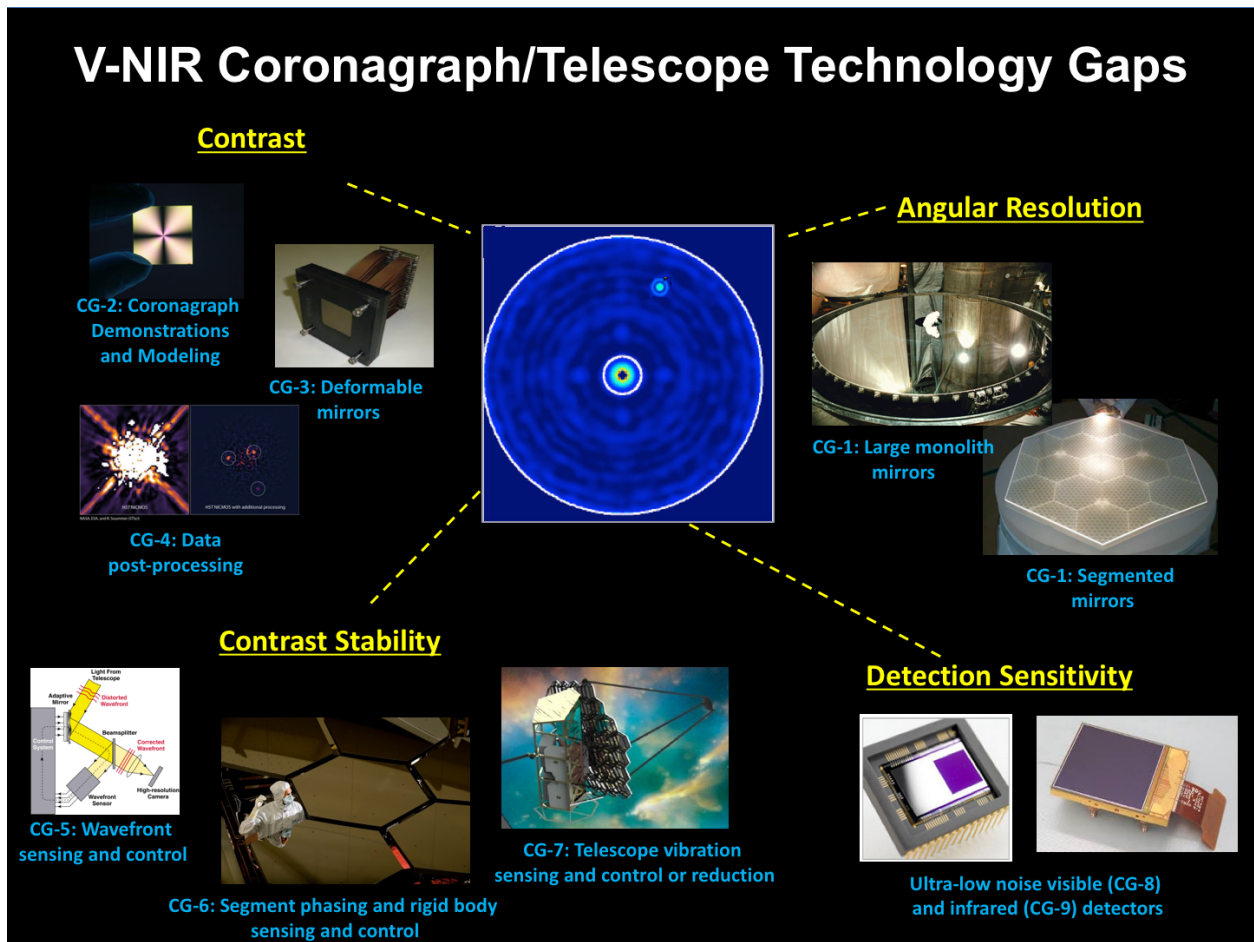


Figure 4: The four Visible-band and Near-Infrared Coronagraph Technology Gaps (in yellow font) to directly image and characterize exo-Earths around Sun-like stars and the candidate technologies for closing the gaps.

### B.1 Contrast

Specialized coronagraph optics suppress on-axis starlight and allow the off-axis planet light to transmit through the instrument achieving the high contrast detection of the planet with respect to its host star. A continuing program to advance the performance of masks, apodizers, and beam-shaping optics, as well as to actively control wavefront error, to exceed WFIRST coronagraph performance requirements ( $< 10^{-8}$ ,  $3 \lambda/D$ , 10% bandwidth) is needed. This should include designs to improve inner working angles ( $< 3 \lambda/D$ ), contrast performance ( $< 10^{-9}$ ),

bandwidth ( $\geq 10\%$ ), and core PSF throughput ( $\geq 10\%$ ), in dynamic vacuum environments on both obscured and segmented apertures.

Coronagraphs using a variety of architectures have achieved contrasts in laboratory tests that begin to approach these requirements.<sup>16</sup> Demonstrated state-of-art results with unobscured pupils at 10% bandwidths are shown in **Figure 5**; **Figure 6** shows contrast demonstrations at a variety of bandwidths. The deepest narrowband (2% bandwidth) simulated starlight suppression achieved is  $1.2 \times 10^{-10}$  raw contrast at 800 nm across angles of  $3-16 \lambda/D$ . It was demonstrated in the HCIT with a Hybrid Lyot Coronagraph (HLC) linear mask on an unobscured pupil in a static vacuum lab environment.<sup>17,18,19</sup>

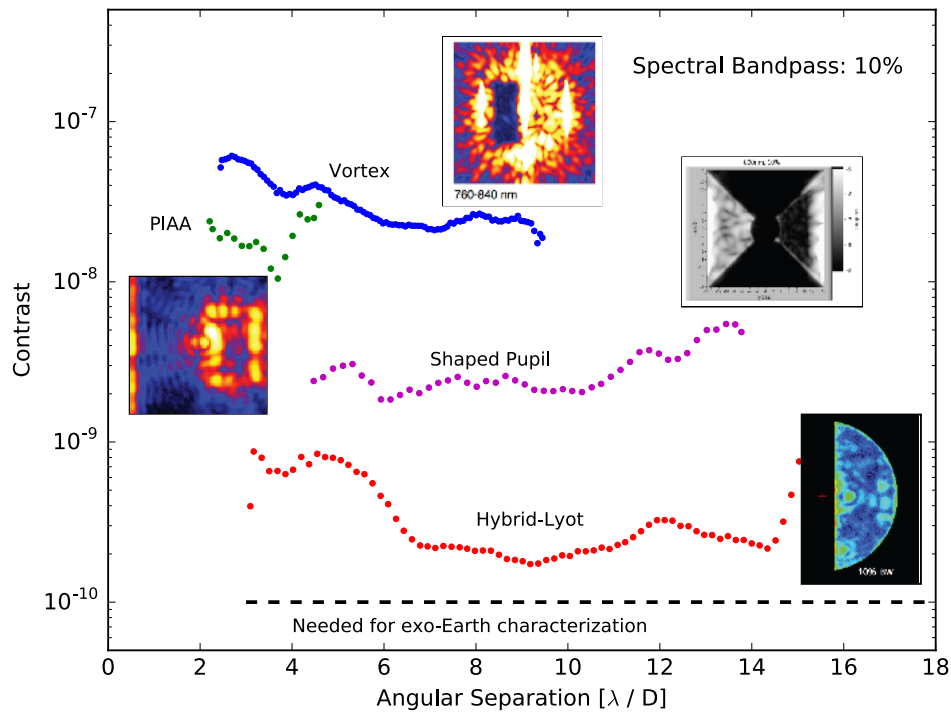


**Figure 5:** Coronagraph laboratory demonstrations using 10% bandwidth visible light. Adapted from Lawson et al (2013)

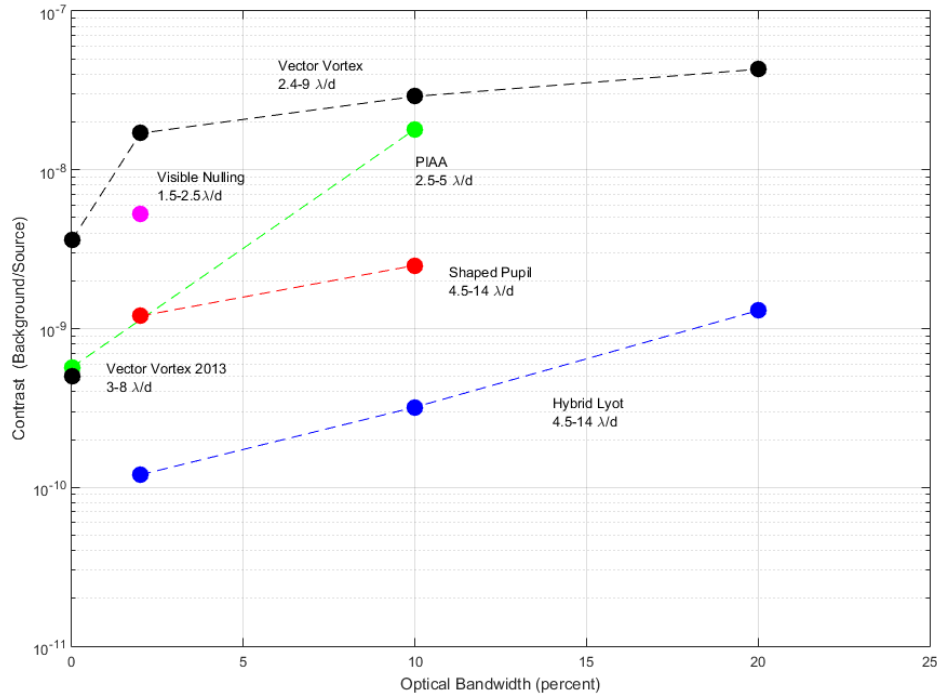


**Figure 6:** Demonstrated coronagraph contrast as a function of bandwidth. All experiments were conducted with unobscured pupils and demonstrated in vacuum chambers under static environment conditions at 800 nm to near-infrared light.

### B.1.1.1 Decadal Survey Testbed

In anticipation of coronagraph demonstrations at  $10^{-10}$  contrast to support large monolithic and segmented telescopes of the future, the ExEP is upgrading one of the High Contrast Imaging Testbeds (HCIT) and vacuum chambers at JPL, building a new testbed to further reduce the noise floor that limits  $10^{-10}$  contrast levels. The new testbed, the Decadal Survey Testbed, has been designed from the ground up to minimize testbed jitter, improve thermal stability, and minimize stray light. In 2018 the testbed was assembled and inserted into the vacuum chamber with a commissioning Lyot coronagraph (this architecture is the laboratory state-of-the-art at 10% bandwidth). As of February 2019, the testbed has demonstrated  $4.5 \times 10^{-10}$  raw contrast averaged over an annular dark hole extending from 3 to 8  $\lambda/D$  and at 10% bandwidth.

Once the  $10^{-10}$  raw contrast milestone is achieved (or testbed limits identified), another coronagraph architecture, a segmented pupil mask, could be inserted to demonstrate static performance of a simulated off-axis segmented telescope such as LUVOIR's architecture B. The subsequent step planned for 2020 could be the addition of a disturbance source to produce a "dynamic" demonstration as well as including a wavefront sensor to correct the wavefront error due to the disturbance. "Static" demonstration here and throughout implies no intentionally introduced line-of-sight errors or other wavefront disturbances, while "dynamic" refers to the experiments where at least some of these disturbances are deliberately introduced into the testbed and the coronagraph is required to sense and compensate for them.

The ExEP will work and consult with other coronagraph testbeds<sup>20</sup> operating in ambient conditions in potentially advancing coronagraph performance from mid-contrast to high-contrast demonstrations. Examples are the HiCat facility at the Space Telescope Science Institute (PI Rémi Soummer), the High Contrast High-Resolution Spectroscopy for Segmented Telescopes Testbed at Caltech's Exoplanet Technology Lab (PI Mawet) and the Ames Coronagraph Experiment testbed at NASA ARC (PI Belikov).

### B.1.2 CG-2: Coronagraph Demonstrations and Modeling

#### CG-2: V/NIR Coronagraph Demonstrations and Modeling

**Description:** The ExEP seeks demonstrations of coronagraph architectures that achieve the necessary contrast, inner working angle, throughput, and bandwidth to directly image and spectrally characterize rocky exoplanets orbiting in the habitable zone of Sun-like stars.

**SOA (Lab):**  $6 \times 10^{-10}$  raw contrast at 10% bandwidth across angles of 3-15  $\lambda/D$  demonstrated with a linear mask and an unobscured pupil in a static vacuum lab environment (Hybrid Lyot) at 700 nm.

$< 1.6 \times 10^{-9}$  raw contrast at 10% bandwidth across angles of 3-9  $\lambda/D$  demonstrated with a circularly-symmetric mask and obscured pupil in a static vacuum lab environment (WFIRST)

**SOA (Flight):**  $10^{-4}$  raw contrast 540 nm at 10  $\lambda/D$  (HST)

**Needed capability:** Coronagraph masks and optics capable of creating circularly symmetric dark regions in the focal plane enabling raw contrasts  $\leq 10^{-10}$ , with minimal contribution from polarization aberration, IWA  $\leq 3 \lambda/D$ , throughput  $\geq 10\%$ , and bandwidth  $\geq 10\%$  on obscured and segmented pupils in a simulated dynamic vacuum environment.

**Supported Missions or Mission Concepts:** WFIRST, LUVOIR, HabEx

#### Current State-of-the-Art:

Demonstrated coronagraph contrast results with unobscured apertures as a function of optical bandwidth are shown in **Figure 6**. Pupil obscurations in on-axis designs (stemming from the secondary mirror and its structural supports) and mirror segmentation further diffract light making deep contrasts more challenging. Resolved angular star sizes due to the larger telescope diameters under consideration provide another level of difficulty for coronagraphs. The WFIRST-CGI has demonstrated  $1.6 \times 10^{-9}$  raw contrast at 10% bandwidth across angles of 3-9  $\lambda/D$  with a circularly-symmetric mask on their highly obscured pupil, in a static vacuum lab environment. Deep-contrast coronagraphs for systems with pupil obscurations and segmentation can be designed in general, but at the expense of throughput and degraded signal-to-noise ratio in the image plane.

#### Progress Over the Last Year:

##### WFIRST

The WFIRST-CGI continued to advance its dual Hybrid Lyot and Shaped Pupil Coronagraphs. In 2018, the Baseline Technology Requirements were defined and reviewed at a Systems Requirement Review<sup>21</sup> and formally entered Phase B.

The CGI performed high contrast tests of the disk science mask set for the Shaped Pupil Coronagraph<sup>22</sup> and has demonstrated an average of  $3 \times 10^{-9}$  contrast in an 360-degree annular dark zone 6.3 - 19.5  $\lambda/D$  in a 10% band centered at 565nm.

The Hybrid Lyot coronagraph in CGI has been demonstrated in a dynamic environment in flight-like stellar flux conditions<sup>23</sup> demonstrating the ability to sense and compensate for flight-like pointing and focus disturbances while observing the equivalent of a 5<sup>th</sup> magnitude star.

##### Segmented Coronagraph Design and Analysis

To meet the challenge of segmented and obscured aperture coronagraphy, the ExEP's Segmented Coronagraph Design and Analysis (SCDA) study continued funding several groups to design and model different coronagraph architectures that enable  $10^{-10}$  contrast sensitivities with throughput and robustness to many wavefront errors. The SCDA teams have worked with the LUVOIR design study team to include both the 15 m LUVOIR-A and the 8 m LUVOIR-B

apertures. Robustness calculations will determine the sensitivities of these coronagraph designs to the effects of optical misalignments, and help to establish error budgets. How these error budgets translate to sensing and control of the wavefront errors through mechanical movements will be a critical question for the future of these architectures.

The team has found designs that achieve the needed performance with an Apodized Pupil Lyot Coronagraph (APLC) are the most successful to-date. In addition to the AP LC, designs based on Hybrid Lyot and Vortex designs also meet  $10^{-10}$  contrast requirements with reasonable throughput and sensitivities. While developing the designs, key lessons about the size of the obscurations and the layout of telescope segments were learned and have influenced the design of the LUVOIR coronagraph concept. Other approaches, such as the use of deformable mirrors to correct the diffraction pattern from the segmentation pattern were explored.<sup>24</sup> A fast coronagraph design code (FALCO) was developed at JPL and released to the public in 2018.<sup>25</sup>

Science yield, given assumptions about an exo-Earth direct imaging mission, was established as a metric for coronagraph performance as part of the SCDA study. The contrast and throughput of coronagraph designs resulting from SCDA work were used in a common yield model and will be presented in a forthcoming publication.<sup>26</sup>

Robustness to segment-to-segment phasing errors is under study. The ExEP's SCDA study is planned to continue advancing design for coronagraphs that work with segmented apertures through at least September of 2019.

### **Decadal Survey Testbed**

In 2018, the newly designed optical testbed (the Decadal Survey Testbed; see Sect. B.1.1.1) was assembled and initially tested in vacuum tank HCIT-2. Phase 1 of the DST commissioning includes a Lyot coronagraph with a clear (unobscured monolithic) pupil; as of February 2019, initial tests were demonstrating  $4.5 \times 10^{-10}$  contrast over a 10% band averaged over an annular dark hole between 3 and  $8 \lambda/D$ . Phase 2 will include a segmented (though static) pupil mask in 2019. Phase 3 (scheduled for 2020) will aim to demonstrate exo-Earth levels of contrast while correcting for wavefront errors expected from segment-to-segment relative piston/tip/tilt. In this phase, the team will implement a high-order wavefront sensor (HOWFS) similar to the one described in Moore and Redding (2018)<sup>27</sup>. The HOWFS can be used to sense and correct dynamic wavefront errors on many temporal and spatial frequencies and will become part of the ExEP-managed facility.

### **Large Mission Concept Studies**

The LUVOIR and HabEx concept studies developed baseline coronagraph designs in preparation for delivering interim reports in 2018. The coronagraph instrument for LUVOIR's architecture A (a telescope with a 15 m primary mirror), ECLIPS, includes a baseline AP LC appropriate for the telescope's segmented 15 m primary mirror and obscuration by the secondary mirror and supports. ECLIPS includes near-UV, visible band, and near-IR channels with integral field spectrograph modes. LUVOIR's architecture B (an off-axis telescope with an 8 m segmented primary mirror) includes a charge-6 vortex coronagraph.

The HabEx mission's initial telescope architecture includes an off-axis 4 m telescope (and thus a clear pupil), supporting a coronagraph with a charge-6 vortex mask, providing robustness to low-order wavefront error modes.

The Origins Space Telescope concept study's interim report includes an optional concept with a coronagraph designed for direct imaging of Saturn and Jupiter analogs at mid-infrared wavelengths. These technologies require specific optimization for longer wavelengths (such as cryogenic operability) but the maturation of UV/O/IR coronagraph technology may be applicable for longer wavelengths as well (see Sect. D for more detail about mid-IR coronagraph technology).

### **TDEMs**

Jim Breckinridge and Russell Chipman's TDEM-15 work is investigating the role of polarization in coronagraphy, calculating the polarization-related degradation of performance for WFIRST, HabEx, and LUVOIR coronagraphs. While polarization effects have not been a limiting factor in laboratory demonstrations approaching  $10^{-10}$  contrast ratio sensitivities, when coupled with telescopes, polarization-induced wavefront aberrations may potentially limit a coronagraph's starlight suppression performance<sup>28,29</sup> This TDEM team launched an effort to model the WFIRST, HabEx, and LUVOIR fore-optics. Using their customized vector ray trace code POLARIS-M, the investigators so far are seeing close agreement with the standard modeling tools. Demonstrations of a vortex coronagraph in the HCIT-2, funded by the Serabyn TDEM-14 award, continued in 2018. The tests have thus far achieved monochromatic contrast of  $5 \times 10^{-10}$  at 785 nm, and  $10^{-8}$  for a 10% band centered at 575 nm for a charge-4 vortex coronagraph averaged across angles of  $3-8 \lambda/D$ .<sup>30</sup> Future demonstrations will also include higher charge vortex masks to improve contrast performance.

A Phase-Induced Amplitude-Apodized/Complex Mask Coronagraph (PIAACMC) design funded by the Belikov TDEM-16 award is currently being assembled in HCIT-2 with testing planned for 2019.

### **Next Steps:**

A gap remains between present capabilities and the needed demonstration of a  $10^{-10}$  contrast ratio visible band coronagraph at  $3 \lambda/D$  inner working angle and 10% bandwidth. A number of activities in modeling, mission concept studies, and laboratory demonstrations continue to work towards this goal and to the eventual maturing of coronagraph technology for infusion into a flight mission.

Prior to delivering their final reports in mid-2019, the HabEx and LUVOIR mission concept studies are further refining their science case and performing preliminary trades at the system level that will help to better define the coronagraph mask and optical layout needs for future exo-Earth-finding missions.

Advances in coronagraph modeling will continue in order to help understand laboratory demonstrations and to perform design work. The SCDA study will continue through 2019, with work focused on robustness of the leading designs for the initial set of SCDA apertures and coordination with the LUVOIR team's selection of large segmented mirror apertures. The TDEM-15 Breckinridge polarization modeling effort will deliver a Final Report assessing

polarization effects and recommending mitigation strategies for HabEx and LUVOIR or other potential exo-Earth missions.

The HCIT will continue to advance the state-of-the-art in laboratory demonstrations. The Serabyn TDEM-14 effort will continue vacuum tests in HCIT in 2019, first aiming for  $10^{-9}$  contrast with a charge-4 mask and later including a charge-6 vortex mask similar to the mask baselined by HabEx. Demonstrations of PIAACMC (PI Belikov, NASA/Ames) and next-generation Lyot coronagraphs (PI Trauger JPL/Caltech) funded by TDEM-16 awards are expected by late 2019 in HCIT. The DST will continue its commissioning tests and will be used as soon as 2019 for TDEM-funded demonstrations.

Three new TDEM efforts were awarded in 2018 to continue to advance the state-of-the-art for coronagraph contrast demonstrations. A TDEM-17 (PI Soummer, STScI) was awarded to advance APLC architecture, and another TDEM-17 (PI Serabyn, JPL/Caltech) was awarded to develop a next-generation vortex coronagraph that can achieve high contrast with segmented/obscured pupils and demonstrate it in HCIT. An additional TDEM-17 (PI Guyon, Arizona) will investigate wavefront control techniques to maintain deep contrast using speckle information outside of the dark hole. Milestone Whitepapers defining the scope of work of these TDEMs will be available in early 2019.

### B.1.3 CG-3: Deformable Mirrors

#### CG-3: Deformable Mirrors

**Description:** Flight-qualified large-format deformable mirrors and their electronics capable of achieving and maintaining  $10^{-10}$  contrast performance.

**SOA (Lab):** Electrostrictive 64×64 actuator DMs have been demonstrated to meet  $\leq 10^{-9}$  contrasts and  $< 10^{-10}$  stability in a vacuum environment and 10% bandwidth; 48×48 actuator DM passed random vibrate testing

**SOA (Flight):** None

**Needed capability:** 4 m primary mirror:  $\geq 96 \times 96$  actuators; 10 m primary mirror:  $\geq 128 \times 128$  actuators. Enable raw contrasts of  $\leq 10^{-9}$  at  $\sim 20\%$  bandwidth and IWA  $\leq 3 \lambda/D$ . Flight-qualified device and drive electronics (radiation hardened, environmentally tested, life-cycled including connectors and cables). Mirror stability maintains  $10^{-10}$  contrast for observation time scales.

**Supported Missions or Mission Concepts:** WFIRST, LUVOIR, HabEx

High-contrast coronagraphs depend critically on deformable mirrors (DMs) to (1) create dark regions by compensating for surface and coating irregularities on the telescope primary mirror, and (2) maintain the dark region (stability). DMs maintain stability of the coronagraph dark region by correcting wavefront errors due to the relatively slow thermal drifts that the observatory will experience in its orbit during science observations. Additionally, in some cases, the DMs can be pre-shaped to work in concert with the coronagraph masks to mitigate the diffraction effects of obscured apertures.<sup>31,32</sup>

#### Current State-of-the-Art:

The WFIRST coronagraph will use two 48×48 element electrostrictive lead magnesium niobate (PMN) DMs made by Adaptive Optics Associates Xinetics in Devens, MA, a subsidiary of Northrop Grumman. These mirrors have been routinely used in the HCIT vacuum testbeds since 2003. With a 500  $\mu\text{m}$  actuator stroke and 1 mm pitch sizes, they have participated in all the HCIT demonstrations better than  $10^{-9}$  with unobscured pupils. These DMs are built up from electro-ceramic blocks with actuators separated by 1 mm (see **Figure 7**). These blocks are

assembled into modules covered by a single-mirror facesheet and driven by a Gen 5 vacuum compatible voltage supply (not multiplexed) with 100 V range and 16-bit resolution. One Xinetics DM has already successfully undergone a 3-axis random vibration test to 10.8 g rms.

Alternative DMs include MEMS devices, such as those fabricated by Boston Micromachines Corp (BMC). These DMs are made of a polysilicon membranes coated with one or more layers for the reflective surface and are actuated by 32×32 or 64×64 electrostatic actuators on the backside. BMC offers both continuous face-sheet and segmented mirrors. Pitch sizes come less than 0.5 mm and maximum stroke is about 5 μm for 250 V drive voltage. These mirrors are currently considered as a backup for the WFIRST coronagraph.

Iris AO DMs are MEMS devices with three electrostatic actuators underneath a segmented mirror surface. The three actuators provide piston, tip, and tilt to a segment. The hexagonal segments are 700 microns wide, vertex to vertex. The actuators are long stroke (8 μm or 5 μm, depending on the model) over 200 V. As of this writing, Iris AO has ceased operations.

### **Progress Over the Last Year:**

The pre-environmental characterization of BMC MEMS deformable mirrors was carried out in the Vacuum Surface Gauge testbed at JPL in 2017. The mirrors were shown to hold a flat surface to better than 1 nm rms over several days. These mirrors were exposed to a random vibration environment commensurate to the Delta-IV launch vehicle planned to carry WFIRST. These DMs are expected to be characterized post-environment testing in early 2019 to evaluate changes in surface figure and actuator performance.

MEMS deformable mirrors, for the first time in the ExEP HCIT, were used in the Serabyn TDEM vortex coronagraph experiments to achieve high-contrast imaging. Contrasts of  $1.3 \times 10^{-8}$  were achieved setting a world record for coronagraphy using MEMS DMs.<sup>33</sup>

Development of a new MEMS DM began as an APRA- and SBIR-funded collaboration between Microscale, Inc and JPL. The Microscale DM is directly mounted on an ASIC in order to enable multiplexing of the large number of interconnects, potentially a path towards miniaturization.

### **Next Steps:**

Future DM needs for larger space telescopes such as HabEx or LUVOIR will include larger format sizes and improved stability with interest in longer stroke and tighter pitch sizes. Larger format DMs allow for larger outer working angles for debris disk science as well as probing the closest exoplanetary systems. Format needs for 4 m-class telescopes may be 96×96 actuators and 10 m-class telescopes may even request 128×128 actuators or larger. Larger Xinetics DMs have been built through mosaicking smaller units. A 64×64 actuator device has operated successfully in the HCIT for over a decade. This larger format was achieved by mosaicking four 32×32 ceramic blocks. A 66×66 unit has also been mosaicked from 11×11 units for the Palm 3000 adaptive optics system at the Palomar Observatory. It is expected that the same technique could be used to meet future large format DM needs although no investments have been made.

While increasing the actuator count of DMs is straightforward, with mosaicking in the case of electrostrictive DMs and with scaling of the wafer design for MEMS, handling the enormous

number of interconnects and the drive electronics channels remains a challenge. Increasing the actuator count of MEMS DMs creates the additional challenge of close-packing large numbers of wire bonds, a subject of APRA- and SBIR-funded investigations that will continue in 2019.

Drive electronics with higher resolution (but flight qualified) digital-to-analog converters (18 bit) will eventually be needed so as to enable finer control (sub-nm) of the actuator motion.

Deformable mirrors with a parabolic shape will be investigated under a directed work package awarded by APD to NASA Goddard Space Flight Center (PI Tyler Groff); this concept potentially can reduce mass and complexity of space coronagraphs by combining the function of off-axis paraboloids and deformable mirrors into a single optical element.

WFIRST will also help advance the DM state-of-the-art over the next few years. Expected activities include:

- Stability measurements of DMs
- Flight qualifying the drive electronics
- Redesigning the electronic interconnects to the actuators
- Miniaturizing the drive electronics
- Improving the facesheet surface figure error so as to gain more stroke
- Life test the DM actuators
- Complete environment testing including thermal, dynamic, and radiation testing

There is interest in smaller pitch sizes ( $< 1$  mm) for future large aperture telescopes to reduce the size of the optical beam and hence, the mass and volume of the optics. Also potentially of interest are in larger stroke ( $> 500$  nm) devices.

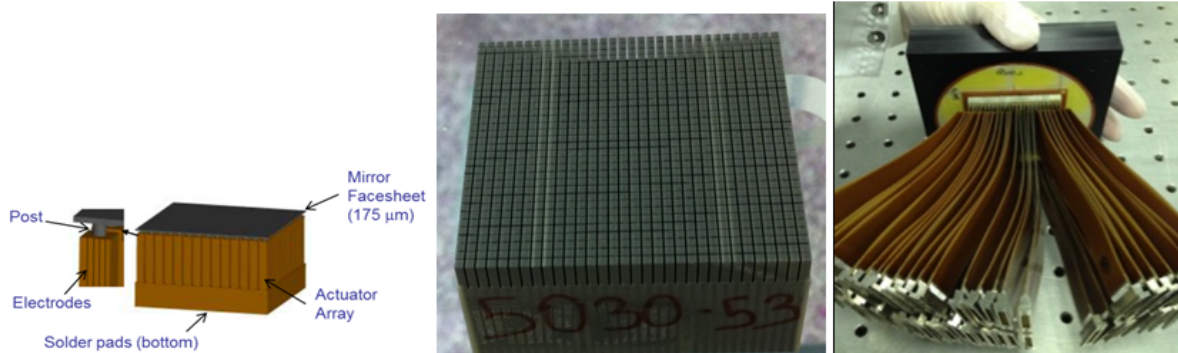


**Figure 7:** (Left) Schematic of the bulk ceramic block with cut actuators mounted to a facesheet. (Center) Bulk block with 1 mm cut posting actuators. (Right) Connector cables extending from the back of the DM.

DEMI, a MIT-led cubesat project that will achieve on-orbit demonstration of active wavefront control with a BMC MEMS DM, passed Preliminary Design Review (PDR) in 2017 and aims for a launch in the next several years.<sup>34</sup>

### B.1.4 CG-4: Data post-processing Algorithms and Techniques

#### CG-4: Data Post-Processing Algorithms and Techniques

**Description:** Data post-processing techniques to remove residual speckle noise at the focal-plane detector further improving contrast sensitivity.

**SOA:** Few 100× speckle suppression has been achieved by HST and by ground-based AO telescopes in the NIR and in contrast regimes of  $10^{-4}$  to  $10^{-5}$ , dominated by phase errors.

**Needed capability:** A 10-fold contrast improvement in the visible from  $10^{-9}$  raw contrast where amplitude errors are expected to be important (or a demonstration of the fundamental limits of post-processing)

**Supported Missions or Mission Concepts:** WFIRST, LUVVOIR, HabEx

The removal of quasi-static speckle noise from imagery data using post-processing techniques can further improve the final contrast and inner working angle capabilities achieved by coronagraphs. Counting on an order of magnitude improvement in the final contrast may loosen both wavefront control and telescope stability requirements needed for raw contrast. Some post-processing techniques require angular diversity by rolling the instrument (and spacecraft) azimuthally with respect to the star, or rely on observing a reference star. The specifics of the post-processing technique, however, levy operational requirements and calibration requirements on the spacecraft system and need to be understood from the system level early in the design process.

#### Current State-of-the-Art:

Remi Soummer et al.<sup>35</sup> applied ground-based techniques to HST NICMOS data and achieved signal-to-noise (SNR) improvements of 100 times for data with an initial contrast of  $10^{-5}$  in the near-infrared. The use of similar techniques to improve contrast in the visible has also been achieved with HST STIS [<https://arxiv.org/abs/1709.10125>], and is under study via simulations in the WFIRST CGI technology development program. Initial results are promising with expected contrast improvement of 5 to  $10^{36, 37}$  for initial contrasts of around  $10^{-9}$  to  $10^{-8}$ , depending on angular separation and the actual post-processing method. However, it is important to note that such post-processing improvements are only obtained in the speckle noise-limited regime, i.e. when shot noise is negligible compared to speckle noise.

#### Progress Over the Last Year:

Zimmerman, Pueyo, and Soummer (2017) demonstrated a principal component separation-based algorithm using WFIRST CGI lab data to remove speckles by reference differential imaging. This is an important milestone since this dataset is the first one for which the amplitude and phase errors are of the same magnitude. The algorithm consistently performed a factor of 3-5 better than simple PSF subtraction. Importantly, they showed that frame-to-frame absolute speckle stability does not by itself determine the post-processing gain. Even when the images become uncorrelated, the diversity of a reference library captured over a long-time baseline can recover the post processing gain observed with highly stable images.

#### Next Steps:

New WFIRST CGI lab data sets will be acquired with a lower flux light source consistent with a typical target star in order to test the interaction of post-processing algorithms with Poisson noise. Post-processing tests will also continue on numerically simulated WFIRST CGI data sets.

The new simulated data will make use of revised coronagraph mask designs, and for the first time will include the effects of pointing jitter, wavefront jitter, and pupil shear errors. Together these efforts will lead to more realistic predictions of contrast gain as the coronagraph instrument is assembled and closer to its final flight design conditions (spectral bandwidth, dynamical perturbations, etc.).

Beyond WFIRST, at the  $10^{-10}$  contrast levels required for exo-Earth detection, it remains to be seen whether speckle noise will be detected at high enough signal-to-noise relative to statistical photon and detector noise, for post-processing algorithms to be able to remove it with enough precision to make significant contrast gains. Characterization of speckle patterns in  $10^{-10}$  coronagraphs should be performed and prospects for their removal should be investigated once PI-led lab demonstrations are meeting this contrast performance.

Algorithms that take advantage of deformable mirror modulation (Coherent Differential Imaging) need to be investigated since they can potentially reduce stability requirements to an even greater extent than what has been demonstrated on the WFIRST CGI testbed data/simulations.

## B.2 Contrast Stability

A coronagraph must maintain its contrast performance long enough to directly image or spectrally characterize a planet. For a system required to achieve contrast sensitivities of  $10^{-10}$ , this places challenging requirements on the telescope system's overall wavefront error stability in the presence of thermal and mechanical disturbances: depending on the system architecture, this can be on order of 10 to 100 pm wavefront error stability over a control loop step (typically 10 minutes). This ambitious stability requirement can be met by designing a telescope and coronagraph with three goals in mind: robustness to disturbance, passive stability, and active control where needed. The technologies listed by the ExEP that address this gap are Mirror Segment Phasing Sensing and Control (CG-6; Section B.2.2), Telescope Vibration Sense/Control or Reduction (CG-7; Section B.2.3), and Wavefront Sensing and Control (CG-5; Section B.2.1).

Because their primary science goals include direct imaging and characterization of exo-Earths, both the LUVOIR and HabEx mission concepts are focusing their system architecture studies on the ability of the overall system to achieve pm-class wavefront error stability through detailed error budgeting. These architectures are advancing rapidly and use multiple levels of disturbance reduction, passive isolation and active control.<sup>38,39,40,41</sup>

While the individual components are needed, subsystem performances are inter-dependent and can be traded between each other. Therefore, a systems-level view is particularly interesting. In addition to systems level demonstrations and assessments, ExEP is interested in the maturation of specific subsystem and component technologies that contribute to the required overall system stability, as long as they can be shown to be applicable to a wide range of architectures.

The NASA Astrophysics Division funded two industry-led studies in 2018 for one-year evaluations of segmented mirror space telescope systems through modeling and associated testbed demonstrations. These studies are expected to return final reports in 2019 including technology gap lists. Phase II of this program will solicit additional proposals (as soon as fall 2019) to advance technologies identified in Phase I.

### B.2.1 CG-5: Wavefront sensing and control

#### CG-5: Wavefront Sensing and Control

**Description:** Sensing and controlling line-of-sight jitter and low-order wavefront drift

**SOA (Lab):** < 0.5 mas rms per axis LOS residual error demonstrated in lab with a fast-steering mirror attenuating a 14 mas LOS jitter and reaction wheel inputs; ~12 pm rms sensitivity to focus (WFIRST)

**SOA (Ground):** Higher low-order modes sensed to 10–100 nm WFE rms on ground-based telescopes

**SOA (Flight):** None

**Needed capability:** Sufficient fast line-of-sight jitter (< 0.5 mas rms residual) and slow thermally-induced WFE sensing and control ( $\leq 10$  pm rms sensitivity) to maintain closed-loop <  $10^{-10}$  raw contrast with an obscured/segmented pupil and simulated dynamic environment.

**Supported Missions or Mission Concepts:** WFIRST, LUVOIR, HabEx

A coronagraph removes starlight diffraction (e.g. Airy rings) and can remove any other starlight leak that is static and known a priori. However, random diffraction speckles (static, quasi-static, and dynamic) remain, and may limit contrast to  $10^{-6}$  to  $10^{-4}$  levels depending on the optical component quality. An adaptive optics (AO) system is necessary for reaching and maintaining the contrast levels needed for exo-Earth imaging. High contrast AO for space missions is typically accomplished by using a focal-plane based Wavefront Control (WFC) system in order to avoid non-common path errors. A DM is used to provide the necessary measurement diversity in focal-plane images as well as to subsequently remove the speckles. To handle wavefront error instabilities on faster time scales, a low- or mid- spatial frequency wavefront sensor can be used, feeding back to the DM. Faster wavefront control of tip/tilt aberrations due to telescope jitter can be achieved with a fast steering mirror.

An additional need is the ability to suppress starlight from a close companion star. This light will be incoherent with light from the target star and thus not suppressible with standard wavefront control algorithms. Many non-M-dwarf stars are in multiple-star systems, thus this capability enlarges the number of stellar systems available for direct imaging observations. Another particularly important binary system is Alpha Centauri, which is 2.4 times closer than any other Sun-like star.

#### Current State-of-the-Art:

The WFIRST coronagraph's Low-order Wavefront Sensing and Control (LOWFS/C) system represents the state-of-the-art for both ground and space systems. It was designed to suppress expected dynamic wavefront error drifts due to thermal and mechanical disturbances, such as vibrations from spacecraft reaction wheels. The WFIRST LOWFS/C consists of a Zernike wavefront sensor which samples on-axis light rejected by the coronagraphic masks. The sensor reads out at high speeds ( $\sim 500$  Hz) and a control system then feeds back to a deformable

mirror and to a fast steering mirror. WFIRST demonstrated in early 2017<sup>42</sup> a coronagraph contrast better than  $10^{-8}$  at working angles from 3 - 9  $\lambda/D$  using the LOWFS/C system in the presence of a WFIRST-telescope-like thermal and mechanical disturbances. The demonstration achieved focus control to 12 pm rms and line-of-sight jitter of 14 mas rms was suppressed to 0.5 mas rms.

To handle binary (or multiple) star systems, a technique called "multi-star wavefront control" has been demonstrated in the lab.<sup>43</sup> This technique does not in principle need any changes in hardware of existing space mission designs like WFIRST, LUVOIR, and HabEx.

### Progress Over the Last Year:

WFIRST-CGI has demonstrated contrast performance in a dynamic environment using realistic low light. A simulated magnitude 3 star was used to perform Electric Field Conjugation (focal plane-based wavefront sensing and control to create the high contrast zone), while the LOWFS was correcting disturbances, then using LOWFS to dynamically correct disturbances using a magnitude 5 star equivalent.<sup>44</sup>

As part of their coronagraph and telescope system designs, the LUVOIR and HabEx mission concepts are investigating the necessary spatial and temporal needs for wavefront stability. Dustin Moore and Dave Redding (2018) proposed a nonlinear Zernicke Wavefront sensor concept<sup>45</sup> that may provide the necessary capability. The Decadal Survey Testbed (see Sect. B.1.2) will include this capability in 2020.

A SAT/TDEM 2017 award (PI Olivier Guyon) will investigate a technique called Linear Dark-field Control<sup>46</sup> the use of brighter speckles outside the region of very high contrast to feed back to the deformable mirror wavefront errors changing on faster time scales and higher order spatial frequencies.

### Next Steps:

A remaining challenge is the achievement of fast wavefront control in the presence of realistically low light levels, and also control of higher order Zernike modes, directions to be investigated by the WFIRST-CGI project. Existing systems are believed to still be orders of magnitude away from fundamental limits of algorithm efficiency and can thus be significantly improved in terms of speed. Additionally, the polarization aberrations induced by the relatively fast primary and secondary mirror optics will be simulated in future CGI demonstrations. Other areas of improvement include achieving control in a wider wavelength band, in combining off-axis wavefront control with on-axis wavefront control to improve the coronagraph sensitivity to line-of-sight jitter, at even deeper contrasts, and in multiple polarization channels.

While the WFIRST LOWFS/C system has achieved pm-class measurement sensitivity to low order wavefront errors, systems level assessments by HabEx and LUVOIR are investigating the higher-order sensing and control needs of the telescope and how these could be coupled in a feed-forward sense to active controls in the opto-mechanical system.

For example, the performance of a coronagraph behind LUVOIR's segmented primary mirror is most sensitive to the relative piston and tip/tilt of the individual segments (see section B.2.2 below) which are not well-described by low-order Zernike modes. An out-of-band wavefront sensor (OBWS; operating in the UV while science observations occur in the visible) could use a

dichroic to feed a Zernike wavefront sensor, avoiding the spatial filtering of the occulting spot reflection, and thus measure the wavefront errors over a much wider range spatial frequencies. The exact sensitivity to temporal and spatial modes depends on the brightness of the guide star, which could potentially be an artificial one created by a cubesat-sized companion spacecraft,<sup>47</sup> and the use of an OBWS in the overall control system must be looked at in concert with other components of the opto-mechanical system.

These assessments could change the requirements on the wavefront sense and control system of a future exo-Earth imaging mission. The demonstrated WFIRST CGI LOWFS sensitivity to line-of-sight jitter translates into 0.03 milliarcseconds for LUVOIR and 0.1 milliarcseconds for HabEx, which will be evaluated.

### B.2.2 CG-6 Mirror Segment Phasing Sensing and Control

#### CG-6: Mirror Segment Phasing Sensing and Control

**Description:** Segmented mirrors require segment phasing and rigid-body sensing and control of the segments and the surface figure to achieve tight static and dynamic wavefront errors.

**SOA (Lab):** 6 nm rms rigid body positioning error and 49 nm rms stability (JWST error budget); SIM and non-NASA: nm accuracy and stability using laser metrology; capacitive gap sensors demonstrated at 10 pm

**SOA (Ground-based):** Keck has achieved 6 nm positioning error rms

**SOA (Flight):** None

**Needed capability:** Systems-level considerations to be evaluated but expect will require WFE stability less than 10 pm rms sensitivity and control over periods of tens of minutes with obscured/segmented pupil and simulated dynamic environment

**Supported Missions or Mission Concepts:** LUVOIR, HabEx

Unlike a traditional monolithic telescope mirror, a multi-segment large-aperture mirror will require phasing and rigid-body sensing and control of the segments to achieve tight static and dynamic wavefront errors at visible and near-infrared wavelengths. Wavefront errors caused by segment rigid body positioning errors, dynamic vibrations, and slow thermal drifts can significantly impact coronagraph coherent imaging and hence contrast. For example, a coronagraph working with a segmented mirror, to avoid speckle noise brighter than typical exoplanets, requires a segment-to-segment dynamic co-phasing error to change less than 10 pm rms between WFSC updates (from a few minutes to many tens of minutes depending on the host star's brightness).<sup>48</sup>

#### Current State-of-the-Art:

The Keck ground-based telescope and JWST sense and control the rigid-body positions of their segments by utilizing wavefront sensing and control, such as phase retrieval, Shack-Hartman sensing, and dispersed fringe sensing.<sup>49</sup> Keck also uses capacitive edge sensors. JWST's optical error budget includes 6 nm rms for rigid body positioning and 49 nm rms stability. While these methods are proven for phasing diffraction-limited segmented optical systems such as JWST, it remains to be seen if they can achieve the tens of picometer-level stability required for exoplanet imaging at visible wavelengths.

Picometer-accuracy laser metrology was demonstrated by the Space Interferometry Mission with large beam launchers. More compact beam launchers, lightweight enough to mount to the edges of segments, have been developed over the last few years for non-NASA customers but were designed to operate at the nanometer-precision level. Additional development in laser metrology is needed if a laser metrology truss is to be used for sensing segment positioning.

### **Progress Over the Last Year:**

The LUVOIR mission concept study is developing an architecture that combines the use of a laser metrology truss to measure positional changes of the large optics to required pm-level stability requirements, complemented by high bandwidth edge sensors. This concept is explored in LUVOIR's interim report and described in detail in Lou et al (2018).<sup>50</sup>

An additional concept for using an external artificial laser guide star on a cubesat flying in formation with the space telescope is explored in Douglas et al. (2019). This idea potentially provides a solution for high signal-to-noise ratio measurements of segment-segment motion, and thus better control authority, for LUVOIR or other segmented space telescopes.<sup>51</sup>

Leboulleux et al (2018)<sup>52</sup> developed a framework for analytic calculations of the effects of segment-to-segment motion on coronagraph contrast by finding the eigenmodes of this motion, in effect determining the combinations of segments whose motion most affects the dark zone.

Babak Saif et al. were awarded a SAT 2017 to continue developing the capability for pm-scale metrology, using stability on fast time scales. In 2017, 25 pm control of an actuator was demonstrated in air, and in 2018 the team plans to set up an ultra-stable vacuum test chamber.

### **Next Steps:**

More work is needed to study the wavefront stability problem at a systems level, of which segment phasing is a component. Requirements definitions will continue to advance within the HabEx and LUVOIR mission concept studies and within the industry systems-level segmented telescope studies. Final reports from all of these efforts are expected in 2019.

In addition, the SCDA study (see Sect. B.1.2) will explore requirements on telescopes segment-segment, building on the work of Nemati et al (2017).<sup>53</sup> It is expected that segment/segment motion on the order of 1 nm rms can be corrected with the coronagraph's DM<sup>54</sup> but this will be studied in detail in 2019.

A picometer-level capacitive sensor, if it is needed as a part of the systems-level solution, should be matured by demonstration in an edge-sensor-like configuration.

### B.2.3 CG-7: Telescope Vibration Sensing and Control or Reduction

#### CG-7: Telescope Vibration Sensing and Control or Reduction

**Description:** Isolation, reduction, and/or damping of spacecraft and payload vibrational disturbances

**SOA (Lab):** 80 dB attenuation at frequencies > 40 Hz (JWST passive isolation); Disturbance-Free Payload demonstrated at TRL 5 for JWST with 70 dB attenuation at high frequencies with 6-DOF low-order active pointing. GAIA cold gas microthrusters or LISA pathfinder colloidal microthrusters for fine pointing can reduce disturbance environment.

**SOA (Flight):** none

**Needed capability:** Vibration Isolation or reduction of vibration disturbance sources to a level that enables < 1nm wavefront error rms stability.

**Supported Missions or Mission Concepts:** LUVOIR, HabEx

Isolation and damping of spacecraft and payload vibrational disturbances, or reducing these disturbances to acceptable levels, is critical in enabling a coronagraph to reach  $10^{-10}$  contrast sensitivities at IWAs less than  $3 \lambda/D$ . Leakage of starlight due to pointing instability or jitter and vibration in the telescope that exceed the control range of the coronagraph's LOWFS/C will potentially scatter light onto the imaging detector and degrade the detection contrast within the dark hole. Precision pointing stability needed by the telescope during integration to keep the star inside the correction capabilities of the coronagraph may need to be better than a few mas<sup>55</sup> (depending on LOWFS/C capability; see Section B.2.1).

The effects of mechanical disturbances on the stability of the telescope can be handled in a number of ways including reduction of the disturbances through design, or by dynamic isolation. For isolation of a telescope system with reaction wheels, typical expected attenuations > 100 dB end-to-end are needed.<sup>56,57</sup> "End-to-end" implies isolation between disturbance source and the optical telescope element and coronagraph instrument. The isolation requirements also critically depend on the mirror stiffness and mass; stiffer mirrors have a lower wavefront error for a constant vibration levels, as do more massive mirrors.

Micropropulsion thrusters for fine pointing, used exclusively or in a hybrid fashion with reaction wheels, is another option to reduce the disturbance levels. Hybridizing the LOWFS/C fast steering mirror system with the fine guidance system is also an approach that could be considered, though there are costs in coronagraph throughput and does not allow control of wavefront errors other than tip/tilt.<sup>58</sup>

#### Current State-of-the-Art:

Several aerospace companies have demonstrated systems that allow for active dynamic isolation candidates. A non-contact isolation system by Lockheed Martin known as the Disturbance-Free Payload<sup>59</sup> demonstrated 68 dB of broadband isolation in a JWST testbed and is self-assessed at TRL 5 for large observatories. The payload and spacecraft bus are separate bodies that fly in close-proximity, allowing precision payload control and simultaneous isolation from spacecraft disturbances.

The use of cold gas microthrusters to achieve extreme spin-rate stability has been demonstrated on-orbit by GAIA. Colloidal microthrusters were used in LISA Pathfinder, which has demonstrated micro-Newton thrust control on orbit.

**Progress Over the Last Year:**

The HabEx and LUVOIR studies are developing architectures which will set the necessary stability requirements on all time scales including the vibration environment. The Lockheed Martin non-contact isolation has been studied in the context of the LUVOIR design and has been shown to provide the needed isolation for LUVOIR's 15 m telescope.<sup>60</sup> The industry systems-level segmented telescope studies will also include the LM concept for non-contact isolation in their trade space.

The HabEx study has explored the option of the use of a microthruster-based fine pointing control system<sup>61</sup> which greatly reduces the vibration environment as compared to standard reaction wheels.

**Next Steps:**

Telescope stability, like wavefront stability in general, is a systems-level challenge and is most efficiently addressed by a reference design that includes selected coronagraph and telescope architectures. Requirements definitions will continue to advance within the HabEx and LUVOIR mission concept studies and within the industry systems-level segmented telescope studies. Final reports from all of these efforts are expected in 2019.

**B.3 Angular Resolution**

An Earth analog orbiting a solar-type star at a distance of 10 pc has a maximum angular extent of 100 mas (see **Figure 3**). To just detect such a planet at 400 nm, a telescope requires an angular resolution of 25 mas if we assume a coronagraph with an inner working angle of  $3 \lambda/D$ . This telescope would have a 3.3 m diameter primary mirror aperture. However, detecting the many spectral biosignatures at longer wavelengths would require even larger apertures. Imposing the same parameters for detecting the planet at 760 nm (oxygen line), a 6.3-m telescope is required; measuring the planet's water line at 940 nm requires a telescope aperture approaching 8 m. Improvements in a coronagraph's inner working angle can help drive the necessary aperture size down, as would investigations of our solar neighborhood limited to within 10 pc.

Aside from angular resolution, large primary mirrors enhance planet sensitivity due to reduction in science integration time with greater collecting areas and throughput enabling probing of a larger number of more distant stars' habitable zones and improved spectral resolution. The telescope's primary mirror size and architecture (monolithic or segmented, obscured versus unobscured) is among the most important decisions a space telescope team will have to make, especially when considering optimizing the performance of a coronagraph.

In addition, the biggest unknown needed to select the telescope size is the fraction of Sun-like stars with Earth-size planets in their habitable zones, also known as  $\eta_{\text{Earth}}$ . As  $\eta_{\text{Earth}}$  increases, the goal of detecting a particular number of Earth-sized planets in habitable zones can be achieved with observations of fewer targets. If  $\eta_{\text{Earth}}$  is near 0.1, then a 10-m-class telescope is required to detect and characterize approximately 30 candidate habitable zones for exo-Earths<sup>62</sup>. If  $\eta_{\text{Earth}}$  is above 0.8 then only a 4 m-class telescope would be required to detect and

characterize the same number of candidate habitable zones.  $\eta_{\text{Earth}}$  is expected to be better constrained in the near future, based on additional analysis of the Kepler data.

### B.3.1 CG-1: Large Aperture Mirrors

#### CG-1: Large Aperture Mirrors

**Description:** Large monolith and multi-segmented mirrors for space that meet tight surface figure error, coating uniformity, and thermal control requirements at visible wavelengths

**SOA (Monolith):** 3.5-m sintered SiC with  $< 3 \mu\text{m}$  SFE (Herschel); 2.4-m ULE with  $\sim 10$  nm SFE (HST); Depth: Waterjet cutting is TRL 9 to 14", but TRL 3 to  $>18$ ". Fused core is TRL 3; slumped fused core is TRL 3 (AMTD).

**SOA (Segmented):** (no flight SOA): 6.5 m Be with 25 nm SFE (JWST); Non-NASA: 6 DOF, 1-m class SiC and ULE,  $< 20$  nm SFE, and  $< 5$  nm wavefront stability over 4 hr with thermal control

**Needed capability:** Aperture: 4–15 m; SFE  $< 10$  nm rms (wavelength coverage 400–2500 nm); Wavefront stability better than 10 pm rms per wavefront control time step; Segmented apertures leverage 6 DOF or higher control authority meter-class segments for wavefront control. Environmentally tested

**Supported Missions or Mission Concepts:** LUV0IR, HabEx

Here we consider large telescope mirror technology with better than 10 nm rms surface figure error and compatible with the 10 pm wavefront error stability needed for exo-Earth coronagraphy. The large primary mirror can be either segmented or a monolith. The exact requirements on the telescope are system-dependent and trades can be made with other subsystems. In this particular technology area, we consider the manufacturability of the mirror, the backing structure, and the thermal control that meets the stability requirements (because thermal control is so integrated in the choice of mirror material and the mounting of the mirror). Mirror coating technology is considered separately (see Section E.1.1). Additionally, the technology for maintaining segment phasing, low order wavefront sense and control, and vibrational isolation and disturbance reduction are considered as separate, though closely related, technologies for closing the Contrast Stability technology gap (Section B.2).

However, here we do include the technology for thermal control of telescopes. Historically, space telescopes use passive thermal control. For example JWST's telescope is in a Sun-shade shadow and HST's telescope is in a heated tube. And again, while not designed to meet the requirements of a UVOIR exoplanet science mission, JWST is predicted to have a 31 nm rms WFE response to a worst-case thermal slew of 0.22 K and take 14 days to passively achieve  $< 10$  pm per 10 min stability. This is too long for a coronagraphic exoplanet mission. HST is a cold-biased telescope heated to an ambient temperature. However, it is not a controlled thermal environment. Thus, HST's wavefront error changes by 10–25 nm every 90 min (1–3 nm per 10 min) as it moves in and out of the Earth's shadow.

When considered for use with a starshade (see Sect. C) instead of a coronagraph instrument, the wavefront error stability requirements of a large aperture telescope are greatly relaxed, and diffraction due to obscurations and segmentation become less of an issue.

### B.3.2 Large Monolithic Mirrors

Monolith primary mirrors in an off-axis telescope provide an ideal unobscured pupil for a coronagraph, but are more limited in size than a deployable segmented mirror. The maximum size monolithic mirror has been limited to approximately 4–6 m by currently available 5-m-class launch vehicle fairings. For example, the largest monolithic space telescope ever flown is the

Herschel Telescope and its primary mirror is 3.5 m. Fortunately, with the advent of NASA's Space Launch System (SLS) and its planned 8.4- and 10-m fairings, it is possible to consider monolithic 4- to 8-m-class mirrors. Alternative rectangular monolith telescope architectures with high aspect ratios could use existing fairings to stow a primary mirror with even greater angular resolution in one direction, though with a non-circular point spread function. This telescope technology is compatible with coronagraphy.<sup>63</sup>

Mirror mass and diameter traditionally have been key telescope design parameters, especially with respect to cost. This has led to light-weighting technologies that continue to be developed. But the SLS's larger fairings and greater mass capacity allow designers to reconsider the benefits of more mass in the overall system (greater stiffness, lower resonance frequencies, greater thermal inertia, etc.).

HabEx is baselining an off-axis telescope with a 4 m monolith.<sup>64,65</sup> Analysis indicates that exoplanet science requires a primary mirror that has a total wavefront error that is stable on the order of 10 pm per wavefront control step.<sup>66</sup> Thermal stability and control is another key challenge that HabEx will have to address in their design. While any future large space mission will probably be in the thermally stable Earth-Sun L2 Lagrange orbit, there will still be thermal load variations as a function of pointing angle relative to the Sun (as shown on JWST).

#### **Current State-of-the-Art:**

The largest monolith mirror optimized for performance in the visible-band is HST, made of ultra-low expansion (ULE) glass with 10 nm surface figure error. WFIRST will be the same size. A 3.5 m monolith primary mirror (made of SiC) flew as part of the Herschel observatory, though it was optimized for mid and far-infrared wavelengths, and had a surface figure error of 3  $\mu\text{m}$ . Glass mirrors in the 8 m or larger class achieving 7-8 nm surface figure error have been manufactured for use in ground-based observatories (Subaru, VLT) though space missions usually need lower density per area, and a higher resonant frequency (stiffness).

#### **Progress Over the Last Year:**

The HabEx design study team considered both ULE and Zerodur as materials for their baseline 4 m primary mirror and developed a detailed point design with United Technologies Aerospace Systems (UTAS) for their 4 m primary mirror telescope.<sup>67</sup> It includes a 35 cm-thick open-back Zerodur mirror by Schott with milling (340 mm pockets/4 mm ribs), giving a 93 Hz first mode (unmounted); 120 Hz first mode mounted design. Four meter Zerodur blanks have been manufactured by Schott in the past. Thermal surface figure distortions, including CTE nonuniformity, have been shown by analysis to create  $\sim 100$  pm of wavefront error on time scales of minutes. According to UTAS heritage, gravity sag can be corrected to  $< 1$  nm. Because the lower first mode increases wavefront error, a lower disturbance environment is required to drive it back down. To that end, the HabEx design team has decided to adopt microthrusters in their design, rather than reaction wheels, for pointing the observatory in an effort to provide a more benign disturbance environment (see Sect. B.2.3).

East et al (2018)<sup>68</sup> presented a thermal analysis of the elements of the mounting assembly of a lightweight ULE mirror showing compatibility of this system with a 10-picometer wavefront stability.

A SAT/TCOR was awarded in 2017 (PI Phil Stahl/NASA Marshall Space Flight Center) to demonstrate predictive thermal control for large glass space mirrors, specifically in the context of enabling pm wavefront error stability for high contrast imaging.<sup>69</sup> As part of this effort in 2018 measurements were made in vacuum of thermal deformations of both ULE and Zerodur<sup>70</sup>

#### **Next Steps:**

The HabEx mission's final report is expected in 2019 and will include a detailed description of the technology needs for their primary mirror.

### **B.3.3 Large Segmented Mirrors**

The development of large segmented mirrors and their supporting structures will enable astronomy to build ever-increasing large telescopes advancing both exoplanet and general astrophysics science, beginning with JWST. However, segmented mirrors have their own challenges to reach  $10^{-10}$  contrast ratio levels at small IWAs. These challenges include diffraction from the segmentation pattern and segment-to-segment rigid body motion (i.e., tip/tilt and piston). See Sect. B.1.2 for descriptions of coronagraph designs that are compatible with this type of pupil, and Sec. B.2 for a discussion of technologies needed to maintain stability of a segmented system. Large apertures often have large corresponding on-axis secondary mirrors which, along with their support structures, provide additional diffraction challenges for a coronagraph instrument.

The experience of controlling 6 degree of freedom segments on JWST can be built upon to gain a higher precision, more stable, segmented aperture for exoplanet imaging. The surface figure error is required to be less than 10 nm rms and drift less than 10 pm due to thermal and dynamic instability during a wavefront control cycle. Previously studied design architectures include the ATLAST (Advanced Technology Large Aperture Space Telescope) design<sup>71</sup> and the High Definition Space Telescope (HDST) concept.<sup>72</sup>

The LUVUOIR design study team is baselining two deployable point designs: architecture A is a 15 m segmented primary mirror, sized to fit the largest fairing expected to be available in the 2030's, and architecture B is based around a 8 m segmented primary mirror and is designed to fit in a 5-m diameter fairing.

#### **Current State-of-the-Art:**

JWST is a segmented aperture telescope scheduled for launch in 2021. Its primary aperture is 6.5 m in diameter composed of 18 gold-coated beryllium segments, each 1.32 m tip-to-tip. Working in the near- to mid-infrared, the telescope operates at a temperature below 50 K. By operating at a warmer temperature, due to its visible to near-infrared observational spectrum, a potential exoplanet imaging mission can use other materials for its optical components and structure. These include ULE glass, and Silicon Carbide with a nanolaminate, which have demonstrated better than 5 nm rms SFE on 1 meter-class segments.

#### **Progress Over the Last Year:**

The LUVOIR design study team is exploring the scientific benefits and technology needs of large segmented primary mirrors. The LUVOIR-A interim report includes a detailed description of LUVOIR's architecture A which uses 120 ULE glass segments with no active surface figure actuation. The segments rely on technology demonstrated by the Advanced Mirror Segment Demonstrator project.<sup>73</sup> Each segment will be connected to a composite backplane structure, whose thermal control system (similar to that considered for the ATLAST study<sup>74</sup>) is compatible with 1 mK control. The interim report does consider the benefits of highly actuated silicon carbide segments and considers this approach to be a viable backup alternative, though with less flight heritage than ULE glass.

#### **Next Steps:**

The LUVOIR final report in 2019 will include a more detailed look at the 8-m architecture B and the results of any additional trade studies undertaken in the last year of its study.

The industry-led systems-level segmented telescope study will also provide a more generic study of the technology needs of a segmented space telescope compatible with exo-Earth direct imaging.

The in-space assembled telescope study (iSAT) will consider possible cost and risk advantages of a robotically assembled segmented space telescope<sup>75</sup> and will deliver a report and a whitepaper to Astro2020 in 2019.

Ultimately, maturing this technology at the level required for exo-Earth direct imaging will require building and testing multiple segments together. This will demonstrate relative phasing, integrated thermal control, and surface figure actuation as needed.

#### **B.4 Detection Sensitivity**

The collected photon flux rate from exo-Earths, depending on the telescope size and the system throughput, is expected to be about one per several minutes. Consequently, the imaging detectors for both the detection and spectrometer channels of a coronagraph instrument must be highly sensitive, have ultra-low noise, and must be radiation hardened. In addition, the need for low spectral-crosstalk spectroscopy and large outer working angles to carry out disk science and imaging of the nearest exoplanets lead to the requirement for large format focal plane array—2k×2k pixels or larger.

Ongoing WFIRST investments are funding electron multiplying charge coupled device (EMCCD) development, though improvements for post-WFIRST missions are needed. These include better QE between 0.85 and 1  $\mu\text{m}$  to help detect important water spectral lines, and longer lifetime in the space radiation environment.

### B.4.1 CG-8: Ultra-low Noise Visible Band Detectors

#### CG-8: Ultra-Low Noise Visible Band Detectors

**Description:** Low-noise visible detectors for faint exoplanet characterization with an Integral Field Spectrograph

**SOA (Lab):** 1k×1k silicon EMCCD detectors provide dark current of  $7 \times 10^{-4}$  e-/px/sec; CIC of 0.01 e-/px/frame; zero effective read noise (in photon counting mode) after irradiation when cooled to 165.15 K (WFIRST); 4k×4k EMCCD fabricated but still under development

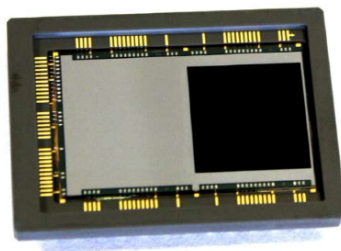
**SOA (Flight):** HST WFC3/UVIS CCD 3.1 e- read noise, dark current  $2 \times 10^{-3}$ , format 2k×2k

**Needed capability:** Effective read noise < 0.1 e- rms; CIC <  $3 \times 10^{-3}$  e-/px/frame; dark current <  $10^{-4}$  e-/px/sec tolerant to a space radiation environment over mission lifetime. ≥ 2k×2k format

**Supported Missions or Mission Concepts:** LUVOIR, HabEx

#### Current State-of-the-Art:

The leading candidate detector technology in the visible is the silicon EMCCD detector, which can provide dark current noise of order  $5 \times 10^{-4}$  e-/px/sec while operating at 165 K, and clock induced charge (CIC) of order 0.01 e-/pix/frame, after (WFIRST) lifetime irradiation. The effective read out noise can be  $\ll 1$  e- rms using electron-multiplying (EM) gain; depending on the device gain of the output amplifier that is being used. In addition, improved quantum efficiency at the long wavelength end of the visible band (closer to 1 micron where silicon becomes transparent) is desirable for biomarker detection, if it can be achieved without a major increase in dark current. In addition, charge trap build-up due to radiation damage leads to degraded performance at end-of-life; the number of pixels that have to be masked in each exposure increases over time thus the effective QE is worse.



WFIRST Detector Performance Requirements				
Specification	Goal	Requirement	Measurement	Unit
Effective read noise w/gain	0.2	0.2	<0.2	e-
Dark current	$1 \times 10^{-4}$	$5 \times 10^{-4}$	$1.01 \times 10^{-4}$ *	e-/pix/sec
Clock induced charge (CIC) @ 5.5σ threshold	0.0010	0.0018	0.0017	e-/pix/fr

**Figure 8:** e2V CCD201-20 (1k×1k) detector and its characterization results conducted at the JPL CCD Detector Lab in 2015; data is beginning of life.

Microwave Kinetic Inductance Detectors (MKID) and Transition Edge Superconducting (TES) arrays are cryogenic alternatives capable of performing at visible wavelengths with essentially no read noise or dark current. Both require operations at cryogenic temperatures, and are less mature than EMCCDs (more about these technologies in Section B.4.2).

Multi-channel plate (MCP) amplifiers can enable photon-counting detectors in the visible band. Commercially available GaAs photocathodes are sensitive to wavelengths 350-850 nm and achieve very low dark current of order 0.2 counts/px/hr with modest cooling to -30 °C. Similar designs are currently operating in space (UVOT on SWIFT, S20 cathode).<sup>76</sup>

P-channel skipper CCD amplifiers, optimized for very low light particle physics experiments, have sub-electron read noise and potentially improved radiation hardness compared to traditional CCDs.<sup>77</sup> These amplifiers have flexibility for tuning the readout scheme of portions of the array. The current designs have very long readout times (hours) in photon-counting

mode that would need to be improved for a space flight application, as well as testing for suitability in low-light astronomical applications.

Low-noise CMOS sensors, such as the photon-counting quanta image sensor,<sup>78</sup> should in principle be less sensitive to the effects of radiation damage as compared to conventional or electron-multiplied CCDs, due to individual pixel readout, but are a relatively recent technological development.

### Progress Over the Last Year:

The WFIRST coronagraph instrument has baselined the e2v CCD201-20 detector (1024×1024; 13×13 μm pixel pitch) for both of the coronagraph science cameras (imaging and IFS) and for the LOWFS camera. The project has carried out full characterization and displacement damage dose radiation testing and while the end-of-life performance has been shown to be adequate, the WFIRST project has worked with Teledyne-e2v to design and implement several changes to the detector that should improve the performance margin. This involves following procedures similar to those implemented on HST/WFC3 CCD detectors,<sup>79</sup> narrowing the path that small charge packets follow reducing the effects of the charge traps created by radiation damage. Customized EMCCD detectors developed for the space flight environment have been developed by Teledyne-e2v in collaboration with WFIRST/CGI. Updates to the commercial design include: narrower charge transfer channels to minimize the impact of radiation-induced traps; a gain register charge overspill to reduce obscuration of photon events by cosmic rays; and a new lower noise amplifier designed to drive larger loads and to reduce read noise, which would enable lower gain operation.

In 2018, Rauscher et al. were awarded a directed work package from NASA's Astrophysics Division to advance hole-multiplying CCD (HMCCD) technology. This work package has the goal of demonstrating photon-counting with a p-channel doped photoconductor with hole multiplication gain. P-channel doping may show improved radiation hardness relative to standard n-channel doped Si.

### Next Steps:

To quantify the combined effects of the detector quantum efficiency and fraction of pixels discarded in an exposure due to cosmic ray transients and effects of radiation damage, we define an Detection Quantum Efficiency (EQE) as  $DQE = QE \epsilon_{PC} \epsilon_{CR} \epsilon_{HP} \epsilon_{CTE}$ , where QE is the fundamental quantum efficiency of the detector,  $\epsilon_{PC}$  is the photon counting efficiency of the device,  $\epsilon_{CR}$  is the fraction of pixels lost in a given exposure due to cosmic ray transients,  $\epsilon_{HP}$  is the fraction of hot pixels that must be discarded in every exposure, and  $\epsilon_{CTE}$  is the fraction of pixels that must be masked due to reduced charge transfer efficiency charge trap build-up effects.  $\epsilon_{HP}$  and  $\epsilon_{CTE}$  are factors that degrade with time in the space radiation environment.

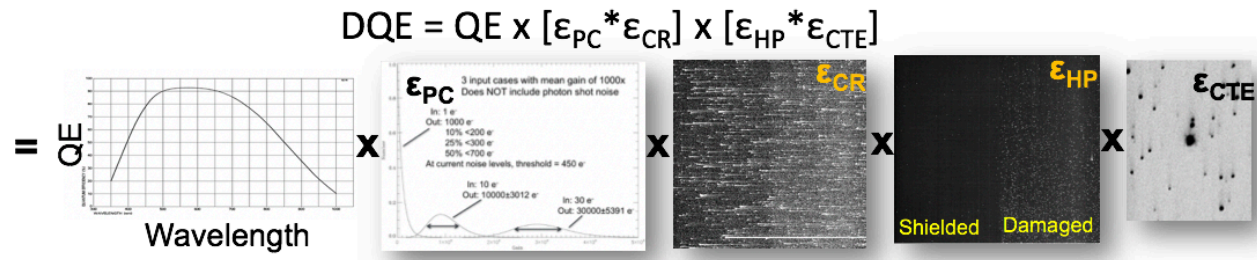


Figure 9: A schematic of the definition of Detection Quantum Efficiency (Courtesy of Leon Harding and Patrick Morrissey).

Requirements for future missions should be developed based on this effective quantum efficiency in order to include radiation hardness.

The customized EMCCD detectors delivered to WFIRST/CGI by Teledyne-e2v will be radiation tested in 2019 leading to a downselect of the flight design.

Additional investigation of silicon detectors (either CCD or CMOS) should study the trade between QE close to 800-1000 nm and dark current.

The HMCCD and Skipper technologies should be explored as potential options to evaluate potential advantages of p-channel-doped silicon detectors. The Rauscher-led work package will test performance of an HMCCD device in low-light (i.e. similar to science observations) conditions in the GSFC Detector Characterization Lab in 2019.

CMOS detectors should be investigated as an alternative to CCD potentially improving on the eCTE terms in the effective quantum efficiency, though read noise and dark current in low-light conditions are not known.

Other superconducting candidate technologies will be further explored. For example, NASA's PICTURE-C balloon experiment is baselined to include a 10–20 kpix MKIDs device in 2019. NASA-GSFC is considering maturing TES devices for future exoplanet imaging missions.<sup>80</sup>

#### B.4.2 CG-9: Ultra-low Noise Near-Infrared Detectors

##### CG-9: Ultra-Low Noise Near-Infrared Detectors

**Description:** Near-infrared wavelength (900 nm to 2.5  $\mu\text{m}$ ), extremely low noise detectors for exo-Earth spectral characterization with Integral Field Spectrographs

**SOA (Lab):** HgCdTe photodiode arrays have read noise  $\lesssim 2$  e- rms with multiple nondestructive reads; 2kx2k format; dark current < 0.001 e-/s/pix; very radiation tolerant (JWST)

HgCdTe APDs have dark current  $\sim 0.025$  e-/s/pix, RN  $\ll 1$  e- rms, and < 1kx1k format

Sub-Kelvin photon-counting detectors (KID, TES): 0 read noise/dark current; radiation tolerance is unknown; <1kx1k format

**SOA (Flight):** HST WFC3/IR HgCdTe dark current 0.05 e-/px/s, 12 e- read noise, 1kx1k format

**Needed capability:** Read noise  $\ll 1$  e- rms, dark current noise < 0.001 e-/pix/s, in a space radiation environment over mission lifetime;  $\geq 2\text{k} \times 2\text{k}$  format

**Supported Missions or Mission Concepts:** LUVOIR, HabEx

Near infrared detectors with high sensitivity in the spectral region of 900 nm to 2.5  $\mu\text{m}$  (and maybe greater) are critical for the spectral characterization of exoplanets and identification of possible biosignatures. Future exo-Earth missions (HabEx, LUVOIR) will consider infrared

spectroscopy capabilities to detect hydrocarbons such as methane (1.00  $\mu\text{m}$ , 1.69  $\mu\text{m}$ , and 2.32  $\mu\text{m}$ ). The presence of methane in an oxygen-rich atmosphere like Earth's is one of the few known spectral combinations that point to a likely biotic origin. Spectral characterization of exo-Earths in the infrared requires sub-electron read noise and the dark current noise  $< 0.001$  e-/pix/s, in a space radiation environment over mission lifetime. These properties in a larger array, such as 2k $\times$ 2k or 4k $\times$ 4k, are desirable.

### **Current State-of-the-Art:**

HgCdTe photodiode arrays hybridized to astronomy readout integrated circuits are the state of the art, with a read noise  $< \sim 2$  e- rms with multiple non-destructive reads, and dark current of  $< 0.001$  e-/s/pix. These detectors have flown in low Earth orbit and have proven to be radiation tolerant. Two large format 4k $\times$ 4k pixel arrays offered by Teledyne Imaging Sensors, with 10 and 15  $\mu\text{m}$  pixel pitch are at TRL 4 (H4RG-10™ and H4RG-15™), though the large format size is needed mainly for spectroscopy.

Other candidate detector technologies are currently less mature but are promising. With appropriately optimized process, the HgCdTe avalanche photodiode (APD) array offers the possibility of the high gain and low effective read noise of EMCCDs while being capable of the same QE performance as the JWST arrays. Because gain is built into each pixel—unlike the EMCCD—they promise photon counting if the dark current is sufficiently suppressed.<sup>81</sup>

Cryogenic (superconducting) detectors such as MKIDS have no read noise or dark current, solving the spurious count rate problem associated with the non-cryogenic devices.<sup>82</sup> These devices are scalable to large arrays. Transition edge sensor microcalorimeter arrays are another candidate cryogenic detectors with built-in energy resolution like the MKIDs. Nanowire single photon detection arrays can operate at higher temperatures and are multiplexed similarly to MKIDs.<sup>83</sup> Cryogenic detectors will require solutions for dynamic isolation, particularly from their cooler vibrations, and resolution (pixel count). The immediate challenge will be providing zero-vibration cooling to maintain compatibility with coronagraph instruments (though a starshade-only space mission will have less stringent vibration requirements). While cooling is not a detector technology, future telescope architectures must minimize vibrations sources to enable the coronagraph performance to reach the dual driving instrument goals of  $10^{-10}$  contrast ratios at  $< 3 \lambda/D$ . Also, their radiation tolerance is unknown. Bernard Rauscher et al.<sup>84</sup> present a summary on the state-of-art and potential detector candidates for low-flux environments.

### **Progress Over the Last Year:**

Lab demonstration of SAPHIRA detectors (by APRA funding) reported 0.025 e-/s/pix dark current in a photon-counting mode.<sup>85</sup> The same work estimates that the dark current inherent to the device itself, and thus representing a potential floor, is on order  $1.5 \times 10^{-3}$  e-/s/pix. This is close to the needs of the program.

MKIDs have recently been demonstrated on two ground-based planet finding instruments, the SDC on the Palomar 200" and SCExAO on the Subaru 8 m. Recent advances include anti-

reflection (AR) coating directly applied to the MKIDs that boost their quantum efficiency to >70% over a wide wavelength range.

**Next Steps:**

The SAPHIRA devices should be developed further, both to improve the dark current to the  $10^{-3}$  e<sup>-</sup>/s/pix level and to increase the format size to make the devices more practical for space-based exoplanet spectroscopy.

Read noise reduction could be further investigated in a (non-avalanche) HgCdTe readout.

## C STARSHADE TECHNOLOGY GAPS

External occulters, or starshades, suppress on-axis starlight so that the reflected starlight from the off-axis planets can be imaged. This is done by blocking most of the on-axis starlight and redirecting the diffraction pattern so that it interferes destructively at the entrance pupil of a telescope creating a shadow. Depending on the size of the telescope and wavelength range, this typically requires the starshade to be tens of meters in diameter and located tens of thousands of kilometers from the telescope (**Figure 10**). The starshade must position itself to maintain the shadow on the telescope, and its petals must maintain a very precise shape to produce the desired reduction in starlight relative to the light reflected by the planet. It must also be opaque and limit the amount of sunlight scattered from the petal edges into the telescope.

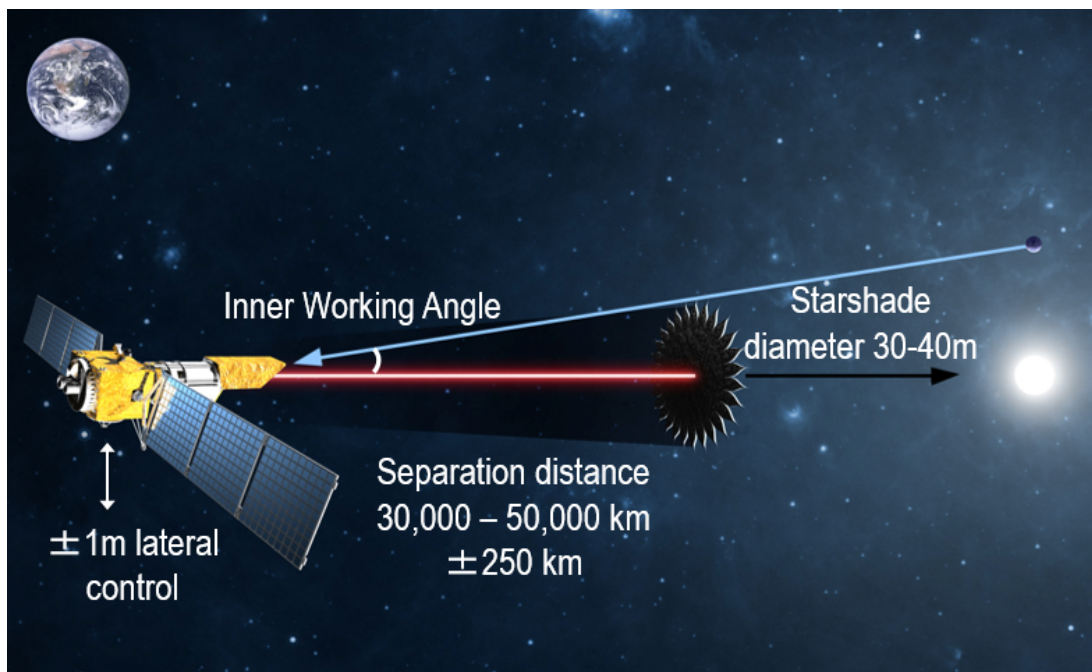


**Figure 10:** A typical starshade/telescope configuration. The starshade blocks starlight from reaching the telescope pupil, but allows light from the exoplanet.

If a circular occulter were used rather than one with numerous shaped petals, a Poisson spot, a circular bright region at the center of the image plane due to constructive interference of diffracted light, would ruin the ability to image faint exoplanets. Independent optical modeling predictions have shown excellent agreement concerning the contrast sensitivity to petal shape errors,<sup>86</sup> and detailed preliminary error budgets have been proposed.<sup>87</sup>

The five starshade technologies tracked by the ExEP are in **Table 1**. They target starshades capable of rendezvous with the WFIRST telescope at the Sun-Earth L2 orbit as well as for a possible larger mission such as the one described by the HabEx mission concept. The technology needs are largely based on a WFIRST Rendezvous reference mission as detailed in the architecture of the NASA Exo-S probe study.<sup>88</sup> This study, sponsored by NASA's Astrophysics Division in 2014, demonstrated the valuable science return of a starshade mission with both a

1.1 m telescope, and alternatively, the 2.4 m WFIRST telescope. This mission concept's starshade had a diameter of 20 - 40 meters. A NASA-chartered probe concept study led by Sara Seager is currently updating the science case for a WFIRST-starshade rendezvous, with a report expected in early 2019. The HabEx mission concept is currently baselining a 70 m-class starshade to accompany its space telescope.<sup>89</sup>

While some of the technology needs for the smaller WFIRST rendezvous concept are directly applicable to a larger starshade, some may require different solutions. Currently the LUVOIR mission does not include a starshade in its baseline architecture, instead, a coronagraph meets its starlight suppression needs. The requirements may change in the coming years as the HabEx and LUVOIR STDTs further advance their mission concepts.

A concept study of a starshade in low-Earth orbit providing starlight suppression for ground-based telescopes (such as the future 30-meter class Extremely Large Telescopes), known as the Remote Occulter, was kicked off in 2018 by a GSFC-based team led by Dr. John Mather and Eliad Peretz. A publication describing the concept is in preparation and will describe the technology needs of this specific concept. These technologies may be similar to those considered here, but may include additional technologies such as adaptive optics to correct atmospheric turbulence.

The starshade technologies in **Table 2** address three starshade technology gaps (shown in **Figure 11**):

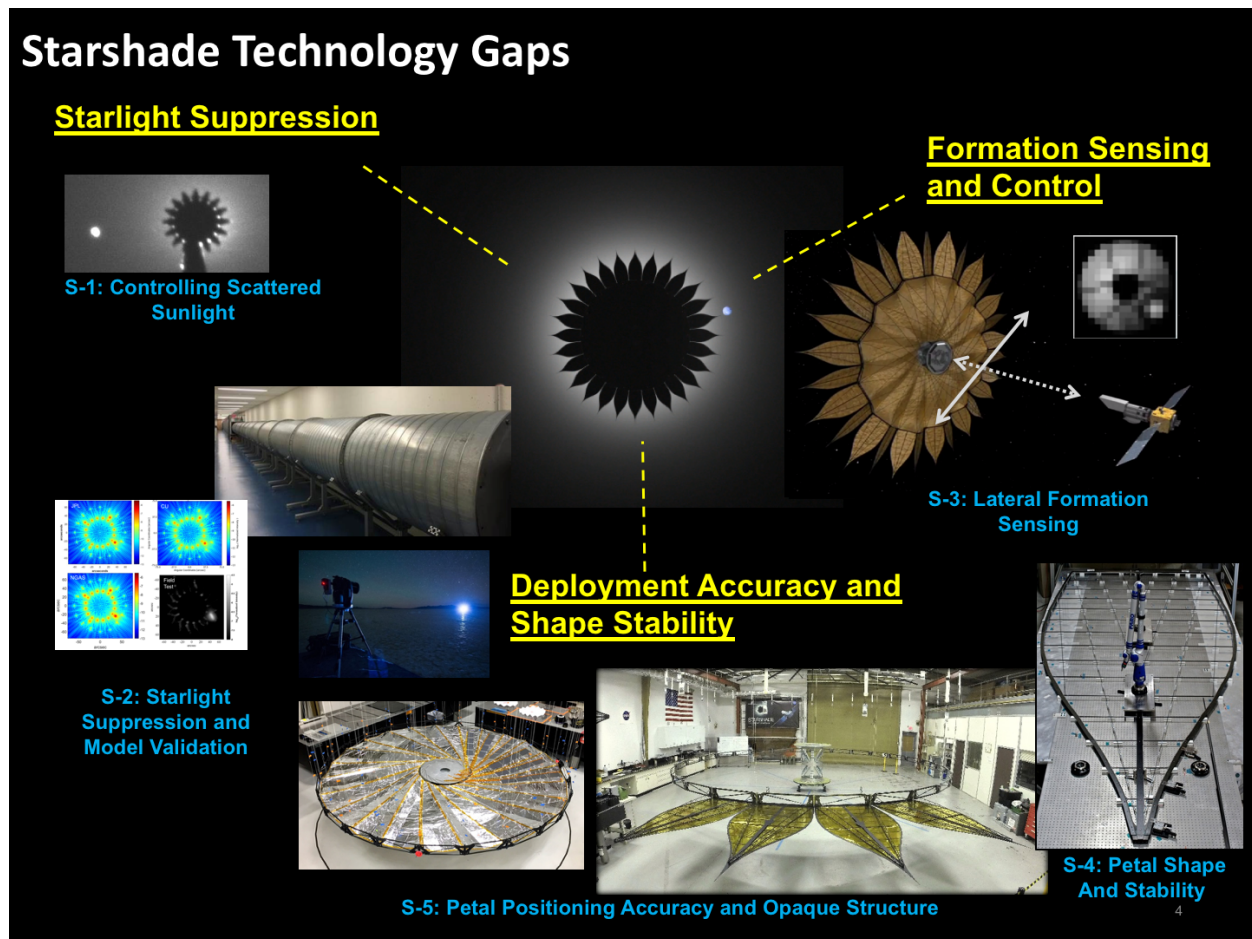


**Figure 11:** The three categories of starshade technology needs (in yellow font) to directly image and characterize exo-Earths around Sun-like stars.

1. **Starlight Suppression** – the starshade must produce the desired shape to within tolerances specified by an error budget to create contrast levels (local ratio of reflected exoplanet light to starlight in the same bandwidth) to better than  $10^{-10}$  at the image plane. The precise positioning and manufacture of the starshade edges that meet design requirements will minimize the diffraction from on-axis starlight and scatter/diffraction from off-axis Sunlight detected at the science focal plane. The starlight suppression capabilities of the starshade must be demonstrated on the ground to validate optical models and the error budget, which are used to predict performance in a space environment.
2. **Deployment Accuracy and Shape Stability** – the ability to stow, survive launch, and deploy the petals and inner disk to within the deployment tolerances budgeted to meet the shape, and ultimately, the contrast requirements. The final shape must be stable throughout operational environments within an allocated error budget. The optical shields within both the petals and the inner disk must fully deploy as an opaque structure.

3. **Formation Sensing and Control** – the ability to sense and control the lateral offset between the starshade and the telescope maintaining the desired contrast long enough for full science integration.

The published literature on starshades is inconsistent in defining starlight suppression, contrast, Fresnel number, and even the radius of the starshade (which can be defined in various ways due to the apodization function). We use the following definitions here, and suggest they be adopted as standards:

*Contrast ratio* is the ratio of starlight irradiance in an arbitrary resolution element of the focal plane to the irradiance that would be seen in that same resolution element were the star to be centered there.

*Suppression* is the ratio of the total starlight that enters the telescope with the starshade in place to that without the starshade. It is measured in the pupil plane.

Contrast ratio is defined at a resolution element in the focal plane. It has meaning for both coronagraphs and starshades. It varies over the focal plane and is only meaningful when a location is specified. In practice, an average value over an annulus between an inner working angle and an outer working angle is sometimes given. Since a “resolution element” depends on the properties of the optical system, including the telescope, the contrast ratio is affected by the performance of the entire system, not just the starshade.

Suppression, on the other hand, depends only weakly on the telescope, and therefore is determined essentially by the starshade alone. Since it involves quantities integrated over the pupil plane, it is always a single number. Because the telescope focuses the residual starlight onto the image plane, forming an image of the starshade, light leaking around starshade petals becomes concentrated into certain areas of the image plane, so that the contrast ratio (e.g.,  $10^{-10}$ ) in most elements is always ‘deeper’ than the suppression (e.g.,  $10^{-9}$ ). The relationship between them depends on the position of interest in the image plane, the telescope resolution and the number of pixels across which the starshade is imaged.

The SAT/TDEM program in the past has succeeded in receiving proposals and funding all of the three key areas of starshade technology gaps shown in **Figure 11**, though now this technology has been advanced through the Starshade Technology Development Activity (below). The Deployment Accuracy and Shape Stability technology gap (Section C.4) has also been the focus of several Small Business Innovation Research (SBIR) awards.

#### **C.1.1.1 Starshade Technology Development Activity (S5)**

After five years of funding starshade through the competed SAT/TDEM program, in March of 2016 the NASA APD Director chartered the formation of a focused starshade technology development activity. This approval allowed technology development for the starshade to transition from a competed, PI-led, SAT-funded effort to a directed, Program-managed and funded activity. The activity’s purpose is to mature the technologies that close the three gaps to TRL 5 for future starshade mission concepts that include WFIRST Rendezvous and HabEx starshades. It is managed using NASA Procedural Requirements (NPR) 7120.8 as a management guideline. Consequently, the SAT/TDEM program no longer accepts starshade proposals.

In 2018, the Starshade Technology Development Activity, known as S5 (starshade technology to TRL 5), developed a Technology Development Plan (TDP).<sup>90</sup> The TDP defined Key Performance Parameters and defined a series of milestones in advancing the starshade technologies listed below to TRL 5. The milestones defined in the TDP, which have been reviewed by the ExoTAC, are reproduced in Figure 12. Once this series of milestones have been achieved, the starshade technology gaps defined here will be closed. Some of the gaps are expected to be closed completely prior to the Astro2020 decadal survey and in other cases, the S5 Activity aims to demonstrate reduced risk a particular technology area prior to Astro2020.

The first S5 milestone (MS #4) was achieved in late 2018 and reviewed by the ExoTAC in January 2019, which formally closed the Formation Sensing and Control Technology Gap (see Sect. C.3). Details are captured in Figure 12 below.

MS #	Milestone	Report Completion Date	Exo-TAC Confirm by Decadal	% Risk Retired by Decadal
1A	Small-scale starshade mask in the Princeton Testbed demonstrates $1 \times 10^{-10}$ instrument contrast at the inner working angle in narrow band visible light and Fresnel number $\leq 15$ .	1/28/19	X	100
1B	Small-scale starshade mask in the Princeton Testbed demonstrates $1 \times 10^{-10}$ instrument contrast at the inner working angle at multiple wavelengths spanning $\geq 10\%$ bandpass at the Fresnel number $\leq 15$ at the longest wavelength.	3/30/19	X	100
2	Small-scale starshade masks in the Princeton Testbed validate contrast vs. shape model to within 25% accuracy for induced contrast between $10^{-9}$ and $10^{-8}$ .	1/15/20	X	100
3	Optical edge segments demonstrate scatter performance consistent with solar glint lobes fainter than visual magnitude 25 after relevant thermal and deploy cycles.	11/1/19	X	100
4	Starshade Lateral Alignment Testbed validates sensor model by demonstrating lateral offset position accuracy to flight equivalent of $\pm 30$ cm. Control system simulation using validated sensor model demonstrates on-orbit lateral position control to within $\pm 1$ m.	11/14/18	X	100
5A	Petal subsystem with <i>shape critical features</i> demonstrates shape stability after deploy cycles (deployed) consistent with a total pre-launch shape accuracy within $\pm 70$ $\mu\text{m}$ .	12/20/19	X	80
5B	Petal subsystem with <i>all features</i> demonstrates total pre-launch shape accuracy (manufacture, deploy cycles, thermal cycles deployed, and storage) to within $\pm 70$ $\mu\text{m}$ .	6/2/23		
6A	Petal subsystem with <i>shape critical features</i> demonstrates on-orbit thermal stability within $\pm 80$ $\mu\text{m}$ by analysis using a validated model of critical dimension vs. temperature.	12/20/19	X	80
6B	Petal subsystem <i>all features</i> demonstrates on-orbit thermal stability within $\pm 80$ $\mu\text{m}$ by analysis using a validated model of critical dimension vs. temperature.	6/2/23		
7A	Truss Bay <i>longeron and node subassemblies</i> demonstrate dimensional stability with thermal cycles (deployed) consistent with a total pre-launch petal position accuracy within $\pm 300$ $\mu\text{m}$ . (Note: SBIR funding dependency)	12/20/19	X	80
7B	Truss Bay <i>assembly</i> demonstrates dimensional stability with thermal cycles (deployed) and storage consistent with a total pre-launch petal position accuracy within $\pm 300$ $\mu\text{m}$ .	6/2/23		
7C	Inner Disk Subsystem with optical shield assembly that includes <i>deployment critical features</i> demonstrates repeatable accuracy consistent with a total pre-launch petal position accuracy within $\pm 300$ $\mu\text{m}$ . (Note: SBIR funding dependency)	12/20/19	X	80
7D	Inner Disk Subsystem with optical shield assembly that includes <i>all features</i> demonstrates repeatable accuracy consistent with a total pre-launch petal position accuracy within $\pm 300$ $\mu\text{m}$ .	6/2/23		
8A	Truss Bay <i>longeron and node subassemblies</i> demonstrate on-orbit thermal stability within $\pm 200$ $\mu\text{m}$ by analysis using a validated model of critical dimension vs. temperature.	12/20/19	X	80
8B	Truss Bay <i>assembly</i> demonstrates on-orbit thermal stability within $\pm 200$ $\mu\text{m}$ by analysis using a validated model of critical dimension vs. temperature.	6/2/23		

Figure 12: Summary of S5 Milestones, reproduced from the Starshade to TRL5 (S5) Technology Development Plan.

## C.2 Starlight Suppression

Starshades must demonstrate experimentally at a subscale level that they can reach  $\leq 10^{-10}$  contrast in a scaled flight-like geometry with Fresnel numbers 8-20 across a broadband optical bandpass. The challenge in this Fresnel number range is that the large starshade-telescope separation distances required for a small inner working angle prohibit ground-based optical

performance verifications of large starshades. Instead performance will need to be verified in a two-part process. One, subscale tests will demonstrate contrast performance consistent with imaging an exo-Earth and validate the optical models, upon which full-scale shape tolerances are based. The scaling approach is to match the flight design in terms of the number of Fresnel zones across the starshade such that the diffraction equations defining the dark shadow are identical. Sub-scale tests will also be used to validate an error budget, using intentionally deformed starshades to verify predicts from optical models. Two, the deployment accuracy and shape tolerances will be verified on a full-scale petal and deployment mechanism. Key capabilities have already been demonstrated via early prototypes, however, only a limited number of tests have been conducted at a flight-like Fresnel number using flight-like materials and manufacturing. Section C.2.2 describes the demonstrations and model validation.

The primary goal of the starshade optical edges is to provide the correct apodization function to suppress starlight to sufficient levels for exoplanet direct imaging. However, in order to do so light emanating from sources other than the target star must also be taken into consideration as this has the potential to significantly degrade the image contrast. Of greatest importance is light from our Sun reflecting off the optical edges and entering the telescope. This solar glint appears primarily as two lobes, originating from a few petals oriented with edges broadside to the Sun. The overall intensity of scattered light must be limited to levels below that from the exozodiacal background so that measurement integration times are not significantly impacted. Section C.2.1 describes the petal edge technology required to meet the scattering requirements.

### C.2.1 S-1: Controlling Scattered Sunlight

#### S-1: Controlling Scattered Sunlight

**Description:** Limit edge-scattered sunlight and diffracted starlight with optical petal edges that also handle any stowed bending strain.

**SOA:** Edges manufactured with machining and electrical discharge machining do not meet scatter requirements; etched amorphous metal edges meet scatter specs integrated in-plane shape tolerance is to be demonstrated.

**Needed capability:** Integrated petal optical edges maintaining precision in-plane shape requirements after deployment trials and limit solar glint contributing  $<10^{-10}$  contrast at petal edges.

**Supported Missions or Mission Concepts:** Starshade Probe for WFIRST, HabEx

The starshade requires an optical edge that can (1) be integrated to the petal's structural edge, (2) meet and maintain precision in-plane shape requirements after deployment and over a broad thermal environment, and (3) limit the intensity of solar glint such that a  $10^{-10}$  contrast sensitivity can be achieved. Based on analyses for an Exo-S petal architecture<sup>91</sup> it was determined that the optical edges should have a sharp beveled edge and/or low reflectivity to meet the requirement on solar glint. A guideline resulting from the Exo-S study is that the product of edge radius and reflectivity should be less than or equal to  $12 \mu\text{m}\%$ , while at the same time maintaining a stable in-plane shape, limiting thermal deformation of the petal and accommodating any stowed bending strain (some mechanical deployment architectures may not have bending strain issues).

The S5 Technology Development Plan specifies the scatter performance in terms of the total sunlight flux scattered by the starshade into the telescope, in units of the visual magnitude of the signal measured at the focal plane. S5's Milestone 3 aims for "Optical edge segments

demonstrate scatter performance consistent with solar glint lobes fainter than visual magnitude 25 after relevant thermal and deploy cycles” expected by November 1, 2019. S5’s overall scheme for optical edges includes independently manufactured meter-scale segments with the needed edge properties which are then precision-bonded onto the petal. This simplifies the design by separating structural requirements of the petal from the scattering performance of the edges.

### **Current State-of-the-Art:**

Suitable edge materials have been demonstrated in several configurations, including very sharp ( $< 1 \mu\text{m}$  radius of curvature) edges and blunt edges with low reflectivity. A thorough investigation into the viability of various coatings on blunt-edged metal was performed in a 2015 TDEM<sup>92</sup> (PI Tiffany Glassman/Northrop Grumman) which included adhesion tests, thermal cycling, and humidity exposure.

Another approach uses amorphous metals fabricated with very sharp and stable ( $< 0.5 \mu\text{m}$  radius of curvature) edges. Chemical etching techniques were used to manufacture the edges as it provides a means to produce the necessary beveled edge and can be implemented at the meter-scale with micron-level in-plane tolerances. The solar glint performance of these coupons was also established using a custom scattered-light testbed and measurements indicate that the scattered flux is predominantly dimmer than the predicted intensity of the background zodiacal light over a broad range of sun angles.<sup>93</sup>

While suitable performance specifications on solar glint have been demonstrated at the coupon level for these amorphous metal edges, in-plane shape requirements have not yet been met on meter scale prototypes, nor have these been demonstrated in relevant environments.

### **Progress Over the Last Year:**

The S5 Technology Development Plan defined the detailed maturation path for the starshade optical edges, which includes demonstration of edge segment scatter properties after thermal and deployment cycles.

Steeves et al (2018)<sup>94</sup> describes details of the ongoing progress of S5 towards the maturation of starshade optical edges. Half-scale optical edge prototypes (0.5 meters long) were produced with the chemical etching process and measured for in-plane accuracy at the level of 10-15  $\mu\text{m}$  RMS, or close to the requirement.

The introduction of anti-reflection coatings such as Enbio SolarBlack and Acktar Magic Black was investigated further and it was found that the etched amorphous metal edge is blunted to a radius of curvature of 15-20 microns once the coating is introduced, and the scattered light performance is no longer met.

Stealth edges can greatly reduce the scattering lobes; this concept uses a serrated petal edge to reduce the amount of light reaching the telescope from specular reflection off the edges. Propagating the measured properties of coupon-scale stealth edges, reflected solar glint is reduced by more than 2 magnitudes.

A Phase II SBIR award to Photonic Cleaning Technologies will investigate a cleaning and protection method for the starshade edges using a polymer coating.

**Next Steps:**

During 2019, per the S5 Technology Development Plan, a fixed-angle scatterometer will be constructed at JPL for demonstrating scattering performance of long edge segments after exposure to the relevant environments (repeated thermal and stow/unstow cycles) aiming to demonstrate the milestone late in 2019.

Once this demonstration has been reached, further engineering work will investigate the effects of contamination, for example quantifying requirements on dust build-up during pre-launch handling, and also the effects of the L2 micrometeoroid environment. Prospects for using stealth edges could also be investigated.

**C.2.2 S-2: Starlight Suppression and Model Validation****S-2: Starlight Suppression and Model Validation**

**Description:** Experimentally validate at flight-like Fresnel numbers the equations that predict the contrasts achievable with a starshade.

**SOA:** Validated optical model with demonstrated  $10^{-6}$  suppression at white light, 58 cm mask, and F (at the starshade tips) = 210;  $6 \times 10^{-6}$  suppression demonstrated at F=15;  $4.6 \times 10^{-8}$  suppression demonstrated at F ~ 27

**Needed capability:** Experimentally validated models with total starlight suppression  $\leq 10^{-8}$  in scaled flight-like geometry, with F between 5 and 40 across a broadband optical bandpass. Validated models are traceable to  $10^{-10}$  contrast system performance in space.

**Supported Missions or Mission Concepts:** Starshade Probe for WFIRST, HabEx

Because full-scale demonstrations of starlight suppression are not feasible on the ground (the telescope-starshade separation is several Earth radii), the validation of the optical properties of a starshade relies heavily on optical modeling and sub-scale validation. In order to accurately compute  $10^{-10}$  contrast, these models must be validated against ground tests, especially in the same diffraction regime (same Fresnel number) as in-flight observations. Harness, Shaklan, Cash, and Dumont (2018)<sup>95</sup> present a comparison of 1D fast modeling approaches based on Green's theorem and those based on 2D Fresnel propagation.

The S5 Activity has two milestones (M/S #1A and M/S 1B) aiming to demonstrate, with a sub-scale starshade in a flight-like configuration, better than  $10^{-10}$  contrast at the inner working angle, first in narrow-band then in broadband ( $\Delta\lambda/\lambda = 10\%$ ) visible-band light, for a Fresnel number  $\leq 15$  (at the longest wavelength). A third Milestone (M/S #2) will use the same testbed to measure the performance of a set of sub-scale starshades with deliberately introduced defects with the goal of showing that the diffraction models agree with measurement to within 25%.

**Current State-of-the-Art:**

Several experiments over the last decade demonstrate the viability of creating a dark shadow with a starshade to contrasts better than  $10^{-10}$  just outside the petal edge. They include lab demonstrations at the University of Colorado,<sup>96,97</sup> Northrop-Grumman,<sup>98,99</sup> Princeton University,<sup>100,101</sup> larger scale tests in a dry lakebed by Northrop Grumman as part of their TDEM-12,<sup>102</sup> and larger scale demonstrations using the McMath Pierce solar observatory on astronomical objects. These measurements are summarized in the 2018 edition of the ExEP Technology Plan Appendix. The best contrast performance to date has been reported from the Princeton Testbed (**Figure 13**) and this testbed is being used by the S5 to achieve its milestones #1A, #1B, and #2.

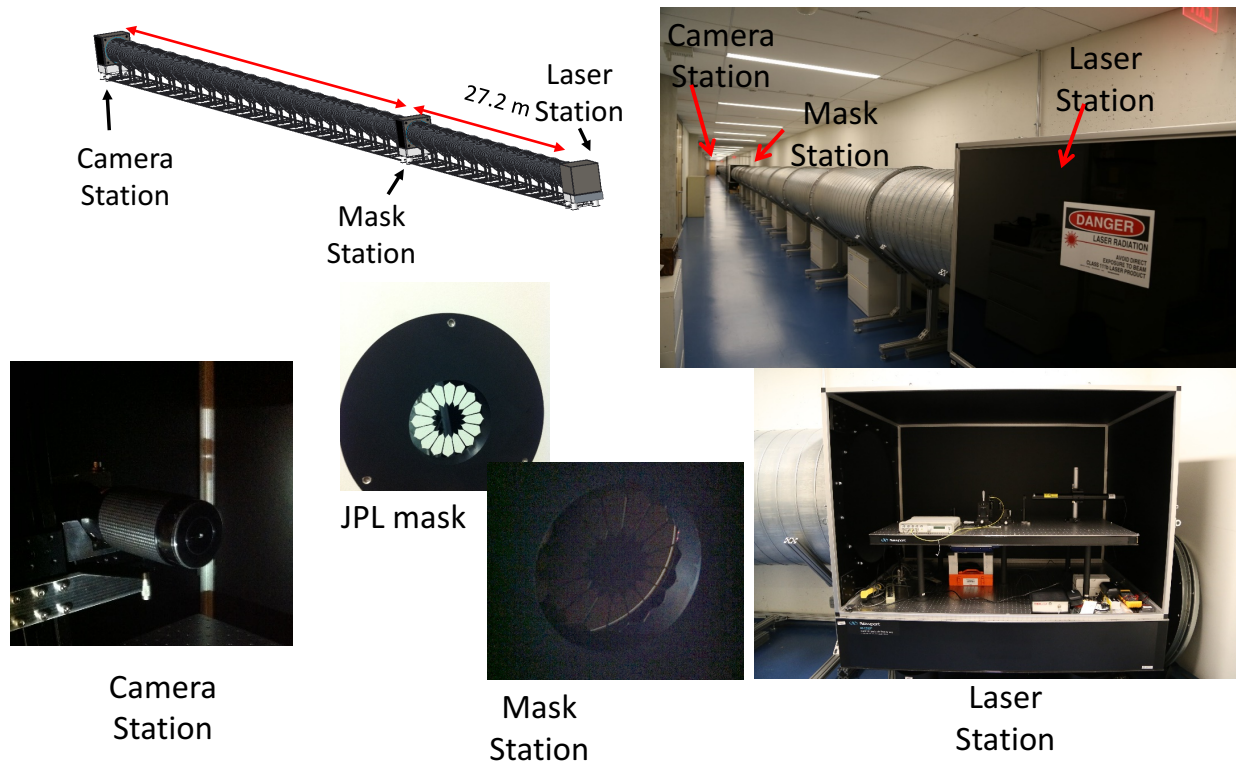


**Figure 13:** Schematic diagrams and pictures of the Princeton University starshade performance testbed (TDEM-12; PI Kasdin). Tubes are each 2 m in length and 1 m in diameter. They are painted with low-reflectivity black paint and include baffles to suppress stray light. (Figure credit: Anthony Harness)

### Progress Over the Last Year:

The Princeton testbed shown in **Figure 13** operates a subscale starshade at a Fresnel number of 13, in the middle of the range of Fresnel numbers at which the HabEx mission will operate, and similar to the WFIRST Rendezvous Fresnel number. In the past year, improvements in the thermal stability of the testbed and in the manufacture of the subscale starshade had led to a published average suppression of  $4.8 \times 10^{-8}$  <sup>103</sup> limited by defects in the subscale starshade at the micron scale. The optical diffraction model has reproduced the experimental results when the as-built defects were included.<sup>104</sup> Further refinements of the mask have allowed improved suppression at the IWA, limited by effects of vector diffraction at the petal valleys. The vector diffraction effects appear to be important for the sub-scale starshade but will be present at a negligible level in the on-orbit configuration.<sup>105</sup> The team is on the cusp of achieving milestone #1A and review by the ExoTAC is expected in early 2019.

### Next Steps:

The tests in the Princeton tube will continue with a further improved subscale starshades until S5 milestones 1A, 1B, and 2 are achieved. These are all expected to occur in calendar year 2019 and to result in closing the technology gap.

To further test the robustness of the optical diffraction model beyond the scope of S5 in preparation for a future starshade mission, engineers could operate the Princeton testbed at longer wavelengths (NIR), also enabling larger starshades.

The X-ray calibration facility (XRCF) facility at Marshall Space Flight Center has a 500 m long, 1.2 m diameter tube, and models have indicated that a subscale starshade test in this facility would be able to achieve flight-levels of suppression and contrast at flight-like Fresnel numbers. It will be considered as a candidate for future subscale starshades in order to validate further the robustness of the optical models in a different region of parameter space.

### C.3 Formation Sensing and Control

The starshade and telescope must maintain a formation such that the darkest part of the shadow, which may only be slightly bigger than the telescope itself, overlaps with the telescope entrance. The S5 activity has matured a sensing scheme based on a pupil-plane camera (such as CGI's LOWFS camera) operating out-of-band with the starshade science observations. The shadow of the starshade is not as deep out-of-band and an Arago spot forms at the center of the pupil and acts as a relative alignment reference. As of January 2019, following the ExoTAC review of the Starshade Technology Activity S5's Milestone 4, this technology gap is closed for the requirements listed in the ExEP Technology List and for the class of missions considered within S5.

#### C.3.1 S-3: Lateral Formation Sensing

##### S-3: Lateral Formation Sensing

**Description:** Demonstrate lateral formation flying sensing accuracy consistent with keeping telescope in starshade's dark shadow.

**SOA:** Sub-scale lab demonstration showing ability to center telescope within  $\pm 1$  m of starshade shadow.

**Needed capability:** Demonstrate sensing lateral errors  $\leq 0.24$  m  $3\sigma$  accuracy at the flight signal-to-noise ratio at scaled flight separations. Demonstrate control algorithms with scaled lateral control error  $\leq 1$  m radius.

**Supported Missions or Mission Concepts:** WFIRST, Starshade Probe for WFIRST, HabEx

Maintaining precise alignment of the telescope, starshade, and target star is imperative to achieving the science goals of an exo-Earth-finding mission. The rapid degradation of starlight suppression as a starshade and space telescope moves radially out of alignment places a tight constraint on the lateral position of the starshade relative to the telescope-star line of sight. According to mission studies for Exo-S,<sup>106</sup> New Worlds Observer,<sup>107</sup> and THEIA,<sup>108</sup> a starshade spacecraft must control its lateral position to within about  $\pm 1$  m of the telescope boresight to keep the telescope within the darkest shadow. The benign disturbance environment at either Earth-Sun L2 or an Earth Drift-Away orbit makes controlling to the meter level straightforward with conventional chemical thrusters: better than 10 cm-level-control is regularly achieved in low Earth orbit for rendezvous and docking.<sup>109</sup> The challenge, however, is to sense the lateral position error to within  $\pm 30$  cm. Comparatively, the axial separation distance, or range, between the starshade and telescope is loosely controlled to only within  $\pm 250$  km,<sup>110</sup> with

sensing knowledge to within  $\pm 1$  km. The range is measured by a proximity radio with two-way ranging. These requirements are well within the state-of-the-art.

#### **Current State-of-the-Art:**

The starshade compatibility study of WFIRST has developed a sensing concept that uses a pupil plane sensor in the telescope for fine formation sensing using light from outside the science bandwidth. In the case of WFIRST, this sensor is the CGI's LOWFS camera. The concept exploits the fact that starshade petal shapes are optimized for extreme suppression within a particular bandpass. Out-of-band, the spot of Arago (see Figure 14) appears at a much brighter level than in-band, and thus the pupil plane signal can be used to sense the misalignment of the starshade and telescope to the centimeter scale. Simulations and scaled benchtop laboratory demonstrations have shown that this is a feasible approach.<sup>111</sup> While the work so far has focused on a potential WFIRST/starshade rendezvous mission, this procedure should be straightforward to scale to larger starshades and space telescopes with different science bands.

Bottom et al (2017)<sup>112</sup> presented a model of formation sensing with a WFIRST-like system, using the pupil-plane camera of the LOWFS, with a bandpass different from the starshade science observations. The approach shows that a library of pre-computed pupil-plane simulations can be fitted to the sensed image with the misalignment as a free parameter, achieving centimeter-level sensitivity to the misalignment. The authors, in addition, used a laboratory testbed at flight Fresnel number to begin validating the model.

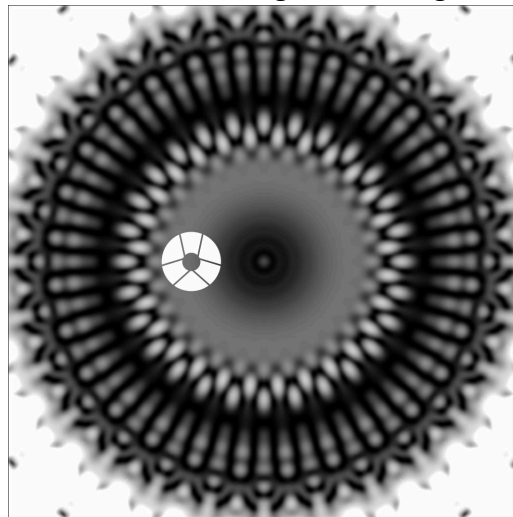


Figure 14: An out-of-band simulated starshade shadow with the WFIRST pupil superposed. The spot of Arago is visible at the center of the shadow. Reproduced from Bottom et al. (2017).

#### **Progress Over the Last Year:**

The starshade Technology Development Activity matured this technology in 2018 in achieving their Milestone #4 (Figure 12).<sup>113</sup> The Starshade Lateral Alignment Testbed Experiment (SLATE) at JPL consists of a collimated source, a 6 mm-diameter starshade, a WFIRST pupil simulator and a pupil plane sensor placed at a scaled distance of about 2 m from the starshade, preserving the Fresnel number of the flight configuration. The model used to generate the pupil-plane image library was validated against testbed measurements. Finally, a model of the

lateral sensing accuracy achieved on the scaled demonstration will be interfaced with a simulation of the spacecraft control loop in order to demonstrate that the sense and control concept achieves the required precision.

The review of the S5 work by the Exo-TAC has formally closed this technology gap and ExEP will no longer be tracking it. The Arago spot sensing scheme is broadly scalable to different starshade and telescope sizes. The control side of the equation is considered to be standard engineering, and the S5 team performed a spot check was done that the spacecraft control loop works with a 52-meter HabEx starshade.

#### C.4 Deployment Accuracy and Shape Stability

To function as an occulter, casting a dark shadow on the formation-flying telescope, the starshade must accurately deploy to, and maintain the correct shape. There are two technologies that must be matured in order to close this gap. First, the petals must meet the in-plane shape and maintain that shape stably over the full range of operational environments (see Sect. C.4.1). Second, Petal Positioning and Opaque Structure (Sect. C.4.2) is the technology needed to deploy petals from their stowed launch configuration to within the required tolerances and maintain that position with an opaque barrier to starlight.

To ensure that S5 is developing the best packaging and deployment architecture, NASA ExEP completed a trade study in 2018. The trade study team was made up of a multi-institutional team of engineers from inside and outside of NASA. The recommended “wrapped” approach (the original S5 baseline) uses a radially deployable perimeter truss, from which attached concentrically-wrapped petals would unfurl (**Figure 15**; left). The architecture leverages the Northrup Grumman Astro Aerospace AstroMesh communications antenna, successfully flown with NASA’s Soil Moisture Active Passive mission (Astro Aerospace is a subsidiary of Northrop Grumman). This is the architecture adopted by the NASA Exo-S mission concept study for 30–40 m-class starshades. Mission concepts currently under consideration, including the Starshade-WFIRST Rendezvous and HabEx, also plan to use this architecture.

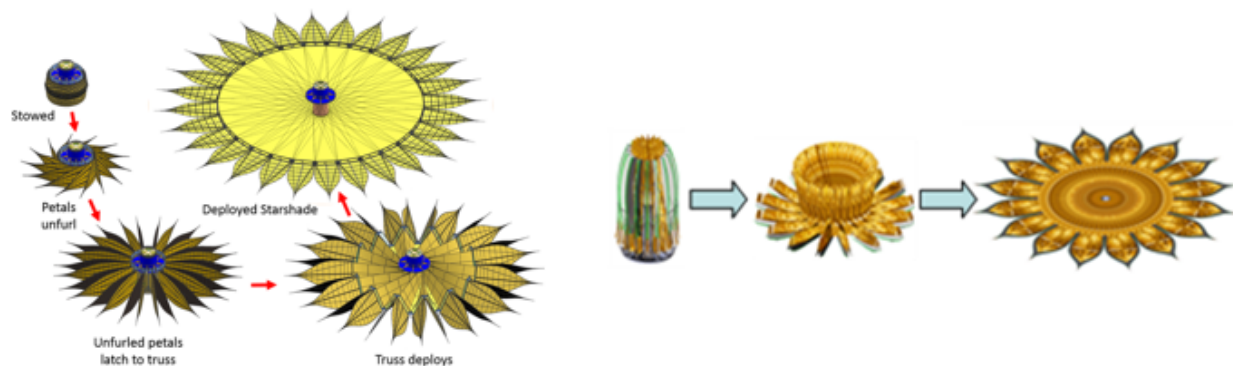


**Figure 15:** Illustration of the two candidate stowing and deployment architectures considered in a trade study: (Left) the “wrapped” architecture<sup>114</sup>; (right) the “folded” architecture<sup>115</sup>.

The S5 Technology Development Plan defines ten milestones related to the Deployment Accuracy and Shape Stability technology gap (Milestones 5A to 8B in Figure 12). Five of these

are scheduled for completion in 2019, in time to inform Astro2020. The remaining five milestones, needed to fully retire the gaps, are scheduled for 2023.

#### **C.4.1 S-4: Petal Shape and Stability**

##### **S-4: Petal Shape and Stability**

**Description:** Demonstrate a high-fidelity, flight-like starshade petal meets petal shape tolerances after exposure to relevant environments.

**SOA:** Manufacturing tolerance ( $\leq 100 \mu\text{m}$ ) verified with low fidelity 6 m prototype and no environmental tests. Petal deployment tests conducted but on prototype petals to demonstrate rib actuation; no shape measurements, no long-duration stowage tests.

**Needed capability:** Tolerances demonstrated to  $\leq 100 \mu\text{m}$  (in-plane tolerance profile for a 7 m petal on the 34 m-diameter Exo-S design; tolerances scale roughly linearly with starshade diameter) with flight-like, minimum half-scale petal fabricated and maintains shape throughout mission lifetime with exposure to relevant environments and is optically opaque.

**Supported Missions or Mission Concepts:** Starshade Probe for WFIRST, HabEx

#### **Current State-of-the-Art:**

The TDEM-09 activity led by PI Jeremy Kasdin of Princeton established the state-of-the-art, using the mathematically optimized shape approach, and successfully demonstrated the allocated manufacturing tolerance ( $\leq 100 \mu\text{m}$ ) of an early 6 m petal prototype. The low fidelity prototype did not include an optical shield that makes the petal opaque, optical edges that effectively minimize the effect of scattered and diffracted sunlight, or undergo environmental testing. A starshade shape tolerancing analysis by Shaklan et al (2017)<sup>116</sup> investigated a set of starshade/telescope combinations, including a hypothetical 26 m starshade paired with WFIRST and a 72 m starshade paired with a 4 m HabEx. A key finding was that physical requirements on the petal shape scale roughly linearly with starshade size.

#### **Progress Over the Last Year:**

The purpose of the petal subsystem of the starshade is to hold the optical edges in the correct position. The current petal design has a carbon fiber composite skeleton that provides a number of thermal stability, flexibility for stowing, and stiffness when deployed. To carry out these tests, a 4-m long (2/3 scale) prototype petal was built by Tenedeg (Figure 16).

**Next Steps:**

The S5 Technology Development Plan defined four milestones related to the petal subsystem, two of which are scheduled for late 2019 and two of which are scheduled for 2023. Milestone 5A will carry out shape measurements of the full-scale prototype petal with thermal and deployment cycling to validate that critical shape features are accurate to within 70  $\mu\text{m}$ . In parallel, milestone 6A will demonstrate with a validated model that on-orbit thermal stability requirements can be met. To advance towards these milestones, the prototype petal will be thermally cycled and its shape measured by Tendeg in early 2019, with supporting thermal and mechanical modeling being carried out in parallel.



Figure 16: prototype petal.

**C.4.2 S-5: Petal Positioning Accuracy and Opaque Structure****S-5: Petal Positioning Accuracy and Opaque Structure**

**Description:** Demonstrate that a starshade can be autonomously deployed to within its budgeted tolerances after exposure to relevant environments.

**SOA:** Petal deployment tolerance ( $\leq 1$  mm) verified with low fidelity 12 m prototype and no optical shield; no environmental testing (Exo-S design).

**Needed capability:** Deployment tolerances demonstrated to  $\leq 1$  mm (in-plane envelope) with flight-like, minimum half-scale structure, with petal optical edge interfaces, that is optically opaque when deployed, and includes interfaces to launch restraint. Verify the structure will meet shape stability (petal edge position) after exposure to relevant environments throughout mission lifetime.

**Supported Missions or Mission Concepts:** Starshade Probe for WFIRST, HabEx

**Current State-of-the-Art:**

Petal deployment was demonstrated to meet tolerances at the 12 m scale using an off-the-shelf retrofitted 12 m diameter Astromesh Antenna and four representative petals. As a more flight-like proof of concept, a 10 m diameter inner disk subsystem was built deploying the inner disk

from a stowed configuration (see Figure 17). To demonstrate the deployment of an opaque optical shield, a 5 m prototype was developed and partially integrated with its inner disk (see **Figure 18**). The optical shield builds on an origami fold pattern that allows for proper interfaces to the central spacecraft and perimeter truss disk.

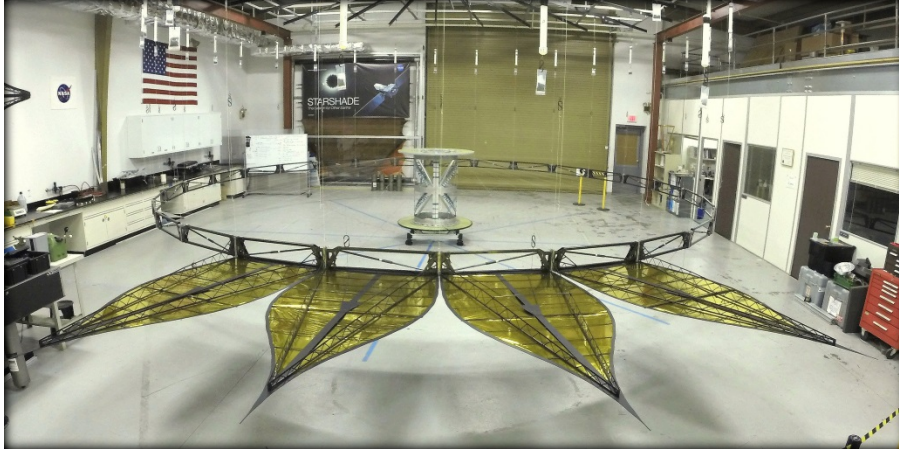


Figure 17: A 10 m inner disk subsystem prototype demonstrates deployment from a stowed configuration and final positioning of the starshade petals. The testbed also allows for studying the petal-inner disk interface. The entire testbed has its weight offloaded by a gravity compensation system. (Image: JPL/Caltech)

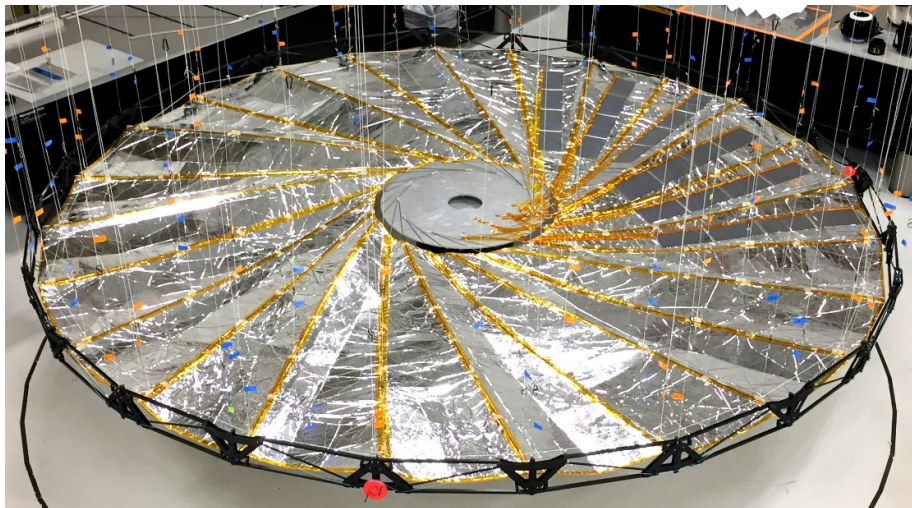


Figure 18: A 5 m prototype starshade inner disk mechanical structure along with its opaque optical shield. The optical shield is constructed of two layers of Mylar separated by a low-density polyurethane foam. Vertical strings are part of the gravity-offloading ground support equipment, designed through an SBIR with Rocco, LLC. (Image: JPL/Caltech)

### Progress Over the Last Year:

The deployable opaque structure is separated into three separate subsystems that the S5 Activity will develop to mature this technology: 1. The inner disc truss bay assembly (Figure 19), 2. The inner disc subsystem (**Figure 18**), and 3. The Petal Launch and Unfurl Subsystem (PLUS; **Figure 20**).

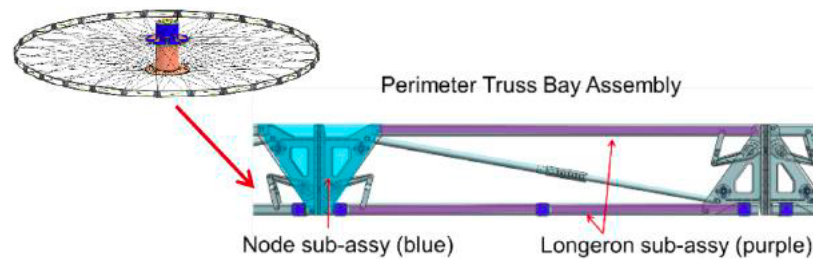


Figure 19: Truss Bay Assembly (Image: JPL/Caltech)

Advancing beyond the 5-meter origami folded inner disk subsystem demonstrated in 2018, a 10-meter inner disk subsystem has been designed and evaluated using a finite element model, with construction planned in 2019.

A preliminary truss bay sub assembly (including a flight-like longeron and node) to be used for thermal testing has been designed.

HabEx's interim report adopted a 52-meter diameter starshade, which is exactly a factor of 2 larger than the reference starshade to be developed by the S5 activity. The technology matured for the 26-meter starshade is expected to be applicable for sizes up to and including the HabEx starshade.



**Figure 20:** The Petal Launch Restraint and Unfurler Subsystem testbed at JPL. It was designed through an SBIR led by Tendeg, LLC. The prototype serves as a proof of concept for the unfurling of the starshade petals from a fully wrapped and stowed launch configuration. The vertical bars serve to restrain the petals from unfurling further and inadvertently making contact with each other. (Image: JPL/Caltech)

An SBIR Phase II was awarded to Tendeg to further develop a motor for autonomous deployment of the edge perimeter truss.<sup>117</sup>

### Next Steps:

The S5 Activity's milestones 7A, 7C, and 8A in Figure 12 are expected to complete in 2019. The dimensional stability of a truss bay longeron and node subassembly prototype after thermal cycles will be demonstrated to be stable to within 300  $\mu\text{m}$  after repeated thermal cycling. A thermal model, validated against measurements, will be used to demonstrate that the truss bay will be thermally stable to within 200  $\mu\text{m}$  on-orbit. Finally, a 10-meter inner disc subsystem prototype that includes deployment critical features will be shown to deploy within 300  $\mu\text{m}$ . This set of milestones will demonstrate the riskiest portions of the deployment architecture. The final milestones for 2023 will build on the experience of 2019 to demonstrate the robustness to the on-orbit thermal environment of a full truss bay assembly, and demonstrate the accurate deployment of a full inner disk subsystem.

A prototype PLUS system will be assembled in 2019 in order to allow petals (see Sect. C.4.1) to be demonstrated for shape stability after repeated stowing and deployment.

HabEx's final report, expected in 2019, will include further analysis and discussion of the 52-meter starshade.

## D MID-IR CORONAGRAPH/TELESCOPE TECHNOLOGY GAPS

The ExEP has traditionally focused its coronagraph technology development on visible wavelengths because for a fixed telescope aperture size, the available inner working angle to study the habitable zones of nearby stars degrades linearly with wavelength. However, in the mid-infrared where a planet could be detected in thermal emission rather than in reflected starlight, the starlight suppression requirement is less stringent. The Origins Space Telescope (OST)<sup>118</sup> is a NASA-chartered large mission concept study focused on far- and mid- infrared science, formulating its mission in parallel with those of HabEX and LUVOIR. The OST team has developed two exoplanet-related science cases with technology gaps and candidate technologies appropriate for tracking and potential development by the ExEP. The first is an ultra-stable mid-infrared detector needed to take a factor ten step beyond JWST's detection capabilities in transit spectroscopy and study the atmospheres of rocky Earth-sized planets orbiting M dwarf stars (see Section E.5.1). The second is a mid-infrared coronagraph capable of directly imaging and spectrally characterizing cool giant exoplanets.

Additionally, planets in the habitable zone of the nearby Alpha Centauri system could be directly imaged with 10 m-class telescopes on the mid-infrared.<sup>119</sup> This will be attempted from the ground using the VLT,<sup>120</sup> but is potentially a science goal for a future mid-infrared space mission.

The mid-infrared direct imaging technology gaps and the technologies required to close them are shown in Figure 21. These are parallel to those for visible/near-infrared direct imaging and are contrast (Section D.1), angular resolution (Section D.2), and detection sensitivity (Section D.3). The gaps are in yellow font and the technologies that address these gaps are shown in blue.

The 2017 Technology Plan Appendix included a mid-IR spectral coronagraph technology (CG-11), a single instrument-level technology. In 2018, the OST STDT team, with the help of the ExEP, broke apart the technology gap to sub-system level technologies that need to be matured, each of which was accepted to the prioritized ExEP Technology List. Consequently, the instrument-level technology CG-11 was replaced on the Program's list.

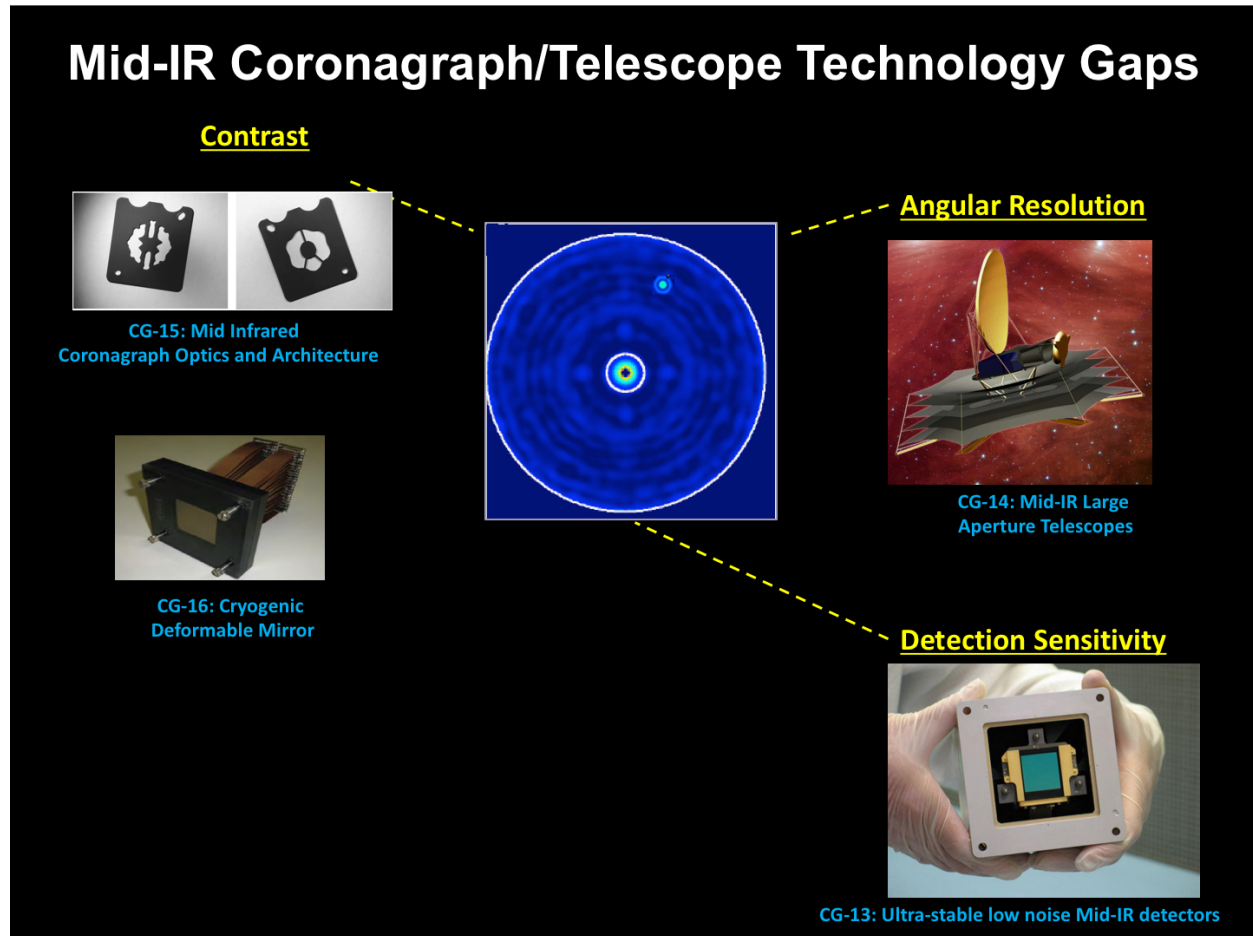


Figure 21: The ExEP mid-infrared coronagraphy technology gaps.

### D.1 Contrast

A coronagraph for use on a mission observing in the mid-infrared can build on technologies originally developed for the Japan Aerospace Exploration Agency's (JAXA's) Space Infrared Telescope for Cosmology and Astrophysics (SPICA).<sup>121</sup> These technologies require specific optimization for the mid-infrared: key optics must operate at cryogenic temperatures in order to minimize thermal background noise, for example a deformable mirror capable of actuation at 5 K. On the other hand, detecting planets in thermal emission rather than in reflected light mitigates the required contrast that a coronagraph must achieve in the mid infrared. Potentially, this allows for looser wavefront and telescope stability requirements as compared to visible/near infrared coronagraphy (for example, fast wavefront sense/control may not be needed).

### D.1.1 CG-15: Mid-infrared Coronagraph Optics and Architecture

#### CG-15: Mid-infrared Coronagraph Optics and Architecture

**Description:** Coronagraph optics and architecture that suppress diffracted starlight by a factor of  $< 10^{-6}$  over a broad mid-IR band (7-30 microns)

**SOA:** The current state of the art for mid-infrared coronagraphs are the three four-quadrant phase masks of JWST-MIRI. These provide narrow-band imaging with contrasts up to  $10^{-4}$  in three narrow bands from 10.65-15.5 micron with inner working angles of 0.33-0.49". The MIRI coronagraphs do not offer spectral dispersion.

**Needed capability:** Contrast should be  $10^{-6}$  at IWA  $3 \lambda/D$  at 10  $\mu\text{m}$ .

**Supported Missions or Mission Concepts:** Origins Space Telescope

The coronagraph architecture requires compatibility with obscured/segmented telescopes (see Sect. B.1 for a discussion of coronagraph technology maturation in the V/NIR). The PIAACMC architecture represents a useful way to reach high contrast at a narrower inner working angle in the mid-infrared, but other architectures are also applicable to this longer wavelength band. Some development in coronagraph optics and architecture technology will overlap with development in the visible band and near infrared, but there are specific optimizations that are needed for the mid-infrared band. In particular, the coronagraph instrument may need to operate entirely at cryogenic temperatures to reduce background noise.

#### Current State-of-the-Art:

The state-of-the-art in mid-infrared coronagraphy are the four-quadrant phase masks on JWST-MIRI (Mid-InfraRed Instrument) which are predicted to achieve contrasts to  $10^{-4}$  at 10.65 to 15.5  $\mu\text{m}$  wavelengths with inner working angles of 0.33 - 0.49" in wide bands (i.e. no spectral dispersion).<sup>122</sup> To achieve its exoplanet imaging science goals, the OST STDT preliminarily estimates that it will need a coronagraph that achieves a contrast  $10^{-6}$  with inner working angle of 0.1" at 10  $\mu\text{m}$ . The maximum spectral dispersion must be sufficient to resolve the 15  $\mu\text{m}$  CO<sub>2</sub> band, implying  $R \sim 500$ . The OST science case and reference design for mid-infrared direct imaging is still in development. A high contrast (i.e. using active wavefront control) mid-infrared coronagraph has not yet been demonstrated.

#### Progress Over the Last Year:

The Origins STDT defined a reference architecture in their interim report, including a Mid-infrared Imager, Spectrometer, and Coronagraph (MISC) instrument that baselines a coronagraph instrument with a cryogenic deformable mirror to enable contrast performance at wavelengths as short as 5 microns.

#### Next Steps:

JWST is scheduled for launch in 2021, and will represent for the first time a systems validation of space-based mid-IR coronagraphy, though it will not include active wavefront control. Gaining experience in operation of the coronagraphic modes in MIRI are likely to provide lessons for future coronagraph design in this wavelength band. The OST STDT will finalize their reference design and instrument needs from which the technology needs will be identified. Assuming direct imaging of exoplanets at mid-infrared wavelengths will be prioritized, performance of a coronagraph must be demonstrated in a lab environment.

Occulting and apodizing mask designs for the mid-IR can also benefit from parallel efforts at shorter wavelengths, for example using results of the SCDA study (see Sect. B.1.2). If PIAA architecture is needed to minimize the inner working angle, this technology will be advanced by the award of a TDEM16 (PI Belikov, NASA/Ames) to specific, though with no specific focus on mid-infrared optimization.

### D.1.2 CG-16: Cryogenic Deformable Mirror

#### CG-16: Cryogenic Deformable Mirror

**Description:** Flight-qualified deformable mirrors operable at cryogenic temperatures, and their drive electronics.

**SOA:** Lab: MEMS DM with 32x32 actuator count operated at 5k demonstrating 2.6 nm rms repeatability

**Needed capability:** Requirements on actuator stroke, stroke resolution, heat dissipation, and actuator count are TBD but must be operable at cryogenic temperatures.

**Supported Missions or Mission Concepts:** Origins Space Telescope

To correct for wavefront errors, particular due to wavefront errors from the primary and secondary mirror, adaptive optics, i.e. deformable mirrors (DM), are needed. For operation in the mid-IR, the DM must be operable at cryogenic temperatures. Requirements need to be set for actuator stroke length and resolution, actuator density, heat dissipation, and will be set by coronagraph and telescope reference designs that are still in progress.

In addition, systems level studies of a mid-IR coronagraph/telescope system may conclude that wavefront control to achieve  $10^{-6}$  contrast can be performed using a deformable secondary mirror of the telescope, in which case, an instrument-level cryogenic deformable mirror may be unnecessary.

#### Current State-of-the-Art:

Prototype MEMS DMs were developed for the SPICA coronagraph, have been demonstrated for functionality at 95 K, and thermally-cycled.<sup>123</sup> A 32x32 MEMS DM built by Boston Micromachines Corporation was operated at 5 K, and achieved repeatability of 2.6 nm rms over three thermal cycles<sup>124</sup>

#### Progress Over the Last Year:

The Origins STDT defined a reference architecture in their interim report, including a Mid-infrared Imager, Spectrometer, and Coronagraph (MISC) instrument that baselines a deformable mirror in to allow diffraction limited performance at 5  $\mu\text{m}$  (the Origins telescope is specified for diffraction limited performance at 30  $\mu\text{m}$ ). This improves the ability to perform transit spectroscopy of the atmospheres of rocky planets orbiting M-dwarf stars.

#### Next Steps:

The requirements for this particular technology must be developed more thoroughly. The necessary stroke length for operations in the 7-30  $\mu\text{m}$  wavelength range must be verified and shown to be compatible with the existing deformable mirror technology (such as the MEMS). Heat dissipation requirements must be established and demonstrated. The actuator density and actuator count must be determined based on science objectives. Finally, a full cryogenic coronagraph must be demonstrated in a lab environment.

## D.2 Angular Resolution

### D.2.1 CG-14: Mid-IR Large Aperture Telescopes

#### CG-14: Mid-IR Large Aperture Telescopes

**Description:** Cryogenic (4K), large-aperture (> 6m) telescopes to achieve high angular resolution needed to direct-image cool exoplanets in wide orbits (> 5 AU)

**SOA:** JWST Be mirror segments may meet requirements now; TRL 3 exists for other materials like SiC. Cryogenic low-dissipation actuators exist at TRL 3-5.

**Needed capability:** Develop a feasible and affordable approach to producing a 6-m-class telescope with sufficiently high specific stiffness, strength, and low areal density to be launched; while maintaining compatibility with cryogenic cooling and FIR surface quality/figure of  $\sim 1\mu\text{m}$  rms. Material property measurements at cryogenic temperatures for structures and optics such as damping, emissivity, thermal conductivity, etc.

**Supported Missions or Mission Concepts:** Origins Space Telescope

A future large aperture infrared space telescope in the 10-m class must have sufficiently high specific stiffness, strength, and low areal density to be launched, while maintaining compatibility with cryogenic cooling (to as low as 4K). The necessary surface quality optimized for the mid-infrared is relatively modest compared to UV/V/NIR telescopes and may be of order  $1\mu\text{m}$  rms. A telescope of that size will be segmented, folded for launch, and autonomously deployed. JWST is a 6.5 m segmented telescope that is passively cooled for operations in the mid-infrared and has advanced deployment technology.

#### Current State-of-the-Art:

JWST Beryllium mirror segments will operate at 40 K and may meet requirements now; Spitzer's Beryllium mirror operated at 5.5 K with 67-nm rms surface figure. SiC or Aluminum may be a lower cost alternative.

#### Progress Over the Last Year:

The Origins design team considered alternatives for a cryogenic telescope meeting the launch fairing requirements. For the concept presented in their interim report,<sup>125</sup> selected an off-axis 3-mirror anastigmat design with a 9.1-m, segmented primary mirror, with a surface figure defined by the requirement to be diffraction-limited at  $30\mu\text{m}$ . Five materials were remaining as potential candidates at the time of the interim report: beryllium, aluminum, AlBeMet (an aluminum/beryllium composite), silicon carbide and fused silica glass.

A separate concept for a segmented, linearized space telescope optimized for coronagraphy<sup>126</sup> with one dimension was presented as an alternative approach to imaging terrestrial planets around FGK-type stars.

#### Next Steps:

The Origins team will continue studying reference designs and mirror material studies will provide an assessment of the maturity of mid- and far-IR telescope components. For example, for some solutions, cryogenic low dissipation surface figure actuators, if available, may save expensive cryo-figuring and allow use of cheaper materials. The Origins final report is expected in 2019. The Systems-Level Segmented Study by Lockheed will deliver a report in 2019 looking at error budgeting and additional trades for segmented cryogenic telescopes. Alternative architectures, such as linear or sparse apertures, should be considered.

## D.3 Detection Sensitivity

### D.3.1 CG-13: Low-noise Mid-IR detectors

#### CG-13: Low noise Mid-IR detectors

**Description:** Low noise and detectors for the mid-infrared band (7 - 20 microns) enabling exoplanet direct imaging.

**SOA:** JWST/MIRI

**Needed capability:** noise requirements TBD, likely to be 10 x better than JWST/MIRI

**Supported Missions or Mission Concepts:** Origins Space Telescope

A mid-infrared coronagraph operating in the 7-30  $\mu\text{m}$  band requires low noise detectors in order to have acceptable signal to noise on an exoplanet while performing spectroscopy at a resolution of 100-500. The exact needed noise performance must be studied in more detail; it is possible that the present-day state-of-the-art (e.g. JWST/MIRI) is acceptable.

Wavefront sensing for a mid-infrared coronagraph could be performed using an architecture similar to that of a UV/V/NIR coronagraph (WFIRST, HabEx, LUVOIR; see Sect. B.2.1), using out-of-band light and thus require ultra-low noise visible detectors such as those being matured by WFIRST (See Sect. B.4.1).

#### Current State-of-the-Art:

JWST's MIRI uses arsenic-doped silicon impurity band conduction (IBC) detector arrays,<sup>127</sup> which have demonstrated read noise of 14 e<sup>-</sup> (in Fowler sampling mode) and 0.2 e<sup>-</sup>/s dark current. These are similar technology to that previously flown on Spitzer's Infrared Array Camera.

#### Progress Over the Last Year:

The OST interim report<sup>128</sup> adopted present-day state-of-the-art IBC detector arrays as a baseline for the MISC instrument. The OST final report, which is expected to include a detector technology roadmap, will better specify whether there is a gap between current performance and the OST science needs.

#### Next Steps:

Requirements must be developed for mid-infrared coronagraphy to determine whether the IBC detectors are sufficient as measured on the ground in MIRI testing and on orbit with Spitzer/IRAC. JWST is expected to establish the on-orbit state of the art for mid-IR detectors after its 2021 launch. Alternative doping for IBC detectors (such as Phosphorous) may be considered as a less-costly alternative to arsenic doping for future missions. In addition, the long wavelength HgCdTe detectors under development for the NeoCAM program could be an alternative.

**E OTHER TECHNOLOGY GAPS**

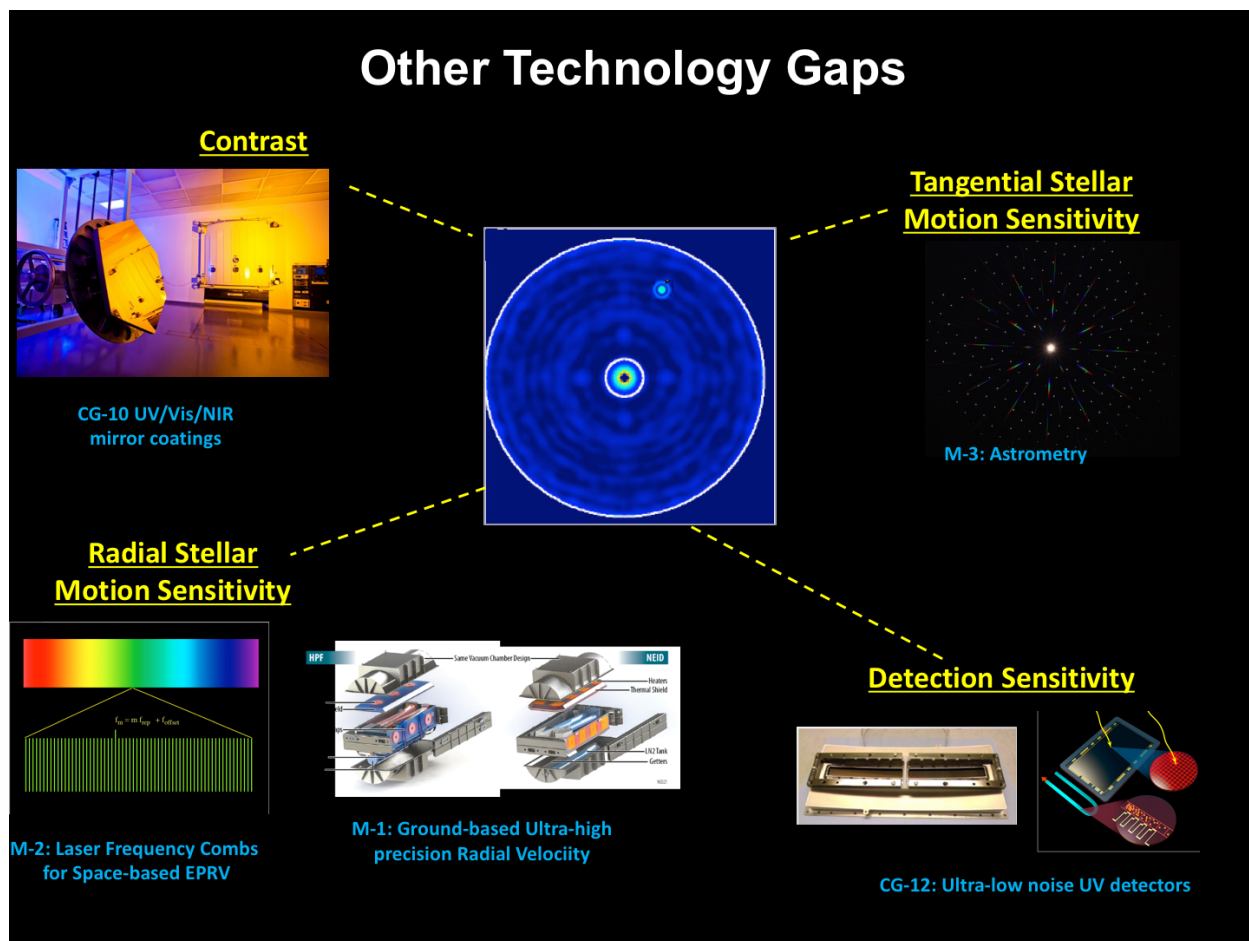


Figure 22: Other technology gaps.

**E.1 Contrast**

**E.1.1 CG-10: UV/V/NIR mirror coatings**

**CG-10: UV/V/NIR mirror coatings**

**Description:** Mirror coatings that enable high reflectivity to wavelengths as short as 90 nm; coating uniformity enables 10-10 coronagraph performance

**SOA:** Al coating with combination of MgF2, LiF, and/or AlF3 overcoat: 90-120 nm: < 50% reflectivity 120-300 nm: 85% reflectivity 300 nm-2 μm: > 90% reflectivity Polarization differences between orthogonal polarization states, uniformity, and durability of coatings on large optics is unknown. Flight: HST uses MgF2; 85% reflectivity at wavelengths > 120 nm; 20% reflectivity for wavelength < 120 nm

**Needed capability:** A mirror coating that that achieves 90-120 nm: > 70% reflectivity; 120-300 nm: > 90% reflectivity; 300 nm-2 μm: > 90% reflectivity; Polarization phase and amplitude difference < 1% between orthogonal polarization states; Uniformity enables 10-10 coronagraph contrast performance.

**Supported Missions or Mission Concepts:** LUVOIR, HabEx

The measurement of broad atmospheric features in the ultraviolet band can enhance the direct detection and characterization of exoplanets. For example, at wavelengths shortward of 300 nm, the reflectivity of planets with O<sub>3</sub> in their atmosphere (such as in an Earth-like planet) is

very low, while a different reflectivity cutoff shortward of 220 nm occurs for planets with SO<sub>4</sub>-rich atmospheres (such as a Venus-like planet).<sup>129</sup> While a future space observatory (such as HabEx or LUVOIR) could be driven to a wavelength cutoff less than 100 nm by general astrophysics science goals, wavelengths less than 200 nm are not likely to benefit exoplanet science directly. However, a space mission that requires both high throughput at wavelengths < 120 nm and wavefront uniformity for coronagraphy must develop appropriate mirror coatings. Coatings are needed to protect aluminum optics, which are reflective to a wide band of light, including at  $\lambda < 120$  nm, from oxidation.

Non-uniformities in these coatings, which may also change with time, can induce cross-polarized wavefront errors, frustrating standard wavefront control with a DM. Hence, achieving 10<sup>-10</sup> contrast in a visible/near-IR coronagraph is likely to require coatings to be uniform to the 0.5% level. The ExEP is therefore interested in technology development particularly in the area of coating uniformity.

#### **Current State-of-the-Art:**

The state-of-the art in space UV mirror coatings is HST and the Galaxy Evolution Explorer, which used aluminum optics coated with a thin layer of MgF<sub>2</sub>. The reflectivity was > 85% for  $\lambda > 120$  nm but dropped to 20% at shorter wavelengths. Hennessy et al (2016)<sup>130</sup> report 2 nm rms coating uniformity for multi-layer coatings on small samples. Quijada et al. (2017)<sup>131</sup> report hot coating processes, under development at GSFC and capable of extremely thin dielectric deposition on aluminum down to 3 nm thickness, allowing for high reflectivity below 100 nm while maintaining broadband performance into the near-infrared. Uniformity for larger mirrors depends strongly on the specific coating process. As one example, JWST showed better than 0.5% uniformity in near-infrared reflectance and < 10 nm peak-to-valley thickness variation in its 18 Au-coated segments.<sup>132,133</sup> In 2004, Kodak (now Harris) demonstrated the uniformity of 34 witness samples in a coating chamber configured to coat a 2.5-m diameter optic to 0.1% across a wide band 400 to 2350 nm.<sup>134</sup>

#### **Progress Over the Last Year:**

In the HabEx and LUVOIR interim reports, both large mission STDTs described their consideration of coatings and are baselining a mirror coat of Aluminum with LiF, with a thin capping layer of MgF<sub>2</sub> or AlF<sub>3</sub> and have studied uniformity requirements. Balasubramanian et al. (2017)<sup>135</sup> presented a summary of the field and also showed that the protective overcoat must maintain a thickness variation better than 2 nm peak-to-valley. APRA-funded research (PI David Sheikh, ZeCoat) developed motion-controlled and battery powered coating filament arrays to improve uniformity and performance between 90 nm and 2500nm and aims to demonstrate in 2019 and 2020 the multi-layer coating needed by HabEx and LUVOIR.

#### **Next Steps:**

While attaining the required coating performance has been shown to be feasible, the polarization performance given feasible uniformity of Al+LiF+MgF<sub>2</sub> must be characterized, to allow modeling of the impact on high-contrast imaging.

Space telescopes tend to have a fast f/# due to tight launch fairing constraints, which in turn

induces additional polarization aberration from steep incidence angle rays which are difficult to compensate with a deformable mirror. A tuned mirror coating could potentially mitigate this systems-level polarization effect, though this has not yet been demonstrated.<sup>136</sup>

The Breckinridge TDEM15 effort seeks to characterize measure the polarization birefringence of a 3.8 m mirror designed for ground-based use at 500 nm, and while the results may not be traceable to future coating processes for space telescopes, the information will be valuable. Contamination by particulate accumulation during the ground testing and integration can also be an issue at the several percent level. For example, HST's primary mirror had a 10% degradation in reflectivity due to pre-launch contamination.<sup>137</sup> Hence, handling protocols must be further refined for future space telescopes.

## E.2 Detection Sensitivity

### E.2.1 CG-12: Ultra-low noise UV detectors

#### CG-12: Ultra-low noise UV detectors

**Description:** Low-noise ultraviolet (200-400 nm) detectors to characterize exoplanets.

**SOA:** Lab: Micro-channel Plates (MCP): 0 read noise,  $\lambda \sim 90 - 300$  nm, spurious count rate 0.05 - 0.5 counts/cm<sup>2</sup>/s; QE 20-45%; resolution element size 20  $\mu$ m. EMCCD: 0 read noise, dark current > 0.005 e-/res/hr; QE 30-50%; resol. el. size 20  $\mu$ m Flight: HST HRC: In relevant UV band (250 nm): QE 33%, read noise 4.7 e-, dark current  $5.8 \times 10^{-3}$ , 1024 $\times$ 1024

**Needed capability:** Read Noise: 0 e-; Dark Current: 0 e- /resolution/s; Spurious Count Rate: < 0.05 counts/cm<sup>2</sup>/s; QE: 75% ; Resolution size  $\leq 10$   $\mu$ m; Tolerant to space radiation environment over mission lifetime.

**Supported Missions or Mission Concepts:** LUVUOIR, HabEx

The measurement of broad atmospheric features in the ultraviolet band can enhance the direct detection and characterization of exoplanets. For example, at wavelengths shortward of 300 nm, the reflectivity of planets with O<sub>3</sub> in their atmosphere (as in an Earth-like planet) is very low, while a different reflectivity cutoff shortward of 220 nm occurs for planets with SO<sub>4</sub>- rich atmospheres (such as a Venus-like planet).<sup>138</sup>

The Habex and LUVUOIR STDTs will determine the detailed requirements for UV detectors for exoplanet science applications during their ongoing studies; the needs listed in **Table 2** represent requirements linked to general astrophysics applications of UV detectors, and include desired sensitivity to wavelengths shorter than 100 nm.

#### Current State-of-the-Art:

Wavelengths shorter than 200 nm are not likely to benefit exoplanet science greatly. In the 200-400 nm band, there are several candidate technologies whose state-of-the-art is close to the needs for imaging spectral characterization of exoplanets, including EMCCD detectors and microchannel plates (MCP): see Bolcar et al. (2016)<sup>139</sup> for a summary and Siegmund et al. (2017)<sup>140</sup> for an assessment of the applicability to HabEx and LUVUOIR. For all of these candidate technologies, noise levels are adequate, but improvement is needed in quantum efficiency and detector lifetimes. Cryogenic MKID and TES detectors can also potentially operate in this band (Section B.4.2).

**Progress Over the Last Year:**

As defined in the LUVUOIR interim report, the coronagraph instrument on LUVUOIR (ECLIPS) has baselined delta-doped EMCCD detectors for its UV (200-525 nm) channel.<sup>141</sup> The HabEx starshade camera may also include a UV channel utilizing delta-doped EMCCD.<sup>142</sup> These detectors meet all sensitivity requirements, though lifetime in the L2 radiation environment is not known. Current state-of-the-art formats of 1k x 1k are acceptable.

**Next Steps:**

To further mature near-UV detectors for future exoplanet missions, radiation hardening may be needed. Radiation testing of delta-doped EMCCD devices will be performed at JPL as part of a SAT/COR effort that began in 2016 (PI Nikzad).

**E.3 Radial Stellar Motion Sensitivity (for planetary mass measurement)**

Precision radial velocity (RV) techniques measure the Doppler shift in stellar absorption lines as orbiting planets cause a gravitational recoil in the star. RV is a historically important technique for discovering exoplanets, and recently was used to discover a planet orbiting our closest neighboring star, Proxima Centauri.<sup>143</sup>

RV is one technique for obtaining a planetary mass measurement. It is needed to interpret spectral biosignature detections by inferring a planet's density and atmospheric scale height. RV could support a future strategic exoplanet space mission in two ways: first, ground-based RV instruments could support a space mission by detecting and characterizing the masses and orbits of direct imaging targets; and second, a dedicated RV instrument could be included on a space telescope to accomplish these ends.

Both paths require new technologies. The reflex motion (radial velocity semi-amplitude) of a Solar-mass star due to an orbiting Earth-mass planet at 1 AU is 9 cm/s. Detection of the Doppler shift of spectral lines to this precision requires exquisite control of instrumental precision and long term accuracy as well as mitigation of "stellar jitter" and of the deleterious effects of telluric atmospheric residuals on the time scales of years, or nearly an order of magnitude improvement in the current-state-of-the-art.<sup>144</sup>

Achieving this improvement requires investment in theoretical studies of stellar stability, as well as practical issues in instrumentation, including the multi-year stability of spectrograph pressure, temperature and optical-mechanical structure and wavelength calibration using gas lamps, Fabry-Perot Etalons or Laser Frequency combs.<sup>145</sup>

The National Academies Exoplanet Science Strategy report emphasized the importance of the mass measurement and in developing the capability of RV, including necessary technology. One of the report's recommendations explicitly states that "NASA and NSF should establish a strategic initiative in extremely precise radial velocities (EPRVs) to develop methods and facilities for measuring the masses of temperate terrestrial planets orbiting Sun-like stars." While such a strategic initiative has not been established as of this writing, ExEP's Technology List described in this document already includes, as a broad category, both space-based and ground-based technology for extreme-precision radial velocity.

### E.3.1 M-2: Laser Frequency Combs for Space-based EPRV

#### M-2: Laser Frequency Combs for Space-based EPRV

**Description:** Laser Frequency Combs (LFCs) are precise calibration sources for extreme-precision radial velocity measurement.

**SOA:** Lab: Electro-optic-modulation frequency combs demonstrated on ground-based observatories with needed mode spacing, need miniaturization and power reduction. Non-NASA work is advancing miniaturization.

Flight: Fiber laser-based optical frequency combs demonstrated on sounding rocket (TEXUS 51 4/15 and TEXUS 53 1/16) w/~ few hundred MHz mode spacing. System mass is > 10 kg.

**Needed capability:** Space-based Laser Frequency Combs to calibrate high resolution, fiber-fed spectrographs for radial velocity precision better than 10 cm/s. Desired parameters are: mode spacing of 5-10 GHz, bandwidth span 380 nm to 2400 nm, Allen deviation < 10<sup>-10</sup>, Low SWaP.

**Supported Missions or Mission Concepts:** LUV0IR, HabEx

Additional sensitivity may be gained by including an RV instrument on a space telescope. A major systematic error faced by ground-based RV measurements is microtelluric absorption lines from the Earth's atmosphere. RV measurements in space would also open near-IR wavelengths to sensitive measurement which might help in reducing the effects of stellar noise. An essential component for obtaining extreme precision, both on ground-based and space-based spectrometers are Laser Frequency Combs (LFCs). LFCs provide an extremely stable and accurate comb of visible and near-infrared lines, creating an ideal calibration source for a high resolution, fiber-fed spectrographs for radial velocity measurements. The key parameters for LFCs for space operation require mode spacings of 5-10 GHz, an overall bandwidth spanning 380 nm to 2400 nm, as well as appropriate packaging for a space mission.

#### Current State-of-the-Art:

Electro-optic-modulation (EOM) frequency combs have been demonstrated on ground-based observatories with the needed mode spacing, though with size and power needs that are not yet appropriate for a space instrument. Non-NASA work is advancing miniaturization. Fiber laser-based optical frequency combs have been demonstrated on sounding rockets (TEXUS 51 4/15 and TEXUS 53 1/16) though without the required mode spacing.

#### Progress Over the Last Year:

An Astrophysics Probe study called EarthFinder (PI Peter Plavchan) was funded by the NASA Astrophysics Directorate in 2017 to study the improvement in measurement errors that could be obtained from observing from space, across a broad wavelength band unaffected by residual atmospheric effects.

Suh et al (2018) have demonstrated on-sky astronomical spectrograph measurements calibrated soliton microcomb<sup>146</sup> with mode spacing of 20 GHz. The device is potentially scalable to centimeter scales and is thus an excellent candidate technology for a space-based LFC.

#### Next Steps:

As of this writing, the Earthfinder study is completed and a final report will be delivered in 2019. The study will define technology needs for a space based RV instrument, including the specifications of a LFC for calibration.

High spectral resolution, fiber-fed, ground-based spectrographs aiming for an ultimate sensitivity of 10 cm/s will be on line in the next several years.<sup>147,148</sup> Experience from these projects relating to instrument stability, mitigation of stellar jitter and atmospheric residuals, and long-term calibration, including the use of LFCs, will be directly applicable to assessing the need for and the technical readiness of space-based RV instrumentation.

Reduction of the footprint of the laser comb with an implementation such as the soliton microcomb would be a step towards a space instrument and obtaining a comb whose bandwidth spans more than an octave will allow self-calibration of the comb, enabling multi-year calibration stability at better than 1 cm/s.

### **E.3.2 M-1: Extreme Precision Ground-based Radial Velocity**

#### **M-1: Extreme Precision Ground-based Radial Velocity**

**Description:** Ground-based radial velocity instrumentation capable of measuring the mass of candidate exo-Earths in the habitable zone and to maximize efficiency of space telescope surveys.

**SOA:** VLT/ESPRESSO demonstrated stability of 28 cm/s over 7 hours; NN-EXPLORE's NEID (WYNN observatory) goal 27 cm/s

**Needed capability:** Signal from exo-Earths is 10 cm/s; Need to reduce systematic errors to 1 cm/s on multi-year timescales; statistical uncertainties of 1 cm/s on monthly timescales for late F, G, and early K stars

**Supported Missions or Mission Concepts:** LUVOIR, HabEx

Ground-based RV measurements provide two important enhancements to a space mission's ability to directly-image and characterize exoplanets. First, dedicated ground-based RV surveys in the Northern and Southern hemispheres could improve the science return of a direct imaging space mission. By pre-selecting stars with known planets, and using RV-measured planet orbits to schedule observations, the yield of a space mission would be improved. Second, precision RV measurements combined with imaging data can unambiguously determine planetary mass which is necessary for assessing potential habitability.<sup>149,150</sup>

To measure the mass of Earth-mass planets orbiting Sun-like stars, a long term accuracy of 1 cm/s over the relevant orbital time scales is needed.<sup>151</sup> Achieving this goal requires investment in theoretical studies of stellar stability, as well as in instrumentation, including wavelength calibration and in the stability of spectrograph pressure, temperature and optical-mechanical structure on one-year time scales. A number of next-generation RV-optimized spectrographs with better stability are coming online currently or in the next year and will push the instrumental limits further. For example, the development of the NEID instrument for the WIYN telescope under the ExEP's NN-EXPLORE program has a goal of 27 cm/s precision.<sup>152</sup>

#### **Current State-of-the-Art:**

In a presentation to SPIE in 2018, Francesco Pepe reported a state-of-the-art RV measurement precision of 28 cm/s over 7 hours using ESPRESSO on the VLT, limited by stellar activity. This is the most precise measurement reported on these time scales.<sup>153</sup>

A similar level of precision (in the 20-30 cm/s range) is expected in the near term by NN-EXPLORE's NEID instrument<sup>154</sup> for the WIYN telescope, and the iLocator<sup>155</sup> instrument for the LBT, both planned for first light in 2019.

#### **Progress Over the Last Year:**

A number of instruments (MINERVA-Australis, iSHELL, MAROON-X) expected to achieve similar stability to that reported by ESPRESSO are now on the sky or close to being commissioned and results should be reported soon. Investigation into the systematic errors to stellar activity continues. Multiple groups have published results investigating the “line-by-line” approach of analyzing each spectral line separately, thus allowing a combination of lines that is optimized for stellar activity noise suppression.<sup>156 157</sup> This has been shown to improve measurements using HARPS to the instrumental noise limit of 70 cm/s in several cases, and is thus a promising technique for even more stable instruments. To investigate one aspect of correcting the systematic error from stellar activity, Hall et al (2018)<sup>158</sup> show via simulations that an optimized observing cadence for the HARPS3 instrument can correct an RV measurement to the 30 cm/s level, or roughly 25% of typical Solar activity.

Sameshima et al (2018)<sup>159</sup> has developed requirements for using a “telluric standard” star to measure and correct contamination of an RV measurement by atmospheric telluric spectral lines.

### Next Steps:

A number of RV instruments, including NEID and EXPRES, are expected to deploy to ground-based telescopes in 2019, several aiming for 10 cm/s precision. Limiting factors are likely to be better understood as experience is gained in using these instruments for science observations. Further theoretical understanding of stellar noise and telluric atmospheric effects, as well as additional improvement in instrumental stability will be needed beyond the current generation of RV spectrometers.

A report on the enhancement of HabEx science using a ground-based radial velocity survey is expected in 2019.

## E.4 Tangential Stellar Motion Sensitivity (for planetary mass measurement)

### E.4.1 M-3: Astrometry

#### M-3: Astrometry

**Description:** Measure the mass and orbital parameters of Earth-like planets by performing astrometry of FGK stars to the sub-micro-arcsecond level.

**SOA:** Flight: GAIA typical uncertainty in astrometry for DR1 catalog is 300 microarcseconds; goal for V band magnitude 7-12 stars is 10 microarcseconds

**Needed capability:** <0.1 microarcsecond uncertainty enables survey of nearby FGK stars. Astrophysical limits (such as variable stellar surface structure) need to be well-understood. Telescope wavefront error stability and detector thermal and mechanical stability must enable sub-microarcsecond astrometry measurements.

**Supported Missions or Mission Concepts:** LUVOIR, HabEx

Precision astrometry determines the Keplerian orbital parameters of an exoplanet, enhancing the direct imaging and characterization of exoplanets by (1) increasing science yield of follow-up coronagraph observations, and (2) determining the mass of a detected exoplanet without the  $\sin(i)$  system inclination uncertainty intrinsic to radial velocity measurements. Masses are necessary to assess habitability by distinguishing Earth-like planets around Sun-like stars from small Neptunes or water worlds, and by helping to constrain the atmospheric scale height, which is crucial to understanding the atmosphere. The precision must be improved to 0.3

microarcseconds in a single measurement in order to enable detection of Earth analogs at 10 pc distance,<sup>160</sup> which is two orders of magnitude beyond the current state-of-the-art. Astrometry is potentially a powerful means of determining the masses of Earth-like planet orbiting the nearest Sun-like stars such as  $\alpha$ -Cen A and B, where the astrometric signal due to reflex motion of an Earth-mass planet would be at the 1-2 micro arcsecond level.<sup>161</sup>

#### **Current State-of-the-Art:**

The current in-flight state of the art is the GAIA mission, preliminarily estimated to achieve 34 microarcsecond measurement error, but ultimately could achieve 10 microarcseconds on bright targets after all systematics are calibrated. GAIA is expected to discover Jupiter-mass exoplanets.<sup>162</sup> In addition, astrometry accuracy of 25 microarcseconds has been achieved with HST.<sup>163</sup> The lab state-of-the art was set by the Bendek TDEM-14 that demonstrated the use of a diffractive pupil to achieve 10 microarcsecond astrometric precision (when installed on a 2.4 m telescope) while showing compatibility of a diffractive pupil with direct imaging using a PIAA coronagraph.<sup>164</sup>

#### **Progress over the Last Year:**

LUVOIR's HDI instrument (the UV/Vis/NIR wide-field imager) includes a precision astrometry mode in order to measure the mass of directly imaged exoplanets. The LUVOIR interim report<sup>165</sup> reports astrometry requirements at the 0.1 microarcsecond level for HDI. The MicroArcsecond Small Satellite (MASS) concept (PI Mike Shao, JPL) was selected for study by APD in September 2018 along with eight other astrophysics smallsats. This study will continue to develop the diffractive pupil concept. The Exoplanet Science Strategy found that that astrometry is a viable option for determining the mass of exoplanets, but considered it as a backup to extreme precision radial velocity. There are some key cases, however, such as in observing the nearest Solar-type stars, where astrometric techniques may prove superior to RV.

#### **Next Steps:**

GAIA's Data Release 2 occurred in 2018, including many astrometric exoplanet detections. In the long run, GAIA is expected to detect thousands of Jupiter-mass planets in orbits between 0.5 and 5 AU of their host stars<sup>166</sup> which will revolutionize the understanding of exoplanetary systems. In addition, a detailed assessment of GAIA's systematic errors and on-orbit stability, including thermal relaxation effects and micrometeoroid impacts, will be critical for designing future missions.

Given the importance of mass measurements for understanding the potential habitability of exo-Earths, the LUVOIR and HabEx STDTs are expected to explore astrometry. Both missions require extreme telescope wavefront error stability for coronagraph performance, which may help astrometric measurements. The diffractive pupil design may enable astrometric solution at the sub microarcsecond level for these large mission concepts.

The MASS smallsat study will explore the feasibility of precise astrometric measurements using a small wide-field telescope with a diffractive pupil, final report expected in spring 2019.

## E.5 Mid-IR Transit and Secondary Eclipse Spectroscopy

Transit spectroscopy has proven to be an essential tool for characterizing the atmospheres of exoplanets. Like photometric transits, transit spectroscopy looks at the decrease in brightness of a host star as a planet passes through our line of sight to the star. By observing the transit in multiple wavelengths, spectroscopic absorption features in the atmosphere of the transiting planet can be measured. Similarly, secondary eclipse spectroscopy measures the spectra of light emitted from transiting planets by comparing signals during and outside of secondary eclipse, when the host star completely occults the planet. These techniques have been used to study the atmospheres of giant planets with HST and Spitzer data.

The mid-infrared wavelength band is rich with spectral features from trace gas constituents and potential biomarkers such as methane, carbon dioxide, ozone, nitrates, sulfates, and others. From its cooled and stable platform at Sun-Earth L2, JWST will be able to carry out transit spectroscopy of many planetary systems. In 2017, A Cycle-1 Early Release Science proposal was selected, entitled “The Transiting Exoplanet Community Early Release Science Program” (PI N. Batalha)<sup>167</sup>, with plans to observe a number of transiting systems with all of JWST’s instruments. JWST will make even deeper inroads into studying the bulk atmospheres of planets via secondary eclipse spectroscopy. This is because JWST will be the first observatory capable of sensitive and high precision mid-IR spectroscopy, and this will be exploited by several Cycle 1 GTO programs that focus on this technique. These and other Cycle 1 programs will reveal much information about exoplanet atmospheres as well as demonstrate JWST’s early performance on transiting planet systems.

The key performance metric for these observations is the stability of the instrument response during the transit, secondary eclipse, or planetary orbit phase curve (typically on the time scale of hours to days). JWST MIRI will use the same detectors<sup>168</sup> as Spitzer/IRAC which has been able to achieve around 60 ppm precision on time scales of several hours, including the phenomenological calibration of on-orbit drifts. Systematic errors for transit observations expected with JWST based on previous are described in Beichman et al (2014).<sup>169</sup>

Beyond JWST, further improvement in the stability of transit and secondary eclipse spectroscopy can enable further characterization of exoplanets. One goal to search for habitable worlds is through the study of the atmospheres of rocky Earth-sized planets orbiting M dwarf stars. The shallower transit depth and secondary eclipse signals of small planets require improvements in the detector system stability to ensure that systematic errors are kept to a level that does not impede measurement of a planet’s spectral features.

The study of the atmospheres of potentially habitable planets orbiting M-dwarf stars is a key science goal for the OST mission concept. OST has specified a needed improvement to ~ 5 ppm stability over 5 hours in mid-IR detectors. This performance is a factor 10 beyond the state-of-the-art, and may likely require new technology.

### E.5.1 M-4: Ultra-Stable Mid-Infrared Detectors

#### M-4: Ultra-Stable Mid-Infrared Detectors

**Description:** Ultrastable detectors for the mid-infrared band (7 - 20 microns) enabling transit spectroscopy of rocky exoplanets in the Habitable Zone of M-dwarfs.

**SOA:** Lab: JWST/MIRI is expected to achieve 10-100 ppm transit stability. Flight: Spitzer IRAC Si:As detector data have demonstrated about 60 ppm precision in transit observations of several hours

**Needed capability:** < 5 ppm stability for 5 hours

**Supported Missions or Mission Concepts:** Origins Space Telescope

Once on orbit, the MIRI detectors are expected to establish the state-of-the-art for transit spectroscopy in the mid-IR band. MIRI uses the same arsenic-doped silicon impurity band conductor (IBC) detector technology as Spitzer/IRAC and a hybridized readout<sup>170</sup> that improves their stability.

#### Current State-of-the-Art:

Spitzer IRAC Si:As detectors have demonstrated about 60 ppm precision in transit observations of several hours. JWST/MIRI is expected to achieve similar or slightly better stability. Limiting factors in stability are currently not identified: some instabilities can be removed by careful calibration in post-processing, and in instrumental design.

#### Progress Over the Last Year:

The Origins Space Telescope interim report<sup>171</sup> identified an architecture for a transit spectrometer as part of its MISC instrument. This architecture is based on a “densified pupil” concept<sup>172</sup> which divides the entrance pupil into subpupils creating independent spectra of the star on the detector plane. This allows the mitigation of a number of stability and calibration issues, including those related to variations in pixel properties across the focal plane. This concept is an important first step towards demonstrating the necessary stability.

A new class of HgCdTe photoconducting arrays with sensitivity to wavelengths as long as 10 microns were developed by Teledyne Imaging Systems and characterized at the University of Rochester under contract with JPL as part of the NeoCAM project;<sup>173</sup> these may provide a higher-stability alternative to IBC technology, for at least part of the mid-infrared band. In principle these devices can be extended to slightly longer wavelengths, perhaps 13 microns.

#### Next Steps:

After the launch of JWST in 2021, MIRI, operated in a Time Series Observation mode,<sup>174</sup> is expected to show some improvement of the state-of-the-art for stability beyond that achieved by Spitzer/IRAC. In particular, additional work in on orbit calibration of transit spectroscopy observations will show how much instability can be corrected in the presence of drifts in the instrument and in the astrophysical sources.

For future missions targeting several parts per million stability, such as OST, a detailed study of sources of instability in mid-IR detector systems will be needed to determine where technology investments will be most effective. This should be done in concert with modeling on-orbit calibration, which will mitigate the detector requirements to some level. The intrinsic stability of the mid-IR detector system may be driven by fundamental detector materials properties, cryogenic detector readout circuitry, or other instabilities in the system. Additionally,

alternative doping for IBC detectors (such as phosphorous) may be considered as a less costly alternative to arsenic doping for mid-IR detectors.

The Origins final report, expected in 2019, will include a technology roadmap that will take an important step towards this error budget, providing system and detector requirements for enabling transit spectroscopy at the 5 ppm stability level and a plan for maturing the technology to achieve the requirements. Alternatives to IBC detectors will be considered including long-wavelength-cutoff HgCdTe and superconducting detectors such as superconducting nanowire detectors.

A lab demonstration of the densified pupil technique would provide confidence that most systematic errors can be addressed and fundamental detector properties will be the limiting factor.

Finally, astrophysical limits should be examined further to show that they will not be limitations for transit measurements at sensitivity levels beyond those achievable by JWST.

## F TECHNOLOGY WATCH LIST

While not meeting the selection criteria to be included on the prioritized Technology List, two of the technologies submitted by the community were determined to still be potentially beneficial to exoplanet science. These technologies will be revisited annually for possible prioritization and are listed in Table 4.

**Table 4:** ExEP Technology Watch List

Gap Title
Advanced Cryocoolers
Sub-Kelvin Coolers

### F.1 Advanced Cryocoolers

Some classes of energy-resolving near-infrared and visible detectors for exoplanet characterization (such as KIDs and TES microcalorimeters; see Sect. B.4.2) require cooling to temperatures  $< 1$  K. To reach these temperatures, sub-Kelvin coolers must be pre-cooled by an advanced cryocooler. Below 25 K, passive cooling in space is not practical and compact cryocoolers are necessary for pre-cooling a sub-Kelvin cooler. Custom solutions have been successful in space for mm-wave space missions such as Planck, but additional development is required in heat lift, lower mass, lower volume, and lifetime. Sorption coolers and mechanical Joule-Thomson, pulse tube, and Stirling coolers are possible solutions, but vibration isolation must be at a level compatible with the sub-nanometer wavefront stability needed for coronagraphy. See Rauscher et al (2016)<sup>175</sup> for a discussion of technology suitable for cryogenic detectors.

### F.2 Sub-Kelvin Coolers

To cool an energy-resolving exoplanet detector system below 1 K starting from a stage pre-cooled by an advanced cryocooler, a sub-Kelvin cooler must be used. While sub-Kelvin coolers have been successfully flown on Herschel and Planck, cooler technology with the necessary heat lift have not advanced beyond TRL 3. Existing candidates include  $^3\text{He}$ - $^4\text{He}$  dilution refrigerators,  $^3\text{He}$  sorption coolers, and adiabatic demagnetization refrigerators. The compatibility of these coolers with sub-nanometer wavefront stability required for a coronagraph is currently unknown.

## G PRIORITIZATION

During 2018, ExEP Technologists worked with their counterparts in the PCOS/COR NASA APD program offices to develop an APD-wide technology selection and prioritization process and a new prioritization of ExEP's technologies was not performed in 2018. The prioritized list derived during the 2017 technology cycle and described in the 2018 ExEP Technology Plan Appendix (see sections A.3 and G in particular) represents the current technology priorities of the program office, with scoring shown again here for convenience.

ID	Technology Title	Impact	Urgency	Trend	Total
	weight:	10	10	5	Score
CG-2	Coronagraph Architecture	4	4	2	90
S-2	Starlight Suppression and Model Validation	4	4	2	90
S-1	Controlling Scattered Sunlight	4	4	2	90
S-3	Lateral Formation Sensing	4	4	2	90
S-5	Petal Positioning Accuracy and Opaque Structure	4	4	2	90
S-4	Petal Shape and Stability	4	4	2	90
CG-3	Deformable Mirrors	4	4	2	90
CG-1	Large Aperture Primary Mirrors	4	3	3	85
CG-6	Mirror Segment Phasing	4	3	3	85
CG-7	Telescope Vibration Sense/Control or Reduction	4	3	3	85
CG-9	Ultra-Low Noise Near-Infrared Detectors	4	3	3	85
CG-5	Wavefront Sensing and Control	4	3	2	80
CG-8	Ultra-Low Noise Visible Detectors	4	3	2	80
M-4	Ultra-Stable Mid-IR detector	3	3	4	80
M-3	Astrometry	3	3	3	75
CG-4	Data Post-Processing Algorithms and Techniques	4	2	2	70
CG-10	Mirror Coatings for UV/NIR/Vis	3	3	2	70
M-2	Space-based Laser Frequency Combs	3	3	2	70
CG-13	Ultra Low-noise Mid-IR detectors	2	3	4	70
M-1	Extreme Precision Ground-based Radial Velocity	2	3	3	65
CG-14	Mid-IR Large Aperture Telescopes	2	3	3	65
CG-15	Mid-IR Coronagraph Optics and Architecture	2	3	3	65
CG-16	Cryogenic Deformable mirror	2	3	3	65
CG-12	Ultra-Low Noise UV Detectors	2	3	2	60

## **H CONCLUSION**

The 2010 Astrophysics Decadal Survey recommended the creation of a technology development program for a potential future exoplanet mission to mature starlight-suppression technology for the detection of spectra of Earth-like exoplanets. The ExEP supports a community-based process to help NASA identify the needed technologies to achieve this goal and to mature the selected concepts to inform the 2020 Decadal Survey committee. This Appendix outlines technology development plans and activities that will lead toward that goal.

Starting in 2019, a new APD-wide Technology Gap List will be assembled in a coordinated way between the three NASA APD program offices. The Gaps related to exoplanet science will be described in detail in future updates to the ExEP Technology Plan Appendix.

## I DOCUMENT CHANGE LOG

This section contains a log of changes to the 2019 ExEP Technology Plan Appendix.

Date	Version	Author	Description

**J ACRONYMS**

ACAD	Adaptive Correction of Aperture Discontinuities
AIP	Astrophysics Implementation Plan
AFTA	Astrophysics Focused Telescope Assets
AMTD	Advanced Mirror Technology Development
APLC	Apodized Pupil Lyot Coronagraph
APRA	Astrophysics Research and Analysis
ATLAST	Advanced Technology Large Aperture Space Telescope
BMC	Boston Micromachines Corporation
CIC	Clock-Induced Charge
CTE	Coefficient of Thermal Expansion
DM	Deformable Mirror
DRM	Design Reference Mission
DST	Decadal Survey Testbed
EMCCD	Electron Multiplying Charge Couple Device
ExEP	Exoplanet Exploration Program
ExoPAG	Exoplanet Program Analysis Group
HabEx	Habitable Exoplanet Observatory
HCIT	High Contrast Imaging Testbed
HDST	High Definition Space Telescope
HiCAT	High Contrast Imager for Complex Aperture Telescopes
HRC	High-Resolution Channel
HST	Hubble Space Telescope
IWA	Inner Working Angle
JWST	James Webb Space Telescope
LOWFS/C	Low-Order Wavefront Sensor and Controller
LTF	Low-temperature Fusion
LTS	Low-temperature Slumping
LUVOIR	Large Ultra-Violet Optical Infrared
MCP	Micro Channel Plate
MEMS	Micro Electro Mechanical Systems
MKID	Microwave Kinetic Inductance Detectors
NG-VNC	Next Generation Visible Nulling Coronagraph
NICMOS	Near-Infrared Camera and Multi-Object Spectrometer
NWNH	New Worlds, New Horizons (2010 Astronomy and Astrophysics Decadal Survey)
OST	Origins Space Telescope
PIAACMC	Phase-Induced Amplitude Apodization Complex Mask Coronagraph
PMN	Lead Magnesium Niobate
PSF	Point Spread Function
QE	Quantum Efficiency
ROSES	Research Opportunities in Space and Earth Sciences
SBIR	Small Business Innovation Research
SIM	Space Interferometry Mission

SLS	Space Launch System
SOA	State of Art
SP	Shaped Pupil
SPLC	Shaped Pupil Lyot Coronagraph
STScI	Space Telescope Science Institute
TCOP	Technology Development for the Cosmic Origins Program
TDEM	Technology Development for Exoplanet Missions
ULE	Ultra-Low Expansion
VNC	Visible Nulling Coronagraph
WFC	Wavefront Control
WFIRST	Wide-Field Infrared Survey Telescope
WFSC	Wavefront Sensing and Control

## K REFERENCES

- <sup>1</sup> 2018 NASA Strategic Plan,  
[https://www.nasa.gov/sites/default/files/atoms/files/nasa\\_2018\\_strategic\\_plan.pdf](https://www.nasa.gov/sites/default/files/atoms/files/nasa_2018_strategic_plan.pdf).
- <sup>2</sup> NASA 2014 Science Plan,  
[http://science.nasa.gov/media/medialibrary/2014/05/02/2014\\_Science\\_Plan-0501\\_tagged.pdf](http://science.nasa.gov/media/medialibrary/2014/05/02/2014_Science_Plan-0501_tagged.pdf) .
- <sup>3</sup> 2014 update to the Astrophysics Implementation Plan,  
[http://science.nasa.gov/media/medialibrary/2015/01/16/ImpPlan\\_Rev2\\_15Apr2013\\_LL\\_15\\_0107TAGGED.pdf](http://science.nasa.gov/media/medialibrary/2015/01/16/ImpPlan_Rev2_15Apr2013_LL_15_0107TAGGED.pdf)
- <sup>4</sup> National Research Council. *Review of Progress Toward the Decadal Survey Vision in New Worlds, New Horizons in Astronomy and Astrophysics*. Washington, DC: The National Academies Press, 2016,  
<https://www.nap.edu/catalog/23560/new-worlds-new-horizons-a-midterm-assessment>
- <sup>5</sup> 2014 update to the Astrophysics Implementation Plan,  
[http://science.nasa.gov/media/medialibrary/2015/01/16/ImpPlan\\_Rev2\\_15Apr2013\\_LL\\_15\\_0107TAGGED.pdf](http://science.nasa.gov/media/medialibrary/2015/01/16/ImpPlan_Rev2_15Apr2013_LL_15_0107TAGGED.pdf)
- <sup>6</sup> Brendan P. Crill, Nicholas Siegler, "Space technology for directly imaging and characterizing exo-Earths," Proc. SPIE 10398, UV/Optical/IR Space Telescopes and Instruments: Innovative Technologies and Concepts VIII, 103980H (5 September 2017); doi: 10.1117/12.2275697
- <sup>7</sup> Exo-C and Exo-S Final Reports (2015); <https://exoplanets.nasa.gov/exep/studies/probe-scale-stdt/>
- <sup>8</sup> WFIRST Home Page: <http://wfirst.gsfc.nasa.gov/index.html>
- <sup>9</sup> LUVOR Interim Report  
[https://asd.gsfc.nasa.gov/luvor/resources/docs/LUVOR\\_Interim\\_Report\\_Final.pdf](https://asd.gsfc.nasa.gov/luvor/resources/docs/LUVOR_Interim_Report_Final.pdf)  
HabEx Interim Report [https://www.jpl.nasa.gov/habex/pdf/HabEx\\_Interim\\_Report.pdf](https://www.jpl.nasa.gov/habex/pdf/HabEx_Interim_Report.pdf)  
OST Interim Report [https://asd.gsfc.nasa.gov/firs/docs/OST\\_Interim\\_Study\\_Report.pdf](https://asd.gsfc.nasa.gov/firs/docs/OST_Interim_Study_Report.pdf)
- <sup>10</sup> LUVOR Science & Technology Definition Team LUVOR Study Office & Members of the LUVOR Technology Working Group. *LUVOR Decadal Mission Concept Study "O1" Deliverable: Technology Gap Assessment for the 2016 Program Office Technology Cycle*, 2016. [http://asd.gsfc.nasa.gov/luvor/docs/tech/2016-05-31-LUVOR-O1-Deliverable\\_rev3.0.pdf](http://asd.gsfc.nasa.gov/luvor/docs/tech/2016-05-31-LUVOR-O1-Deliverable_rev3.0.pdf)
- <sup>11</sup> TDEM past awards:  
<https://exoplanets.nasa.gov/exep/technology/TDEM-awards/>
- <sup>12</sup> NSPIRES APRA past awards:  
<https://nspires.nasaprs.com/external/solicitations/solicitations.do?method=closedPastIni&stack=push>
- <sup>13</sup> Committee on Exoplanet Science Strategy "Exoplanet Science Strategy" (2018).  
<https://www.nap.edu/catalog/25187/exoplanet-science-strategy>.
- <sup>14</sup> ExEP Technology Website; <http://exoplanets.nasa.gov/technology/>.

- <sup>15</sup> Pham, T., Ganel, O., & Thronson, H. (2018). NASA's physics of the cosmos and cosmic origins programs manage strategic astrophysics technology development in preparation for the next decadal survey. In H. A. MacEwen, M. Lystrup, G. G. Fazio, N. Batalha, E. C. Tong, & N. Siegler (Eds.), *Space Telescopes and Instrumentation 2018: Optical, Infrared, and Millimeter Wave* (Vol. 10698, p. 106986J). International Society for Optics and Photonics. <http://doi.org/10.1117/12.2314832>
- <sup>16</sup> Lawson, P. R., Belikov, R., Cash, W., et al. 2013, "Survey of experimental results in high-contrast imaging for future exoplanet missions," Proc. SPIE 8864, 88641F, <http://spiedigitallibrary.org/proceeding.aspx?articleid=1744192&resultClick=1>.
- <sup>17</sup> Moody, D. C., Gordon, B. L., & Trauger, J. T. 2008, "Design and demonstration of hybrid Lyot coronagraph masks for improved spectral bandwidth and throughput," Proc. SPIE 7010, 70103P, <http://spiedigitallibrary.org/proceeding.aspx?articleid=787868&resultClick=1>
- <sup>18</sup> Trauger, J., Moody, D., Gordon, B., Krist, J., Mawet, D. 2011, "A hybrid Lyot Coronagraph for the direct imaging and spectroscopy of exoplanet systems," Proc. SPIE 8151, 81510G, <http://spiedigitallibrary.org/proceeding.aspx?articleid=1342401&resultClick=1>.
- <sup>19</sup> Trauger, J. et al, TDEM-09 Final Report:  
[http://exoplanets.nasa.gov/files/exep/Lyot\\_TDEM\\_Report\\_121215\\_signed.pdf](http://exoplanets.nasa.gov/files/exep/Lyot_TDEM_Report_121215_signed.pdf)
- <sup>20</sup> <https://sites.google.com/view/highcontrastlabs/home>
- <sup>21</sup> Douglas, E. S., Carlton, A. K., Cahoy, K. L., Kasdin, N. J., Turnbull, M., & Macintosh, B. (2018). WFIRST coronagraph technology requirements: status update and systems engineering approach. In G. Z. Angeli & P. Dierickx (Eds.), *Modeling, Systems Engineering, and Project Management for Astronomy VIII* (Vol. 10705, p. 1070526). International Society for Optics and Photonics. <http://doi.org/10.1117/12.2314221>
- <sup>22</sup> Marx, D., Cady, E., Riggs, A. J. E., Prada, C., Kern, B., Seo, B.-J., & Shi, F. (2018). Shaped pupil coronagraph: disk science mask experimental verification and testing. In H. A. MacEwen, M. Lystrup, G. G. Fazio, N. Batalha, E. C. Tong, & N. Siegler (Eds.), *Space Telescopes and Instrumentation 2018: Optical, Infrared, and Millimeter Wave* (Vol. 10698, p. 106981E). International Society for Optics and Photonics. <http://doi.org/10.1117/12.2312602>
- <sup>23</sup> Seo, B.-J., Shi, F., Balasubramanian, B., Cady, E., Gordon, B., Kern, B., et al. (2018). Hybrid lyot coronagraph for WFIRST: high contrast testbed demonstration in flight-like low flux environment. In *Space Telescopes and Instrumentation 2018: Optical, Infrared, and Millimeter Wave* (Vol. 10698, p. 106982P). International Society for Optics and Photonics. <http://doi.org/10.1117/12.2314358>
- <sup>24</sup> Ruane, G., Mawet, D., Mennesson, B., Jewell, J., & Shaklan, S. (2018). Vortex coronagraphs for the Habitable Exoplanet Imaging Mission concept: theoretical performance and telescope requirements. *Journal of Astronomical Telescopes, Instruments, and Systems*, 4(1), 015004. <http://doi.org/10.1117/1.JATIS.4.1.015004>
- <sup>25</sup> Riggs, A. J. E., Ruane, G., Sidick, E., Coker, C., Kern, B. D., & Shaklan, S. B. (2018). Fast linearized coronagraph optimizer (FALCO) I: a software toolbox for rapid coronagraphic design and wavefront correction. In H. A. MacEwen, M. Lystrup, G. G. Fazio, N. Batalha, E. C.

- Tong, & N. Siegler (Eds.), *Space Telescopes and Instrumentation 2018: Optical, Infrared, and Millimeter Wave* (Vol. 10698, p. 106982V). International Society for Optics and Photonics. <http://doi.org/10.1117/12.2313812>
- <sup>26</sup> Stark et al. (2019) JATIS, submitted.
- <sup>27</sup> Moore, D. B., & Redding, D. C. (2018). Picometer differential wavefront metrology by nonlinear Zernike wavefront sensing for LUVVOIR. In H. A. MacEwen, M. Lystrup, G. G. Fazio, N. Batalha, E. C. Tong, & N. Siegler (Eds.), *Space Telescopes and Instrumentation 2018: Optical, Infrared, and Millimeter Wave* (Vol. 10698, p. 1069841). International Society for Optics and Photonics. <http://doi.org/10.1117/12.2312600>
- <sup>28</sup> Breckinridge, J., W. Lam, and R. Chipman, 2015, "Polarization Aberrations in Astronomical Telescopes: The Point Spread Function". *Publications of the Astronomical Society of the Pacific*, 127: 445-468. <http://dx.doi.org/10.1086/681280>
- <sup>29</sup> Krist, J., B. Nemati, and B. Mennesson, 2016, "Numerical modeling of the proposed WFIRST-AFTA coronagraphs and their predicted performances," *J. Astron. Telesc. Instrum. Syst.* 2016; 2 (1): 011003, <http://astronomicaltelescopes.spiedigitallibrary.org/article.aspx?articleid=2468019>.
- <sup>30</sup> Serabyn, E., C. Mejia Prada, P. Chen, and D. Mawet. 2019 "Vector vortex coronagraphy for exoplanet detection with spatially-variant diffractive waveplates.", *JOSA-B*, in press.
- <sup>31</sup> Pueyo, L, and Norman, C. 2013, "High-contrast Imaging with an Arbitrary Aperture: Active Compensation of Aperture Discontinuities ", *ApJ* 769, 102, [http://adsabs.harvard.edu/cgi-bin/nph-data\\_query?bibcode=2013ApJ...769..102P&db\\_key=AST&link\\_type=ABSTRACT&high=5697e4cfa22878](http://adsabs.harvard.edu/cgi-bin/nph-data_query?bibcode=2013ApJ...769..102P&db_key=AST&link_type=ABSTRACT&high=5697e4cfa22878)
- <sup>32</sup> John Trauger; Dwight Moody; John Krist; Brian Gordon, *J. Astron. Telesc. Instrum. Syst.* 2016; 2(1):011013. doi: 10.1117/1.JATIS.2.1.011013
- <sup>33</sup> Serabyn, E., Prada, C. M., Chen, P., & Mawet, D. (2019). Vector vortex coronagraphy for exoplanet detection with spatially variant diffractive waveplates. *Journal of the Optical Society of America B*, 36(5), D13–D19. <http://doi.org/10.1364/JOSAB.36.000D13>
- <sup>34</sup> Douglas, E. S., Allan, G., Barnes, D., Figura, J. S., Haughwout, C. A., Gubner, J. N., et al. (2017). Design of the deformable mirror demonstration CubeSat (DeMi). In S. Shaklan (Ed.), *Techniques and Instrumentation for Detection of Exoplanets VIII* (Vol. 10400, p. 1040013). International Society for Optics and Photonics. <http://doi.org/10.1117/12.2274430>
- <sup>35</sup> Soummer, R., et al., 2014, "Five Debris Disks Newly Revealed in Scattered Light from the Hubble Space Telescope NICMOS Archive," *The Astrophysical Journal Letters* 786 (23S), [http://adsabs.harvard.edu/cgi-bin/nph-data\\_query?bibcode=2014ApJ...786L..23S&db\\_key=AST&link\\_type=ABSTRACT&high=5697e4cfa04593](http://adsabs.harvard.edu/cgi-bin/nph-data_query?bibcode=2014ApJ...786L..23S&db_key=AST&link_type=ABSTRACT&high=5697e4cfa04593)
- <sup>36</sup> Menesson, D., 2015, "AFTA coronagraph performance feedback from post-processing studies to overall design," *Proc. SPIE* 9605, <http://spiedigitallibrary.org/proceeding.aspx?articleid=2443259&resultClick=1>

- <sup>37</sup> Ygouf, M., et al., 2015, "Data processing and algorithm development for the WFIRST-AFTA coronagraph: reduction of noise free simulated images, analysis and spectrum extraction with reference star differential imaging" Proc. SPIE 9605 9605 0S, <http://spiedigitallibrary.org/proceeding.aspx?articleid=2443266&resultClick=1>
- <sup>38</sup> Paul A. Lightsey, J. Scott Knight, Lee D. Feinberg, Matthew R. Bolcar, Stuart B. Shaklan, "First-order error budgeting for LUVOIR mission," Proc. SPIE 10398, UV/Optical/IR Space Telescopes and Instruments: Innovative Technologies and Concepts VIII, 103980C (5 September 2017);
- <sup>39</sup> J. Brent Knight, H. Philip Stahl, Andy Singleton, Ron Hunt, Melissa Therrell, Kate Caldwell, Jay Garcia, Mike Baysinger, "Dynamic/jitter assessment of multiple potential HabEx structural designs," Proc. SPIE 10374, Optical Modeling and Performance Predictions IX, 1037402 (6 September 2017);
- <sup>40</sup> Lee Feinberg, Matthew Bolcar, Scott Knight, David Redding, "Ultra-stable segmented telescope sensing and control architecture," Proc. SPIE 10398, UV/Optical/IR Space Telescopes and Instruments: Innovative Technologies and Concepts VIII, 103980E (5 September 2017);
- <sup>41</sup> Sang C. Park, Michael J. Eisenhower, Marcel Bluth, Matthew R. Bolcar, Lee D. Feinberg, J. Scott Knight, David C. Redding, "LUVOIR backplane thermal architecture development through the composite CTE sensitivity study," Proc. SPIE 10398, UV/Optical/IR Space Telescopes and Instruments: Innovative Technologies and Concepts VIII, 103980D (5 September 2017);
- <sup>42</sup> Fang Shi, Eric Cady, Byoung-Joon Seo, Xin An, Kunjithapatham Balasubramanian, Brian Kern, Raymond Lam, David Marx, Dwight Moody, Camilo Mejia Prada, Keith Patterson, Ilya Poberezhskiy, Joel Shields, Erkin Sidick, Hong Tang, John Trauger, Tuan Truong, Victor White, Daniel Wilson, Hanying Zhou, "Dynamic testbed demonstration of WFIRST coronagraph low order wavefront sensing and control (LOWFS/C)," Proc. SPIE 10400, Techniques and Instrumentation for Detection of Exoplanets VIII, 104000D (1 September 2017);
- <sup>43</sup> Belikov, R., Bendek, E., Pluzhnik, E., Sirbu, D., Thomas, S.J., 2016, "High contrast imaging in multi-star systems: technology development and first lab results," Proc SPIE 9904. <http://proceedings.spiedigitallibrary.org/proceeding.aspx?articleid=2541995>
- <sup>44</sup> Seo, B.-J., Shi, F., Balasubramanian, B., Cady, E., Gordon, B., Kern, B., et al. (2018). Hybrid lyot coronagraph for WFIRST: high contrast testbed demonstration in flight-like low flux environment. In Space Telescopes and Instrumentation 2018: Optical, Infrared, and Millimeter Wave (Vol. 10698, p. 106982P). International Society for Optics and Photonics. <http://doi.org/10.1117/12.2314358>
- <sup>45</sup> Moore, D. B., & Redding, D. C. (2018). Picometer differential wavefront metrology by nonlinear Zernike wavefront sensing for LUVOIR. In H. A. MacEwen, M. Lystrup, G. G. Fazio, N. Batalha, E. C. Tong, & N. Siegler (Eds.), Space Telescopes and Instrumentation 2018:

- Optical, Infrared, and Millimeter Wave (Vol. 10698, p. 1069841). International Society for Optics and Photonics. <http://doi.org/10.1117/12.2312600>
- <sup>46</sup> Kelsey Miller, Olivier Guyon, Jared Males, "Spatial linear dark field control: stabilizing deep contrast for exoplanet imaging using bright speckles," *J. Astron. Telesc. Instrum. Syst.* 3(4) 049002 (30 October 2017)
- <sup>47</sup> E. Douglas, A. Carlton, J. Clark, O. Guyon, J. Lumbres, J. Males, W. Marlow, & K. Cahoy "Laser Guide Star for Large Segmented Aperture Space Telescopes, Part I: Implications for Observatory Stability." In-prep.
- <sup>48</sup> Lee Feinberg, Matthew Bolcar, Scott Knight, David Redding, "Ultra-stable segmented telescope sensing and control architecture," *Proc. SPIE 10398, UV/Optical/IR Space Telescopes and Instruments: Innovative Technologies and Concepts VIII*, 103980E (5 September 2017);
- <sup>49</sup> Albanese, M., et al. 2006, "Verification of the James Webb Space Telescope coarse phase sensor using the Keck Telescope," *Proc. SPIE 6265 05*, <http://spiedigitallibrary.org/proceeding.aspx?articleid=1326681&resultClick=1>
- <sup>50</sup> Lou, J. Z., Redding, D. C., Nissen, J. A., & Shelton, C. (2018). LUVVOIR primary mirror segment alignment control with joint laser metrology and segment edge sensing. In H. A. MacEwen, M. Lystrup, G. G. Fazio, N. Batalha, E. C. Tong, & N. Siegler (Eds.), *Space Telescopes and Instrumentation 2018: Optical, Infrared, and Millimeter Wave* (Vol. 10698, p. 1069840). International Society for Optics and Photonics. <http://doi.org/10.1117/12.2311495>
- <sup>51</sup> Douglas, E. S., Males, J. R., Clark, J., Guyon, O., Lumbres, J., Marlow, W., & Cahoy, K. L. (2019). Laser Guide Star for Large Segmented-aperture Space Telescopes. I. Implications for Terrestrial Exoplanet Detection and Observatory Stability. *The Astronomical Journal*, 157(1), 36. <http://doi.org/10.3847/1538-3881/aaf385>
- <sup>52</sup> Sensitivity analysis for high-contrast imaging with segmented space telescopes. (2018). Sensitivity analysis for high-contrast imaging with segmented space telescopes (Vol. 10698, p. 106986H). International Society for Optics and Photonics. <http://doi.org/10.1117/12.2313904>
- <sup>53</sup> Bijan Nemati, Mark T. Stahl, H. Philip Stahl, Stuart B. Shaklan, "The effects of space telescope primary mirror segment errors on coronagraph instrument performance," *Proc. SPIE 10398, UV/Optical/IR Space Telescopes and Instruments: Innovative Technologies and Concepts VIII*, 103980G (5 September 2017);
- <sup>54</sup> Roser Juanola-Parramon, Neil Zimmerman, Maxime Rizzo, Hari Subedi, Giada Arney, Tyler Groff, Laurent Pueyo, Chris Stark, Rémi Soummer, Matthew Bolcar, Aki Roberge, "Modelling exoplanet detection with the LUVVOIR coronagraph (Conference Presentation)," *Proc. SPIE 10698, Space Telescopes and Instrumentation 2018: Optical, Infrared, and Millimeter Wave*, 1069810 (10 July 2018); <https://doi.org/10.1117/12.2312837>
- <sup>55</sup> Stahl, H. P., Postman, M., Smith, W. S. 2013, "Engineering specifications for large aperture UVO space telescopes derived from science requirements," *Proc. SPIE 8860*, <http://spiedigitallibrary.org/proceeding.aspx?articleid=1762023&resultClick=1>

- <sup>56</sup> Stahl, M. T., Shaklan, S. B., Stahl, H. P. 2015, "Preliminary Analysis of effect of random segment errors on coronagraph performance," Proc SPIE 9605 0P, <http://spiedigitallibrary.org/proceeding.aspx?articleid=2446862&resultClick=1>
- <sup>57</sup> Stahl, H. P., Postman, M., Smith, W. S. 2013, "Engineering specifications for large aperture UVO space telescopes derived from science requirements," Proc. SPIE 8860 06, <http://spiedigitallibrary.org/proceeding.aspx?articleid=1762023&resultClick=1>
- <sup>58</sup> Feinberg, L.D., et al. 2009, "Large segmented UV-optical space telescope using a Hybrid Sensor Active Control (HSAC) architecture," Proc. SPIE 7436 08, <http://spiedigitallibrary.org/proceeding.aspx?articleid=785987&resultClick=1>
- <sup>59</sup> Gonzales, M. A., et al., "Unprecedented Vibration isolation Demonstration using the Disturbance Free Payload Concept," AIAA 2004-5247, (2004), <http://arc.aiaa.org/doi/pdf/10.2514/6.2004-5247>
- <sup>60</sup> Larry D. Dewell, Kiarash Tajdaran, Raymond M. Bell, Kuo-Chia Liu, Matthew R. Bolcar, Lia W. Sacks, Julie A. Crooke, Carl Blaurock, "Dynamic stability with the disturbance-free payload architecture as applied to the Large UV/Optical/Infrared (LUVOIR) Mission," Proc. SPIE 10398, UV/Optical/IR Space Telescopes and Instruments: Innovative Technologies and Concepts VIII, 103980B (5 September 2017).
- Sacks, L. W., Blaurock, C., Dewell, L. D., Tajdaran, K., Liu, K.-C., Collins, C., et al. (2018). Preliminary jitter stability results for the large UV/optical/infrared (LUVOIR) surveyor concept using a non-contact vibration isolation and precision pointing system. In H. A. MacEwen, M. Lystrup, G. G. Fazio, N. Batalha, E. C. Tong, & N. Siegler (Eds.), *Space Telescopes and Instrumentation 2018: Optical, Infrared, and Millimeter Wave* (Vol. 10698, p. 1069842). International Society for Optics and Photonics. <http://doi.org/10.1117/12.2313762>
- <sup>61</sup> Mandić, M., Alvarez-Salazar, O., & Kiessling, A. A. (2018). HabEx: A high-precision pointing architecture using microthrusters and a fine steering mirror. In H. A. MacEwen, M. Lystrup, G. G. Fazio, N. Batalha, E. C. Tong, & N. Siegler (Eds.), *Space Telescopes and Instrumentation 2018: Optical, Infrared, and Millimeter Wave* (Vol. 10698, p. 106980U). International Society for Optics and Photonics. <http://doi.org/10.1117/12.2315545>
- <sup>62</sup> Chris Stark et al. 2015, "Lower Limits on Aperture Size for an ExoEarth Detecting Coronagraphic Mission", ApJ 808 149S, <http://adsabs.harvard.edu/abs/2015ApJ...808..149S>
- <sup>63</sup> Rafanelli, G. L., Cosner, C. M., Spencer, S. B., Wolfe, D., Newman, A., Polidan, R., & Chakrabarti, S. (2017). Revolutionary astrophysics using an incoherent synthetic optical aperture. In *UV/Optical/IR Space Telescopes and Instruments: Innovative Technologies and Concepts VIII* (Vol. 10398, p. 103980P). International Society for Optics and Photonics. <http://doi.org/10.1117/12.2272782>

- <sup>64</sup> H. Philip Stahl, "Habitable exoplanet imager optical telescope concept design," Proc. SPIE 10398, UV/Optical/IR Space Telescopes and Instruments: Innovative Technologies and Concepts VIII, 1039806 (5 September 2017);
- <sup>65</sup> J. Brent Knight, H. Philip Stahl, Andy Singleton, Ron Hunt, Melissa Therrell, Kate Caldwell, Jay Garcia, Mike Baysinger, "Dynamic/jitter assessment of multiple potential HabEx structural designs," Proc. SPIE 10374, Optical Modeling and Performance Predictions IX, 1037402 (6 September 2017);
- <sup>66</sup> Stahl, H. P., Postman, M., Smith, W. S. 2013, "Engineering specifications for large aperture UVO space telescopes derived from science requirements," Proc. SPIE 8860 06, <http://spiedigitallibrary.org/proceeding.aspx?articleid=1762023&resultClick=1>
- <sup>67</sup> Davis, J. M., Stahl, P. H., Arnold, W. R., & Smith, W. S. (2017). HabEx primary mirror trade studies. In D. M. Stubbs & A. E. Hatheway (Eds.), *Optomechanical Engineering 2017* (Vol. 10371, p. 103710B). International Society for Optics and Photonics. <http://doi.org/10.1117/12.2274476>
- <sup>68</sup> East, M., Redding, D., Sullivan, C., Mooney, T., & Allen, L. (2018). Picometer level stability of a mounted mirror assembly. In H. A. MacEwen, M. Lystrup, G. G. Fazio, N. Batalha, E. C. Tong, & N. Siegler (Eds.), *Space Telescopes and Instrumentation 2018: Optical, Infrared, and Millimeter Wave* (Vol. 10698, p. 106980Y). International Society for Optics and Photonics. <http://doi.org/10.1117/12.2314332>
- <sup>69</sup> Brooks, T. E. (2017). Predictive thermal control applied to HabEx. In *UV/Optical/IR Space Telescopes and Instruments: Innovative Technologies and Concepts VIII* (Vol. 10398, p. 1039814). International Society for Optics and Photonics. <http://doi.org/10.1117/12.2274338>
- <sup>70</sup> Brooks, T. E., Eng, R., & Stahl, H. P. (2018). Optothermal stability of large ULE and Zerodur mirrors. In *Optical Modeling and Performance Predictions X* (Vol. 10743, p. 107430A). International Society for Optics and Photonics. <http://doi.org/10.1117/12.2321275>
- <sup>71</sup> Postman, M., et al., 2009, "Advanced Technology Large-Aperture Space Telescope (ATLAST): A Technology Roadmap for the Next Decade," [http://www.stsci.edu/institute/atlast/documents/ATLAST\\_NASA\\_ASMCS\\_Public\\_Report.pdf](http://www.stsci.edu/institute/atlast/documents/ATLAST_NASA_ASMCS_Public_Report.pdf)
- <sup>72</sup> Dalcanton, J. and Seager, S., et al. [From Cosmic Birth to Living Earths], Association for Universities for Research in Astronomy, Washington, DC, (2015).
- <sup>73</sup> <https://ntrs.nasa.gov/archive/nasa/casi.ntrs.nasa.gov/20160013273.pdf>
- <sup>74</sup> Eisenhower, M. J., Cohen, L. M., Feinberg, L. D., Matthews, G. W., Nissen, J. A., Park, S. C., & Peabody, H. L. (2015). ATLAST ULE mirror segment performance analytical predictions based on thermally induced distortions. In H. A. MacEwen & J. B. Breckinridge (Eds.), *UV/Optical/IR Space Telescopes and Instruments: Innovative Technologies and Concepts VII* (Vol. 9602, p. 96020A). International Society for Optics and Photonics. <http://doi.org/10.1117/12.2188008>

- <sup>75</sup> Polidan, R. S., Belvin, W. K., Greenhouse, M. A., Grunsfeld, J. M., Guidi, J., MacEwen, H. A., et al. (2018). Servicing and assembly: enabling the most ambitious future space observatories. In H. A. MacEwen, M. Lystrup, G. G. Fazio, N. Batalha, E. C. Tong, & N. Siegler (Eds.), *Space Telescopes and Instrumentation 2018: Optical, Infrared, and Millimeter Wave* (Vol. 10698, p. 1069825). International Society for Optics and Photonics. <http://doi.org/10.1117/12.2313013>
- <sup>76</sup> Roming et al. 2005, "The SWIFT Ultra-violet and Optical Telescope", *Space Science Reviews* (2005) 120: 95–142, <https://link.springer.com/content/pdf/10.1007/s11214-005-5095-4.pdf>
- <sup>77</sup> Tiffenberg et al. 2017, "Single-Electron and Single-Photon Sensitivity with a Silicon Skipper CCD" *Phys. Rev. Lett* 199, 131082, <https://journals.aps.org/prl/abstract/10.1103/PhysRevLett.119.131802>
- <sup>78</sup> E. Fossum, "The Quanta Image Sensor (QIS): Concepts and Challenges," in *Imaging and Applied Optics*, OSA Technical Digest (CD) (Optical Society of America, 2011), paper JTuE1.
- <sup>79</sup> S. M. Baggett, J. Anderson, M. Sosey, C. Gosmeyer, M. Bourque, V. Bajaj, H. Khandrika, C. Martlin, "HST/WFC3: understanding and mitigating radiation damage effects in the CCD detectors," *Proc. SPIE 9904, Space Telescopes and Instrumentation 2016: Optical, Infrared, and Millimeter Wave*, 99045D (29 July 2016);
- <sup>80</sup> Private communications with Bernie Rauscher (December 2015)
- <sup>81</sup> Rauscher, B. et al. 2015, "ATLAST detector needs for direct spectroscopic biosignature characterization in the visible and near-IR", *SPIE 9602, 96020D*, <http://spiedigitallibrary.org/proceeding.aspx?articleid=2444184&resultClick=1>
- <sup>82</sup> Mazin, B. A., et al., "A superconducting focal plane array for ultraviolet, optical, and near-infrared astrophysics," *Opt. Express* 20, 1503-1511 (2012), <http://arxiv.org/pdf/1112.0004v1.pdf>
- <sup>83</sup> Allman, M. S., Verma, V. B., Stevens, M., Gerrits, T., Horansky, R. D., Lita, A. E., et al. (2015). A near-infrared 64-pixel superconducting nanowire single photon detector array with integrated multiplexed readout. *Applied Physics Letters*, 106(19), 192601. <http://doi.org/10.1063/1.4921318>
- <sup>84</sup> Rauscher, B., et al., 2015, "ATLAST detector needs for direct spectroscopic biosignature characterization in the visible and near-IR", *SPIE 9602, 96020D*, <http://spiedigitallibrary.org/proceeding.aspx?articleid=2444184&resultClick=1>
- <sup>85</sup> Atkinson, D., Hall, D., Goebel, S., Jacobson, S., & Baker, I. (2018). Observatory deployment and characterization of SAPHIRA HgCdTe APD arrays. In *High Energy, Optical, and Infrared Detectors for Astronomy VIII* (Vol. 10709, p. 107091H). International Society for Optics and Photonics. <http://doi.org/10.1117/12.2311814>
- <sup>86</sup> Shaklan, S. B., Noecker, M. C., Glassman, T., et al. 2010, "Error budgeting and tolerancing of starshades for exoplanet detection," *Proc. SPIE 7731, 77312G*, <http://spiedigitallibrary.org/proceeding.aspx?articleid=749972&resultClick=1>

- <sup>87</sup> Shaklan, S. B., Marchen, L., Lisman, P. D., et al. 2011, "A starshade petal error budget for exo-earth detection and characterization," Proc. SPIE 8151, 815113, <http://spiedigitallibrary.org/proceeding.aspx?articleid=1268343&resultClick=1>
- <sup>88</sup> Exo-S Final Report, <https://exoplanets.nasa.gov/exep/studies/probe-scale-stdt/>
- <sup>89</sup> Manan Arya, David Webb, James McGown, P. Douglas Lisman, Stuart Shaklan, S. Case Bradford, John Steeves, Evan Hilgemann, Brian Trease, Mark Thomson, Steve Warwick, Gregg Freebury, Jamie Gull, "Starshade mechanical design for the Habitable Exoplanet imaging mission concept (HabEx)," Proc. SPIE 10400, Techniques and Instrumentation for Detection of Exoplanets VIII, 104001C (12 September 2017);
- <sup>90</sup> Starshade Technology Development Plan (2018) [https://exoplanets.nasa.gov/internal\\_resources/1033/](https://exoplanets.nasa.gov/internal_resources/1033/)
- <sup>91</sup> Martin, S. R., Shaklan, S. B., Crawford, S. L., et al. 2013, "Starshade optical edge modelling, requirements, and laboratory tests," Proc. SPIE 8864, 88641A, <http://spiedigitallibrary.org/proceeding.aspx?articleid=1744188&resultClick=1>
- <sup>92</sup> Casement et al., TDEM-12 Whitepaper "Starshade Stray Light Mitigation through Edge Scatter Modeling and Sharp-Edge Materials Development"; [http://exoplanets.nasa.gov/technology/casement\\_whitepaper.pdf](http://exoplanets.nasa.gov/technology/casement_whitepaper.pdf)
- <sup>93</sup> Steeves, J.S., Martin, S. R., et. al. 2016, "Precision optical edges for a starshade external occulter", Proc. SPIE 9912, 991220, <http://proceedings.spiedigitallibrary.org/proceeding.aspx?articleid=2538386>
- <sup>94</sup> Steeves, J., Lee, H. J., Hilgemann, E., McKeithen, D., Bradley, C., Webb, D., et al. (2018). Development of low-scatter optical edges for starshades. In R. Geyl & R. Navarro (Eds.), Advances in Optical and Mechanical Technologies for Telescopes and Instrumentation III (Vol. 10706, p. 107065K). International Society for Optics and Photonics. <http://doi.org/10.1117/12.2312694>
- <sup>95</sup> Harness, A., Dumont, P., Shaklan, S., & Cash, W. (2018). Advances in edge diffraction algorithms. Josa A, 35(2), 275–285. <http://doi.org/10.1364/JOSAA.35.000275>
- <sup>96</sup> Schindhelm, E., Shipley, A., Oakley, P., et al. 2007, "Laboratory studies of petal-shaped occulter" Proc. SPIE 6693, 669305, <http://spiedigitallibrary.org/proceeding.aspx?articleid=817922&resultClick=1>
- <sup>97</sup> Leviton, D. B., Cash, W. C., Gleason, B., et al. 2007, "White-light demonstration of one hundred parts per billion irradiance suppression in air by new starshade occulter." Proc. SPIE 6687 66871B, <http://spiedigitallibrary.org/proceeding.aspx?articleid=817377&resultClick=1>
- <sup>98</sup> Lo, A. S., Glassman, T., Dailey, D., Sterk, K., Green, J., Cash, W., Soummer, R. 2010, "New Worlds Probe," Proc. SPIE 7731, 77312E, <http://spiedigitallibrary.org/proceeding.aspx?articleid=749969&resultClick=1>
- <sup>99</sup> Samuele, R., Varshneya, R., Johnson, T. P., et al. 2010, "Progress at the starshade testbed at Northrop Grumman Aerospace Systems: comparisons with computer simulations," Proc.

- SPIE 7731, 773151,  
<http://spiedigitallibrary.org/proceeding.aspx?articleid=750104&resultClick=1>
- <sup>100</sup> Cady, E. et al. 2010, "Broadband suppression and occulter position sensing at the Princeton occulter testbed." Proc. SPIE 7731, 77312F,  
<http://spiedigitallibrary.org/proceeding.aspx?articleid=749970&resultClick=1>
- <sup>101</sup> Sirbu, D., Kasdin, N. J., Vanderbei, R. J., 2013, "Progress on optical verification for occulter-based high contrast imaging," Proc. SPIE 8864, 886419,  
<http://spiedigitallibrary.org/proceeding.aspx?articleid=1744187&resultClick=1>
- <sup>102</sup> Glassman, T. et al., TDEM-12 Final Report, "Demonstration of Starshade Starlight-Suppression Performance in the Field";  
[http://exoplanets.nasa.gov/files/exep/GlassmanTDEM2012\\_FinalReport.pdf](http://exoplanets.nasa.gov/files/exep/GlassmanTDEM2012_FinalReport.pdf)
- <sup>103</sup> Yunjong Kim, Anthony Harness, Dan Sirbu, Mengya Hu, Mike Galvin, N. Jeremy Kasdin, Robert J. Vanderbei, Stuart B. Shaklan, "Optical demonstration of a starshade at flight Fresnel numbers," Proc. SPIE 10400, Techniques and Instrumentation for Detection of Exoplanets VIII, 104001A (1 September 2017);
- <sup>104</sup> Anthony Harness, Stuart Shaklan, Philip Dumont, Yunjong Kim, N. Jeremy Kasdin, "Modeling and performance predictions for the Princeton Starshade Testbed," Proc. SPIE 10400, Techniques and Instrumentation for Detection of Exoplanets VIII, 1040019 (1 September 2017);
- <sup>105</sup> Harness, A., Kasdin, J., Shaklan, S., Dumont, P., & Balasubramanian, K. (2018). Modeling non-scalar diffraction in the Princeton starshade testbed. In H. A. MacEwen, M. Lystrup, G. G. Fazio, N. Batalha, E. C. Tong, & N. Siegler (Eds.), *Space Telescopes and Instrumentation 2018: Optical, Infrared, and Millimeter Wave* (Vol. 10698, p. 1069865). International Society for Optics and Photonics. <http://doi.org/10.1117/12.2310187>
- <sup>106</sup> Seager, S., et al., 2015, "Exo-S: starshade probe-class exoplanet direct imaging mission concept, Final Report," [https://exoplanets.nasa.gov/exep/stdt/Exo-S\\_Starshade\\_Probe\\_Class\\_Final\\_Report\\_150312\\_URS250118.pdf](https://exoplanets.nasa.gov/exep/stdt/Exo-S_Starshade_Probe_Class_Final_Report_150312_URS250118.pdf)
- <sup>107</sup> Cash, W., Kendrick, S., Noecker, et al., 2009, "The New Worlds Observer: the astrophysics strategic mission concept study," Proc. SPIE 7436,  
<http://spiedigitallibrary.org/proceeding.aspx?articleid=785984&resultClick=1>
- <sup>108</sup> N.J. Kasdin et al., 2009, "Occulter design for THEIA," Proc. SPIE 7440,  
<http://proceedings.spiedigitallibrary.org/proceeding.aspx?articleid=786370>
- <sup>109</sup> D.P.Scharf,S.R.Martin,C.C.Liebe,Z.H.Rahman,C.R.Seubert,M.C.Noecker,andG.H.Purcell,"Precision formation flying at megameter separations for exoplanet characterization," *Acta Astronautica* 123, pp. 420–434, June 2016.
- <sup>110</sup> Exo-S Final Report, <https://exoplanets.nasa.gov/exep/studies/probe-scale-stdt/>
- <sup>111</sup> Michael Bottom, Stefan Martin, Carl Seubert, Eric Cady, Shannon Kian Zareh, Stuart Shaklan, "Precise starshade stationkeeping and pointing with a Zernike wavefront sensor," Proc. SPIE

- 10400, Techniques and Instrumentation for Detection of Exoplanets VIII, 104001B (1 September 2017);
- <sup>112</sup> *ibid*
- <sup>113</sup> S5: Starshade technology to TRL5 Milestone 4 Final Report: Lateral formation sensing and control [https://exoplanets.nasa.gov/internal\\_resources/1077](https://exoplanets.nasa.gov/internal_resources/1077)
- <sup>114</sup> Exo-S Final Report, <https://exoplanets.nasa.gov/exep/studies/probe-scale-stdt/>
- <sup>115</sup> Cash, W., Kendrick, S., Noecker, et al., 2009, "The New Worlds Observer: the astrophysics strategic mission concept study," Proc. SPIE 7436.  
<http://spiedigitallibrary.org/proceeding.aspx?articleid=785984&resultClick=1>
- <sup>116</sup> Stuart B. Shaklan, Luis Marchen, Eric Cady, "Shape accuracy requirements on starshades for large and small apertures," Proc. SPIE 10400, Techniques and Instrumentation for Detection of Exoplanets VIII, 104001T (1 September 2017); doi: 10.1117/12.2273436
- <sup>117</sup> See deployment video <https://exoplanets.nasa.gov/resources/2185/starshade-deployment-animation/>
- <sup>118</sup> <http://asd.gsfc.nasa.gov/firs/>
- <sup>119</sup> Males, J. R., Close, L. M., Guyon, O., Morzinski, K., Puglisi, A., Hinz, P., et al. (2014). Direct imaging of exoplanets in the habitable zone with adaptive optics. In E. Marchetti, L. M. Close, & J.-P. Véran (Eds.), *Adaptive Optics Systems IV* (Vol. 9148, p. 914820). International Society for Optics and Photonics. <http://doi.org/10.1117/12.2057135>
- <sup>120</sup> ESO news release 9 January 2017 "ESO Signs Agreement with Breakthrough Initiatives" <https://www.eso.org/public/usa/news/eso1702/>
- <sup>121</sup> Enya, K., Abe, L., Haze, K., Tanaka, S., Nakagawa, T., Kataza, H., et al. (2008). Mid-infrared coronagraph for SPICA. In J. M. Oschmann Jr, M. W. M. de Graauw, & H. A. MacEwen (Eds.), *Space Telescopes and Instrumentation 2008: Optical, Infrared, and Millimeter* (Vol. 7010, p. 70102Z). International Society for Optics and Photonics. <http://doi.org/10.1117/12.788509>
- <sup>122</sup> Boccaletti, A., et al., 2015, "The Mid-Infrared Instrument for the James Webb Space Telescope, V: Predicted Performance of the MIRI Coronagraphs," Publications of the Astronomical Society of the Pacific Vol 127, 953,  
<http://iopscience.iop.org/article/10.1086/682256>
- <sup>123</sup> Enya, K., Abe, L., Haze, K., Tanaka, S., Nakagawa, T., Kataza, H., et al. (2008). Mid-infrared coronagraph for SPICA. In J. M. Oschmann Jr, M. W. M. de Graauw, & H. A. MacEwen (Eds.), *Space Telescopes and Instrumentation 2008: Optical, Infrared, and Millimeter* (Vol. 7010, p. 70102Z). International Society for Optics and Photonics. <http://doi.org/10.1117/12.788509>
- <sup>124</sup> Takahashi, A., Lam, C., Matsuhara, H., Kataza, H., Haze, K., Enya, K., et al. (2017). Laboratory demonstration of a cryogenic deformable mirror for wavefront correction of space-borne infrared telescopes. *Applied Optics*, 56(23), 6694–6708.  
<http://doi.org/10.1364/AO.56.006694>
- <sup>125</sup> OST Interim Report [https://asd.gsfc.nasa.gov/firs/docs/OST\\_Interim\\_Study\\_Report.pdf](https://asd.gsfc.nasa.gov/firs/docs/OST_Interim_Study_Report.pdf)

- <sup>126</sup> Green, J. J., Bradford, S. C., Gautier, T., Rodgers, M., Sidick, E., & Vasisht, G. (2018). Architecture for space-based exoplanet spectroscopy in the mid-infrared. In H. A. MacEwen, M. Lystrup, G. G. Fazio, N. Batalha, E. C. Tong, & N. Siegler (Eds.), *Space Telescopes and Instrumentation 2018: Optical, Infrared, and Millimeter Wave* (Vol. 10698, p. 106981C). International Society for Optics and Photonics. <http://doi.org/10.1117/12.2314338>
- <sup>127</sup> Rieke, G. H., Ressler, M. E., Morrison, J. E., Bergeron, L., Bouchet, P., García-Marín, M., et al. (2015). The Mid-Infrared Instrument for the James Webb Space Telescope, VII: The MIRI Detectors. *Publications of the Astronomical Society of the Pacific*, 127(953), 665–674. <http://doi.org/10.1086/682257>
- <sup>128</sup> OST Interim Report [https://asd.gsfc.nasa.gov/firs/docs/OST\\_Interim\\_Study\\_Report.pdf](https://asd.gsfc.nasa.gov/firs/docs/OST_Interim_Study_Report.pdf)
- <sup>129</sup> Robinson, T., et al., 2014, “Detection of Ocean Glint and Ozone Absorption using LCROSS Earth Observations”, *ApJ* 787: 171. <http://dx.doi.org/10.1088/0004-637X/787/2/171>
- <sup>130</sup> Hennessy, J., et al., 2016, “Performance and prospects of far ultraviolet aluminum mirrors protected by atomic layer deposition” *J. Astron. Telesc. Instrum. Syst.* 2(4), 041206 (Jun 07, 2016). doi:10.1117/1.JATIS.2.4.041206  
<http://astronomicaltelescopes.spiedigitallibrary.org/article.aspx?articleid=2528070>
- <sup>131</sup> Quijada, M. A., Del Hoyo, J., Boris, D. R., & Walton, S. G. (2017). Improved mirror coatings for use in the Lyman Ultraviolet to enhance astronomical instrument capabilities. In H. A. MacEwen & J. B. Breckinridge (Eds.), *UV/Optical/IR Space Telescopes and Instruments: Innovative Technologies and Concepts VIII* (Vol. 10398, p. 103980Z). International Society for Optics and Photonics. <http://doi.org/10.1117/12.2274790>
- <sup>132</sup> Lightsey, P. A., Atkinson, C. B., Clampin, M. C., & Feinberg, L. D. (2012). James Webb Space Telescope: large deployable cryogenic telescope in space. *Optical Engineering*, 51(1), 0111003. <http://doi.org/10.1117/1.OE.51.1.0111003>
- <sup>133</sup> Lightsey, P. A., Gallagher, B. B., Nickles, N., & Copp, T. (2012). Optical transmission for the James Webb Space Telescope. In M. C. Clampin, G. G. Fazio, H. A. MacEwen, & J. M. Oschmann (Eds.), *Space Telescopes and Instrumentation 2012: Optical, Infrared, and Millimeter Wave* (Vol. 8442, p. 84423A). International Society for Optics and Photonics. <http://doi.org/10.1117/12.924841>
- <sup>134</sup> Cohen, E. J., & Hull, T. (2004). Selection of a mirror technology for the 1.8-m Terrestrial Planet Finder demonstrator mission. In E. Atad-Etchedgui & P. Dierickx (Eds.), *Optical Fabrication, Metrology, and Material Advancements for Telescopes* (Vol. 5494, pp. 350–366). International Society for Optics and Photonics. <http://doi.org/10.1117/12.552329>
- <sup>135</sup> Balasubramanian, K., Hennessy, J., Raouf, N., Nikzad, S., Del Hoyo, J., & Quijada, M. (2017). Mirror coatings for large aperture UV optical infrared telescope optics. In H. A. MacEwen & J. B. Breckinridge (Eds.), *UV/Optical/IR Space Telescopes and Instruments: Innovative Technologies and Concepts VIII* (Vol. 10398, p. 103980X). International Society for Optics and Photonics. <http://doi.org/10.1117/12.2274794>
- <sup>136</sup> Balasubramanian, K., Shaklan, S., Give'on, A., Cady, E., & Marchen, L. (2011). Deep UV to NIR space telescopes and exoplanet coronagraphs: a trade study on throughput, polarization,

- mirror coating options and requirements. In S. Shaklan (Ed.), (Vol. 8151, pp. 81511G–14). Presented at the SPIE Optical Engineering + Applications, SPIE.  
<http://doi.org/10.1117/12.902440>
- <sup>137</sup> Hubble Space Telescope Optical Telescope Assembly Handbook version 1.0 May 1990, NASA-CR-189.751, Space Telescope Science Institute (1990)
- <sup>138</sup> Robinson, T., et al., 2014, “Detection of Ocean Glint and Ozone Absorption using LCROSS Earth Observations”, *ApJ* 787: 171. <http://dx.doi.org/10.1088/0004-637X/787/2/171>
- <sup>139</sup> Bolcar, M., et al., 2016, “Technology Gap Assessment for a Future Large-aperture Ultraviolet-Optical-Infrared Space Telescope,” *J. Astron. Telesc. Instrum. Syst.* 2(4), 041209.  
doi:10.1117/1.JATIS.2.4.041209  
<http://astronomicaltelescopes.spiedigitallibrary.org/article.aspx>
- <sup>140</sup> O. H. W. Siegmund, C. Ertley, J. V. Vallerga, E. R. Schindhelm, A. Harwit, B. T. Fleming, K. C. France, J. C. Green, S. R. McCandliss, W. M. Harris, "Microchannel plate detector technology potential for LUVOIR and HabEx," *Proc. SPIE 10397, UV, X-Ray, and Gamma-Ray Space Instrumentation for Astronomy XX*, 1039711 (29 August 2017); doi: 10.1117/12.2274281
- <sup>141</sup> Pueyo, L., Zimmerman, N., Bolcar, M., Groff, T., Stark, C., Ruane, G., et al. (2017). The LUVOIR architecture “A” coronagraph instrument. In H. A. MacEwen & J. B. Breckinridge (Eds.), *UV/Optical/IR Space Telescopes and Instruments: Innovative Technologies and Concepts VIII* (Vol. 10398, p. 103980F). International Society for Optics and Photonics.  
<http://doi.org/10.1117/12.2274654>
- <sup>142</sup> HabEx Interim Report [https://www.jpl.nasa.gov/habex/pdf/HabEx\\_Interim\\_Report.pdf](https://www.jpl.nasa.gov/habex/pdf/HabEx_Interim_Report.pdf)
- <sup>143</sup> Anglada-Escudé, G., Amado, P. J., Barnes, J., Berdiñas, Z. M., Butler, R. P., Coleman, G. A. L., et al. (2016). A terrestrial planet candidate in a temperate orbit around Proxima Centauri. *Nature*, 536(7617), 437–440. <http://doi.org/10.1038/nature19106>
- <sup>144</sup> Fischer, D. A., Anglada-Escudé, G., Arriagada, P., Baluev, R. V., Bean, J. L., Bouchy, F., et al. (2016). State of the Field: Extreme Precision Radial Velocities\*. *Publications of the Astronomical Society of the Pacific*, 128(964), 066001. <http://doi.org/10.1088/1538-3873/128/964/066001>
- <sup>145</sup> Plavchan, P., et al., 2015, “Radial Velocity Prospects Current and Future: A White Paper Report prepared by the Study Analysis Group 8 for the Exoplanet Program Analysis Group (ExoPAG)” <https://arxiv.org/abs/1503.01770>
- <sup>146</sup> Suh, M.-G., Yi, X., Lai, Y.-H., Leifer, S., Grudinin, I. S., Vasisht, G., et al. (2019). Searching for exoplanets using a microresonator astrocomb. *Nature Photonics*, 13(1), 25.  
<http://doi.org/10.1038/s41566-018-0312-3>
- <sup>147</sup> Schwab, C., et al, 2016, “Design of NEID, an extreme precision Doppler spectrograph for WIYN”, *Proc. SPIE 9908, Ground-based and Airborne Instrumentation for Astronomy VI*, 99087H (August 9, 2016); doi:10.1117/12.2234411  
<http://proceedings.spiedigitallibrary.org/proceeding.aspx?articleid=2544294>

- <sup>148</sup> Crepp, J, et al, 2016, “iLocater: A Diffraction-limited Doppler Spectrometer for the Large Binocular Telescope”, Proc. SPIE 9908, Ground-based and Airborne Instrumentation for Astronomy VI, 990819 (4 August 2016); doi:10.1117/12.2233135, <http://proceedings.spiedigitallibrary.org/proceeding.aspx?articleid=2543021>
- <sup>149</sup> Plavchan, P., et al., 2015, “Radial Velocity Prospects Current and Future: A White Paper Report prepared by the Study Analysis Group 8 for the Exoplanet Program Analysis Group (ExoPAG)” <https://arxiv.org/abs/1503.01770>
- <sup>150</sup> Fischer, D. A., Anglada-Escudé, G., Arriagada, P., Baluev, R. V., Bean, J. L., Bouchy, F., et al. (2016). State of the Field: Extreme Precision Radial Velocities\*. *Publications of the Astronomical Society of the Pacific*, 128(964), 066001. <http://doi.org/10.1088/1538-3873/128/964/066001>
- <sup>151</sup> Plavchan, P., et al., 2015, “Radial Velocity Prospects Current and Future: A White Paper Report prepared by the Study Analysis Group 8 for the Exoplanet Program Analysis Group (ExoPAG)” <https://arxiv.org/abs/1503.01770>
- <sup>152</sup> Halverson, S., Terrien, R., Mahadevan, S., Roy, A., Bender, C., Stefánsson, G. K., et al. (2016). A comprehensive radial velocity error budget for next generation Doppler spectrometers. In C. J. Evans, L. Simard, & H. Takami (Eds.), *Ground-based and Airborne Instrumentation for Astronomy VI* (Vol. 9908, p. 99086P). International Society for Optics and Photonics. <http://doi.org/10.1117/12.2232761>
- <sup>153</sup> Francesco Pepe, "ESPRESSO@VLT: an instrument for advanced exoplanet research (Conference Presentation)", Proc. SPIE 10702, Ground-based and Airborne Instrumentation for Astronomy VII, 107020X (9 July 2018); doi: 10.1117/12.2315126; <https://doi.org/10.1117/12.2315126>
- <sup>154</sup> Schwab, C., et al, 2016, “Design of NEID, an extreme precision Doppler spectrograph for WIYN”, Proc. SPIE 9908, Ground-based and Airborne Instrumentation for Astronomy VI, 99087H (August 9, 2016); doi:10.1117/12.2234411 <http://proceedings.spiedigitallibrary.org/proceeding.aspx?articleid=2544294>
- <sup>155</sup> Crepp, J, et al, 2016, “iLocater: A Diffraction-limited Doppler Spectrometer for the Large Binocular Telescope”, Proc. SPIE 9908, Ground-based and Airborne Instrumentation for Astronomy VI, 990819 (4 August 2016); doi:10.1117/12.2233135, <http://proceedings.spiedigitallibrary.org/proceeding.aspx?articleid=2543021>
- <sup>156</sup> Lanza, A. F., Malavolta, L., Benatti, S., Desidera, S., Bignamini, A., Bonomo, A. S., et al. (2018). The GAPS Programme with HARPS-N at TNG - XVII. Line profile indicators and kernel regression as diagnostics of radial-velocity variations due to stellar activity in solar-like stars. *Astronomy and Astrophysics*, 616, A155. <http://doi.org/10.1051/0004-6361/201731010>
- <sup>157</sup> Dumusque, X. (2018). Measuring precise radial velocities on individual spectral lines - I. Validation of the method and application to mitigate stellar activity. *Astronomy and Astrophysics*, 620, A47. <http://doi.org/10.1051/0004-6361/201833795>

- <sup>158</sup> Hall, R. D., Thompson, S. J., Handley, W., & Queloz, D. (2018). On the Feasibility of Intense Radial Velocity Surveys for Earth-Twin Discoveries. *Monthly Notices of the Royal Astronomical Society*, 479(3), 2968–2987. <http://doi.org/10.1093/mnras/sty1464>
- <sup>159</sup> Sameshima, H., Matsunaga, N., Kobayashi, N., Kawakita, H., Hamano, S., Ikeda, Y., et al. (2018). Correction of Near-infrared High-resolution Spectra for Telluric Absorption at 0.90–1.35  $\mu\text{m}$ . *Publications of the Astronomical Society of the Pacific*, 130(989), 074502. <http://doi.org/10.1088/1538-3873/aac1b4>
- <sup>160</sup> Catanzarite, J, et al., 2006, “Astrometric Detection of Terrestrial Planets in the Habitable Zone of Nearby Stars with SIM PlanetQuest” *PASP* 118, 847  
<http://iopscience.iop.org/article/10.1086/504442>
- <sup>161</sup> Bendek, E., Tuthill, P., Guyon, O., Vasisht, G., Belikov, R., Larkin, K., et al. (2018). Precision astrometry mission for exoplanet detection around binary stars. In *Space Telescopes and Instrumentation 2018: Optical, Infrared, and Millimeter Wave* (Vol. 10698, p. 106980G). International Society for Optics and Photonics. <http://doi.org/10.1117/12.2313919>
- <sup>162</sup> Perryman, M., et al., 2014, “Astrometric Exoplanet Detection with GAIA”, *ApJ* 797, 14, <http://iopscience.iop.org/article/10.1088/0004-637X/797/1/14/meta>
- <sup>163</sup> Riess, A. G., Casertano, S., Anderson, J., MacKenty, J., Filippenko, A., “Parallax beyond a kiloparsec from spatially scanning the wide field camera 3 on the Hubble space telescope,” *ApJ*, 785, 2, 2014
- <sup>164</sup> Bendek, E., et al., TDEM-13 Final Report: “Enhanced Direct Imaging Exoplanet Detection with Astrometry Mass Determination,” <http://exoplanets.nasa.gov/technology>
- <sup>165</sup> LUVVOIR Interim Report  
[https://asd.gsfc.nasa.gov/luvvoir/resources/docs/LUVVOIR\\_Interim\\_Report\\_Final.pdf](https://asd.gsfc.nasa.gov/luvvoir/resources/docs/LUVVOIR_Interim_Report_Final.pdf)
- <sup>166</sup> Sozzetti, A. (2017). Gaia and exoplanets: a revolution in the making. In S. Shaklan (Ed.), *Techniques and Instrumentation for Detection of Exoplanets VIII* (Vol. 10400, p. 104001E). International Society for Optics and Photonics. <http://doi.org/10.1117/12.2276987>
- <sup>167</sup> Stevenson, K. B., Lewis, N. K., Bean, J. L., Beichman, C., Fraine, J., Kilpatrick, B. M., et al. (2016). Transiting Exoplanet Studies and Community Targets for JWST’s Early Release Science Program. *Publications of the Astronomical Society of the Pacific*, 128(967), 094401. <http://doi.org/10.1088/1538-3873/128/967/094401>
- <sup>168</sup> Rieke, G. H., Ressler, M. E., Morrison, J. E., Bergeron, L., Bouchet, P., García-Marín, M., et al. (2015). The Mid-Infrared Instrument for the James Webb Space Telescope, VII: The MIRI Detectors. *Publications of the Astronomical Society of the Pacific*, 127(953), 665–674. <http://doi.org/10.1086/682257>
- <sup>169</sup> Beichman, C., Benneke, B., Knutson, H., Smith, R., Lagage, P.-O., Dressing, C., et al. (2014). Observations of Transiting Exoplanets with the James Webb Space Telescope (JWST). *Publications of the Astronomical Society of the Pacific*, 126(946), 1134–1173. <http://doi.org/10.1086/679566>

- <sup>170</sup> Lum, N. A., Asbrock, J. F., White, R., Kelchner, R. E., Lum, L., Le T Pham, et al. (1993). Low-noise, low-temperature 256 x 256 Si:As IBC staring FPA. In A. M. Fowler (Ed.), *Infrared Detectors and Instrumentation* (Vol. 1946, pp. 100–110). International Society for Optics and Photonics. <http://doi.org/10.1117/12.158664>
- <sup>171</sup> OST Interim Report [https://asd.gsfc.nasa.gov/firs/docs/OST\\_Interim\\_Study\\_Report.pdf](https://asd.gsfc.nasa.gov/firs/docs/OST_Interim_Study_Report.pdf)
- <sup>172</sup> Matsuo, T., Greene, T., Roellig, T. L., McMurray, R. E., Johnson, R. R., Kashani, A., et al. (2018). A highly stable spectrophotometric capability for the Origins Space Telescope (OST) mid-infrared imager, spectrometer, coronagraph (MISC). In H. A. MacEwen, M. Lystrup, G. G. Fazio, N. Batalha, E. C. Tong, & N. Siegler (Eds.), *Space Telescopes and Instrumentation 2018: Optical, Infrared, and Millimeter Wave* (Vol. 10698, p. 1069844). International Society for Optics and Photonics. <http://doi.org/10.1117/12.2311896>
- <sup>173</sup> Dorn, M., McMurtry, C., Pipher, J., Forrest, W., Cabrera, M., Wong, A., et al. (2018). A monolithic 2k x 2k LWIR HgCdTe detector array for passively cooled space missions. In A. D. Holland & J. Beletic (Eds.), *High Energy, Optical, and Infrared Detectors for Astronomy VIII* (Vol. 10709, p. 1070907). International Society for Optics and Photonics. <http://doi.org/10.1117/12.2313521>
- <sup>174</sup> Kendrew, S., Dicken, D., Bouwman, J., Marin, M. G., Greene, T. P., Lagage, P.-O., et al. (2018). Time series observations with the mid-infrared instrument (MIRI) on JWST. In H. A. MacEwen, M. Lystrup, G. G. Fazio, N. Batalha, E. C. Tong, & N. Siegler (Eds.), *Space Telescopes and Instrumentation 2018: Optical, Infrared, and Millimeter Wave* (Vol. 10698, p. 106983U). International Society for Optics and Photonics. <http://doi.org/10.1117/12.2313951>
- <sup>175</sup> Rauscher, B, et al., 2016, “Detectors and cooling technology for direct spectroscopic biosignature characterization” *J. Astron. Telesc. Instrum. Syst.* 2(4), <http://astronomicaltelescopes.spiedigitallibrary.org/article.aspx?articleid=2545567>